AD_____

Award Number: DAMD17-99-1-9213

TITLE: Developing Novel Anticancer DNA-Binding Drugs to Disrupt ETS-Mediated Transcription Associated with Breast Cancer: Use of the C-Fos Serum Response Element as a Model System

PRINCIPAL INVESTIGATOR: Christine M. White

CONTRACTING ORGANIZATION: Health Research, Incorporated
Buffalo, New York 14263

REPORT DATE: June 2001

TYPE OF REPORT: Annual Summary

PREPARED FOR: U.S. Army Medical Research and Materiel Command
Fort Detrick, Maryland 21702-5012

REPORT DOCUMENTATION PAGE

Form Approved
OMB No. 074-0188

1. AGENCY USE ONLY (Leave blank)	2. REPORT DATE	3. REPORT TYPE AND DATES COVERED
	June 2001	Annual Summary (15 May 00 - 14 May 01)

4. TITLE AND SUBTITLE
Developing Novel Anticancer DNA-Binding Drugs to Disrupt ETS-Mediated Transcription Associated with Breast Cancer: Use of the C-Fos Serum Response Element as Model System

5. FUNDING NUMBERS
DAMD17-99-1-9213

6. AUTHOR(S)
Christine M. White

7. PERFORMING ORGANIZATION NAME(S) AND ADDRESS(ES)
Health Research, Incorporated
Buffalo, New York 14263

E-Mail: Christien.White@Roswellpark.org

8. PERFORMING ORGANIZATION REPORT NUMBER

9. SPONSORING / MONITORING AGENCY NAME(S) AND ADDRESS(ES)
U.S. Army Medical Research and Materiel Command
Fort Detrick, Maryland 21702-5012

10. SPONSORING / MONITORING AGENCY REPORT NUMBER

11. SUPPLEMENTARY NOTES

12a. DISTRIBUTION / AVAILABILITY STATEMENT
Approved for Public Release; Distribution Unlimited

12b. DISTRIBUTION CODE

13. ABSTRACT *(Maximum 200 Words)*

Disregulated transcription factor (TF)-mediated activation of gene expression can play a key role in oncogenesis, especially in breast cancer. Preventing TF/DNA interactions using small molecule DNA-reactive agents may decrease oncogenic gene expression and potentially halt cancer development. Our goal is to improve DNA-binding drugs' abilities to inhibit specific TF/DNA interactions using the human c-fos promoter's serum response element (SRE) as a target. In an effort to improve drug effectiveness, the novel minor groove-binding fluorescent microgonotropens (FMGTs) were developed. These A/T selective bisbenzimidazole-based agents have polyamine tails that extend to contact DNA's phosphodiester backbone, allowing them to bind with very high affinity. Here, we explore the potential of these agents to inhibit TF/DNA complex formation in a series of increasingly complex assays in the c-fos model and assess whether their ability to contact both groove makes them more effective than classical minor groove-binding drugs. Analyzing these agents using a well-defined gene regulatory element and TFs have provided insight into the relationship between their chemical structure and biological activities and form the basis for further drug development.

14. SUBJECT TERMS
Breast Cancer, Oncogenic gene expression, Ets transcription factors, DNA-binding drugs, Anticancer drugs, c-fos, DNA

15. NUMBER OF PAGES
73

16. PRICE CODE

17. SECURITY CLASSIFICATION OF REPORT	18. SECURITY CLASSIFICATION OF THIS PAGE	19. SECURITY CLASSIFICATION OF ABSTRACT	20. LIMITATION OF ABSTRACT
Unclassified	Unclassified	Unclassified	Unlimited

Table of Contents

Introduction

Disregulated gene expression, which may contribute to the development and progression of various diseases, including breast cancer, often occurs at the level of transcription. This aberrant transcription may result from the inappropriate binding of transcription factors (TFs) to their target DNA sequences in gene promoters (1). For example, overexpression of certain *ets* family TFs, such as PEA3 and ESX, is associated with early stage breast cancer development and the upregulation of Her2/Neu, a receptor tyrosine kinase overexpressed in nearly 30% of breast cancer cases (2, 3). Disrupting specific TF/DNA complexes on key growth-controlling genes may inhibit cancer development and progression and is therefore a desirable first step in the design of therapeutically useful agents (4). While classical DNA-binding drugs, such as the A/T selective minor groove binders distamycin or Hoechst 33342, can inhibit TF/DNA complex formation through steric hindrance and deformation of the DNA helix, such agents lack specificity (5, 6). Since they bind to many sites on DNA, they inhibit general transcription and disrupt other template related activities, leading to significant toxicity in both normal and cancer cells. Our studies focus on evaluating DNA-binding drugs as inhibitors of TF/DNA complex formation in order to identify agents with enhanced sequence selectivity, potency and cellular activity; a key step in using such agents to understand and modify regulation of gene expression or even as an ultimate basis for the development of therapeutics. We chose the well-defined human c-fos serum response element (SRE) as a model system to study drug effects on TF/DNA complexes and resultant transcription and to develop paradigms for drug targeting in increasingly complex assay environments. The binding of serum response factor (SRF) to an A/T rich site and the subsequent recruitment of the *ets* TF Elk-1 to a GGA core sequence provide the opportunity to study drug effects on these TFs separately or the resulting ternary complex as a whole (see manuscript 1 in Appendix III) (7). In an effort to improve drug potency, the novel, rationally designed DNA-binding microgonotropens (MGTs) were developed in collaboration with Dr. Thomas C. Bruice at the University of Santa Barbara, California (8, 9). These agents have an A/T selective, minor groove-binding polypyrrole or bisbenzimidazole backbone attached to a major groove-associating polyamine tail (see Fig. 1 in Appendix II). The c-fos SRE model was used to explore the potential of these agents as inhibitors of TF/DNA complex formation and assessed whether their ability to contact both grooves makes them more effective than their classical minor groove-binding parent compounds, Hoechst 33342 and Hoechst 33258 (see manuscript 3 in Appendix V). Our systematic evaluation provides insight into structure/activity relationships that can potentially be used to strategically improve the chemical design of the MGTs and make them more effective inhibitors of gene expression.

Summary of Research and Training

Materials and Methods/Protocol Development:

My previous report detailed the establishment of the SRE of the human c-fos promoter as a model system to study, understand, and develop paradigms for drug targeting of TF/DNA complexes in cell-free and cellular assays. This work has since been published (see manuscript in Appendix III). In brief, the ability of DNA-binding drugs to inhibit TF complex formation on the SRE is assessed in electrophoretic mobility shift assays (EMSAs), a simple system consisting of purified proteins and short oligonucleotides. The c-fos promoter-driven cell-free transcription assay, which uses a nuclear lysate to drive transcription from a plasmid, analyzes drug effects in a more complicated environment. Effects of agents on endogenous c-fos expression in whole cells are assessed using Northern blot assays. Cytotoxicity and RNA synthesis assays determine how drugs affect cells in general. The IC_{50} values (the concentration of drug needed to inhibit the observed activity by 50%) were used to compare drug potencies in each assay.

We also wished to determine if drugs could disrupt other DNA-template activities in a nuclear environment and whether this activity correlated to the EMSA or cell-free transcription assay results. Therefore, in addition to these methods, an additional assay was established to assess drug effects on topoisomerase II (topo II) activity in isolated nuclei. As an enzymatic mediator of DNA topology, topo II associates with DNA and nicks both strands, becoming covalently bound to the free DNA ends in a "cleavable complex." After cellular DNA is labeled with [^{14}C]-thymidine and nuclei are isolated, covalent topo II/DNA complexes are induced by the epipodophyllotoxin VM-26 (10). These cleavable complexes are then precipitated in the presence of sodium dodecyl sulfate and quantitated through scintillation counting. In the presence of minor groove-binding agents such as Hoechst 33342, cleavable complex formation is inhibited (11). This assay provides a more complex environment than cell-free assays, but barriers to drug uptake do not exist and DNA-template effects can therefore be measured directly. Detailed protocols for this and the aforementioned assays are provided in the attached manuscripts in Appendices III and V.

Thus, the c-fos SRE model offers well-defined, systematic assays to evaluate DNA-binding drugs in increasingly complex environments. The binding of SRF and Elk-1 to A/T rich and mixed sequences, respectively, and their mode of binding to DNA (primary interactions in the major groove coupled with minor groove contacts) are amenable to our drug targeting strategies and allow us to study drug effects on more than one TF in a single system. In my last summary, I reported on the evaluation of a series of classical DNA-binding drugs with contrasting sequence selectivities and modes of binding. This work, which furthered understanding on how the DNA-binding characteristics of drugs influence their ability to inhibit transcription, has since been published in *Biochemistry* (see Appendix III). The c-fos model is now being employed to analyze novel, rationally-designed DNA-binding agents as described below.

Summary of Findings and Results:

Part 1: Evaluation of the fluorescent microgonotropens (FMGTs).

Most TFs, including SRF and Elk-1, primarily interact with the major groove of DNA but may gain increased specificity through minor groove contacts (12, 13). With their ability to approach the helix from the opposite groove and alter DNA conformation, minor groove-binding drugs can inhibit major groove-binding TFs from binding their target sites (14). However, drugs that contact both grooves with high affinity have the potential to more effectively inhibit a wider range of TFs. The MGTs, developed by the Bruice lab, were designed with this goal in mind. They consist of minor groove-binding backbones equipped with major groove-associating functional

groups. The first MGTs were based on a polypyrrole structure, similar to distamycin (see Fig. 1 in Appendix II). Polyamine tails extending from the central pyrrole electrostatically interact with the phosphodiester backbone of DNA, allowing these compounds to bind with affinities equal to or greater than those of TFs and resulting in significant bending of the helix (8). These agents were orders of magnitude more potent than distamycin in inhibiting the E2F1 TF from binding to its target promoter site. This success spurred investigation of whether other minor groove-binding agents could be functionalized with major groove-binding moieties and whether such additions improved their ability to inhibit TF/DNA interactions. The bisbenzimidazole backbone of the Hoechst family of A/T selective minor groove-binding drugs was therefore equipped with polyamine tails to yield FMGTs (structures are shown in Fig. 2, manuscript 3, Appendix V) (9, 15). These agents are capable of forming 2:1 complexes on DNA with up to five fold higher affinity than Hoechst 33258. FMGTs with polyamine tails of varying lengths and degrees of branching were synthesized and evaluated for their ability to inhibit TF/DNA interactions using the c-fos model. Preliminary evaluations of these compounds were included in my last summary report, but these studies have since been completed and have recently been submitted for publication. Notable findings from this study include:

- **The potencies of FMGT-1, FMGT-2 and FMGT-3 in inhibiting TF complex formation in EMSAs were approximately an order of magnitude greater than their parent compounds Hoechst 33342 and 33258.**

  The order of binding affinity on 5 contiguous A/T bp as determined in chemical studies was: FMGT-2 > FMGT-5 = FMGT-1 ~ FMGT-3 >> Hoechst 33258.
  Their order of potency in inhibiting ternary complex formation on the SRE was:
  FMGT-2 > FMGT-1 ~ FMGT-3 > FMGT-5 > Hoechst 33342 = Hoechst 33258.
  The order of absolute polyamine tail length for these compounds is:
  FMGT-5 > FMGT-3 > FMGT-2 > FMGT-1.
  The degree of polyamine tail branching is:
  FMGT-5 > FMGT-3 > FMGT-1 > FMGT-2.

Binding affinity alone therefore fails to explain the EMSA results. The findings suggest that a minimum polyamine tail length is required for contacting the phosphodiester backbone, but further increases in length or branching may interfere with the abilities of FMGTs to inhibit TF complexes. The helical distortions caused by FMGTs, their ability to form higher order complexes, and their ability to contact both grooves may all contribute to the ability of these agents to be more effective inhibitors of TF complex formation than the Hoechst compounds.

- **FMGT-1 and FMGT-2 were able to inhibit c-fos promoter-driven cell-free transcription in a more complicated environment consisting of more proteins and additional DNA with greater sequence complexity. However, these agents were equipotent to the Hoechst compounds in this assay.**

Higher amounts of DNA with greater sequence variation may provide additional lower affinity binding sites for the agents and therefore act as a drug "sink". Alternatively, additional proteins may be interfering with drug binding. A decrease in drug potency as assay conditions become more complex has been seen in several systems and was therefore expected (16-18). However, the relative loss of potency of the FMGTs compared to Hoechst compounds was not. While we had hoped that functionalizing the bisbenzimidazoles with major groove binding tails would overcome this limitation, it appears that the ratio of improvement between drugs in EMSAs is not easily maintained in more complex environments.

- **All of the compounds inhibited topo II activity in isolated nuclei.**

However, there was a lack of correlation between the potencies of FMGTs in these assays and in the EMSAs and cell-free transcription assays. This suggests that characteristics that make the FMGTs good inhibitors of TF complex formation may differ from those needed to inhibit other DNA related activities, especially those which require processive movement of a protein along the DNA, as in the case of topo II.

- **The FMGTs were unable to decrease endogenous c-fos expression in NIH3T3 cells.**

Additional studies demonstrated that they were also unable to cause cell death, even after a three day continuous exposure. Their inability to do so may stem from poor cellular permeability or poor nuclear localization.

Part 2: Characterization of the A/T selective minor groove binder, Hoechst 33377.

In addition to evaluating the FMGTs as summarized above, we collaborated with the Bruice lab in analyzing an additional bisbenzimidazole compound, Hoechst 33377. Its structure is on the first page of the second manuscript, Appendix IV). Very few studies of Hoechst 33377 have been performed. The Bruice lab was interested in characterizing it more fully because of its potential to recognize longer DNA sequences. We therefore analyzed Hoechst 33377 in a series of cellular experiments, including a cytotoxicity assay, its ability to inhibit endogenous c-fos expression in NIH3T3 cells, and visualization of its cellular localization through fluorescence microscopy. These studies complemented the DNA-binding affinity, stoichiometry, and sequence recognition analyses carried out by the Bruice lab. Notable findings include:

- **Chemical analyses carried out by the Bruice lab revealed that Hoechst 33377:**
  -- can bind dsDNA in 2:1 stoichiometries in an antiparallel, side-by-side arrangement, similar to distamycin.
  -- requires at least 4 contiguous A/T bp for binding.
  -- exhibited higher sequence selectivity than Hoechst 33342 or Hoechst 33258 in that it preferentially stabilized duplexes lacking 5'-TpA-3' steps.

Our evaluations using cellular assays demonstrated the following:

- **Hoechst 33377 localized to nuclei of live NIH3T3 cells and exhibited a speckled staining pattern similar to Hoechst 33342.**

The increase in fluorescence exhibited by Hoechst 33377 upon binding to nucleic acids facilitated its visualization in cells using fluorescence microscopy.

- **Northern blot analysis demonstrated that following a 16 h exposure, Hoechst 33377 inhibited endogenous c-fos transcription in NIH3T3 cells by 50% at 4 μM.**

- **Following a three day continuous exposure, the LD_{50} of Hoechst 33377 in NIH3T3 cells was 3.4 μM.**

The ability of Hoechst 33377 to downregulate gene expression may be contributing to its ability to cause cell death.

Part 3: Ongoing and future studies.

While the rationally-designed FMGTs show promise as inhibitors of TF/DNA complex

formation, their lack of cellular activity ultimately needs to be addressed. In addition, our evaluation suggested that polyamine tail length and degree of branching may be important determinants in the ability of the FMGTs to inhibit TF/DNA interactions. Our work with Hoechst 33377 demonstrated that it was cell permeable and capable of decreasing endogenous gene expression. Combining a more lipophilic bisbenzimidazole backbone with polyamine tails may therefore result in a more effective FMGT. However, difficulties with chemical synthesis may prohibit extensive alterations to the bisbenzimidazole backbone itself. Changes in the configuration and chemical characteristics of the polyamine tail may be easier to accomplish through solid-phase chemistry and may also endow the FMGTs with both the ability to contact the major groove as well as increased cellular permeability.

We therefore plan to further explore the effects of systematic alterations to the polyamine tails of FMGTs and MGTs in collaboration with Dr. Bruice. Series of FMGTs with logical, incremental increases in polyamine tail length or number, changes in branching positions or number, and changes in polyamine chemistry can be evaluated for effects on TF/DNA complexes and gene expression using the c-fos model. Comparing and contrasting the potencies of such agents should provide a better understanding of how the chemistry of the polyamine tails influence the biological activity of the drug molecule. We are currently discussing how best to pursue logical changes in FMGT design with members of the Bruice lab.

Comments on deviations from the original "Statement of Work":
Progress in this project has led to some deviations from the goals originally outlined in my submitted grant.

- Our studies have increasingly focused on biological characterization of the novel DNA-binding drugs, such as the FMGTs. The binding and chemical characteristics of these compounds are determined in greater detail by our collaborators in the Bruice lab. Therefore, we have found little need to investigate where and how these agents bind using DNA footprinting as noted in *Task 1* of the original grant.

- We first presumed that transient transfections were needed to evaluate drug effects on gene expression in whole cells, as outlined in *Task 3*. However, the serum inducibility of the endogenous c-fos gene and the robustness of its expression in NIH3T3 cells make transfections unnecessary. Less manipulation of the cells has been beneficial since complications in evaluating drug effects following transfections do not exist.

- In an ongoing effort to better characterize the biological activity of novel DNA-binding drugs, we have established two additional methods not outlined in the original *Statement of Work*. The topo II activity assay evaluates drug effects on the DNA template in isolated nuclei. Additionally, the use of fluorescence microscopy facilitated the characterization of Hoechst 33377.

- In my original grant, I outlined plans to evaluate a second series of novel DNA-binding agents using the c-fos model: the sequence specific polyamides developed by Dr. Peter Dervan of the California Institute of Technology. These agents continue to be studied by other members of the Beerman lab, especially in regards to their effects on the *ets* binding site on the Her2/Neu promoter. However, their minimal cellular activity has prompted more extensive studies of what parameters affect their intracellular localization. Until these problems are resolved, the polyamides appear to be unlikely candidates for evaluation using the c-fos model.

Training:

My work on this project has allowed me to learn additional methods for the molecular and cellular characterization of DNA-binding drugs. More importantly, my work has continued to hone my data evaluation and presentation skills. Writing the enclosed manuscripts was particularly helpful in this regard, and I have also learned how to communicate effectively with scientific journals during the publication process.

I have found my collaboration with the Bruice lab to be especially informative and helpful. It has given me the opportunity to directly apply my findings in the strategic design of agents and has allowed me to gain a better perspective on drug chemistry. My open dialogue with the Bruice lab has prompted me to think more critically about my own work and has allowed me to pursue more extensive studies on the biological and pharmacological characteristics of novel DNA-binding drugs.

Key Research Accomplishments

1. Completed evaluation of a series of novel, rationally designed FMGTs using the c-fos model.

Results obtained from the analysis of five FMGTs (designated 1, 2, 3 and 5) with polyamine tails of varying lengths and degrees of branching were compared to their parent compounds, Hoechst 33342 and Hoechst 33258.

- Analyzed ability of drugs to inhibit the following TF/DNA complex formation in EMSAs:
  -- SRF complexes
  -- Elk-1 complexes
  -- SRF + Elk-1 (ternary complex): both forward and reverse EMSAs.

- Analyzed ability of drugs to inhibit c-fos promoter-driven cell-free transcription.

- Assessed the ability of drugs to inhibit endogenous c-fos expression in NIH3T3 cells.

- Determined the ability of these agents to inhibit topo II-mediated cleavable complex formation in isolated nuclei.

2. Evaluated the biological activity of Hoechst 33377.

Little work has previously been done to characterize Hoechst 33377. Our evaluation of its biological activity complements the chemical analyses carried out by the Bruice lab

- Visualized the localization of Hoechst 33377 in live cells and compared its staining pattern to the extensively studied Hoechst 33342.

- Investigated the effects of Hoechst 33377 on endogenous c-fos expression in cells.

- Evaluated the cytotoxic effect of Hoechst 33377.

Reportable Outcomes

Manuscripts:

One original and two copies of each of the manuscripts below have been enclosed.

White, C.M., Heidenreich, O., Nordheim, A., and Beerman, T.A. Evaluation of the effectiveness of DNA-binding drugs to inhibit transcription using the c-fos serum response element as a target. *Biochemistry* 39: 12262-12273 (2000).

Satz, A.L., **White, C.M.**, Beerman, T.A., and Bruice, T.C. The dsDNA binding characteristics and subcellular distribution of a minor groove binding diphenylether bisbenzimidazole. (In press, *Biochemistry*) (2001). A copy of the version published on the internet (from http://pubs.acs.org/journals/bichaw/) is enclosed.

White, C.M., Satz, A.L., Bruice, T.C., and Beerman, T.A. Inhibiting transcription factor/DNA complexes using fluorescent microgonotropens (FMGTs). (Manuscript submitted).

Presentations:

White, C.M., Satz, A.L., Bruice, T.C., and Beerman, T.A. Developing novel minor groove-binding agents to disrupt gene expression: Microgonotropens as inhibitors of transcription factor/DNA complex formation. American Association for Cancer Research National Meeting. New Orleans, Louisiana, 2001.

Conclusions

Our analysis of the novel FMGTs using the c-fos SRE model was the first to determine the biological effects of these agents. Our studies demonstrate the potential of adding major groove-binding functional groups to minor groove-binding bisbenzimidazoles to enhance their effectiveness as inhibitors of TF/DNA complex formation. Previous work showed that equipping a tripyrrole moeity with a major groove-binding tail significantly increased its DNA-binding affinity and potency in inhibiting TF/DNA interactions (8, 19). Our evaluation of the FMGTs demonstrates that this concept can be applied to other minor groove-binding compounds, thereby confirming proof-of-principle and expanding the potential number of compounds that can functionalized with major groove-binding groups. However, while the FMGTs were more potent than classical Hoechst compounds in cell-free EMSAs, they were unable to affect endogenous c-fos gene expression. Problems with the cellular permeability of small molecules designed to target DNA is not uncommon, as evidenced by the poor uptake of triplex forming oligonucleotides and peptide nucleic acids in other studies (20, 21). Using the information gained in our first study of the FMGTs, we will pursue design strategies in an attempt to improve the activity of these compounds as discussed on page 4.

The studies of Hoechst 33377 demonstrated that the unique side-by-side binding mode of this agent appears to impart a rare ability to distinguish between certain A/T rich sites. The lipophilic phenyl group on this compound may contribute to its ability to penetrate cell membranes and localize to the nucleus. Its chemical characteristics, combined with its biological effects in whole cells, may make Hoechst 33377 a potentially useful starting compound in the development of other sequence selective agents.

Furthermore, our studies demonstrate the convenience and utility of the c-fos model in analyzing a variety of DNA-binding agents in increasingly complex assay environments. Systematic evaluation of these agents should provide a better understanding of how structure correlates with ability to inhibit gene expression. Identifying agents with improved potency and effectiveness in inhibiting TF/DNA interactions is a key step in using such agents to modify regulation of transcription and develop potentially more effective therapeutic strategies to treat breast cancer.

References

1. Papavassiliou, A. G. Transcription factors: Structure, function, and implication in malignant growth, Anticancer Res. *15:* 891-894, 1995.
2. Benz, C. C., O'Hagan, R. C., Richter, B., Scott, G. K., Chang, C. H., Xiong, X. H., Chew, K., Ljung, B. M., Edgerton, S., Thor, A., and Hassell, J. A. HER2/Neu and the Ets transcription activator PEA3 are coordinately upregulated in human breast cancer, Oncogene. *15:* 1513-1525, 1997.
3. Chang, C., Scott, G. K., Kuo, W., Xiong, X., Suzdaltseva, Y., Park, J. W., Sayre, P., Erny, K., Collins, C., Gray, J. W., and Benz, C. C. ESX: A structurally unique Ets overexpressed early during human breast tumorigenesis, Oncogene. *14:* 1617-1622, 1997.
4. Hurst, H. C. Transcription factors as drug targets in cancer, Eur J Cancer [A]. *32A:* 1857-1863, 1996.
5. Broggini, M. and D'Incalci, M. Modulation of transcription factor--DNA interactions by anticancer drugs, Anticancer Drug Des. *9:* 373-87., 1994.
6. Chiang, S. Y., Welch, J., Rauscher, F. J., 3rd, and Beerman, T. A. Effects of minor groove binding drugs on the interaction of TATA box binding protein and TFIIA with DNA, Biochemistry. *33:* 7033-40, 1994.
7. Treisman, R. The serum response element, Trends Biochem Sci. *17:* 423-6, 1992.
8. Bruice, T. C., Houng, Y. M., Gong, X. H., and Lopez, V. Rational design of substituted tripyrrole peptides that complex with DNA by both selective minor-groove binding and electrostatic interaction with the phosphate backbone, Proc Natl Acad Sci USA. *89:* 1700-1704, 1992.
9. Satz, A. L. and Bruice, T. C. Synthesis of a fluorescent microgonotropen (FMGT-1) and its interactions with the dodecamer d(CCGGAATTCCGG), Bioorg Med Chem Lett. *9:* 3261-6, 1999.
10. Chen, G. L., Yang, L., Rowe, T. C., Halligan, B. D., Tewey, K. M., and Liu, L. F. Nonintercalative antitumor drugs interfere with the breakage-reunion reaction of mammalian DNA topoisomerase II, J Biol Chem. *259:* 13560-6., 1984.
11. Woynarowski, J. M., Sigmund, R. D., and Beerman, T. A. DNA minor groove binding agents interfere with topoisomerase II mediated lesions induced by epipodophyllotoxin derivative VM-26 and acridine derivative m-AMSA in nuclei from L1210 cells, Biochemistry. *28:* 3850-5., 1989.
12. Pellegrini, L., Tan, S., and Richmond, T. J. Structure of serum response factor core bound to DNA, Nature. *376:* 490-8, 1995.
13. Mo, Y., Vaessen, B., Johnston, K., and Marmorstein, R. Structure of the elk-1-DNA complex reveals how DNA-distal residues affect ETS domain recognition of DNA, Nat Struct Biol. *7:* 292-7., 2000.
14. Dorn, A., Affolter, M., Muller, M., Gehring, W. J., and Leupin, W. Distamycin-induced inhibition of homeodomain-DNA complexes, The EMBO Journal. *11:* 279-286, 1992.
15. Satz, A. L. and Bruice, T. C. Synthesis of fluorescent microgonotropens (FMGTs) and their interactions with dsDNA, Bioorg Med Chem. *8:* 1871-80., 2000.
16. Chiang, S. Y., Azizkhan, J. C., and Beerman, T. A. A comparison of DNA-binding drugs as inhibitors of E2F1- and Sp1-DNA complexes and associated gene expression, Biochemistry. *37:* 3109-3115, 1998.

17. Chiang, S. Y., Burli, R. W., Benz, C. C., Gawron, L., Scott, G. K., Dervan, P. B., and Beerman, T. A. Targeting the Ets binding site of the HER2/neu promoter with pyrrole-imidazole polyamides, J Biol Chem, 2000.
18. White, C. M., Heidenreich, O., Nordheim, A., and Beerman, T. A. Evaluation of the effectiveness of DNA-binding drugs To inhibit transcription using the c-fos serum response element as a target, Biochemistry. *39:* 12262-73., 2000.
19. Chiang, S. Y., Bruice, T. C., Azizkhan, J. C., Gawron, L., and Beerman, T. A. Targeting E2F1-DNA complexes with microgonotropen DNA binding agents, Proc Natl Acad Sci USA. *94:* 2811-6, 1997.
20. Wickstrom, E. Strategies for administering targeted therapeutic oligodeoxynucleotides, Trends Biotechnol. *10:* 281-7., 1992.
21. Nielsen, P. E. Peptide nucleic acids as therapeutic agents, Curr Opin Struct Biol. *9:* 353-7., 1999.

Appendix I: Abbreviations

A	Adenine
bp	Base pair(s)
C	Cytosine
EMSA	Electrophoretic mobility shift assay
FMGT	Fluorescent microgonotropen
G	Guanine
h	Hour(s)
IC_{50}	Concentration of drug needed to inhibit the observed activity by fifty percent
LD_{50}	Concentration of drug needed to kill fifty percent of cells in a cytotoxicity assay
MGT	Microgonotropen
Oligo	Oligonucleotide
PNA	Peptide nucleic acid
SRE	Serum response element
SRF	Serum response factor
T	Thymine
TF	Transcription factor
Topo	Topoisomerase
μM	Micromolar

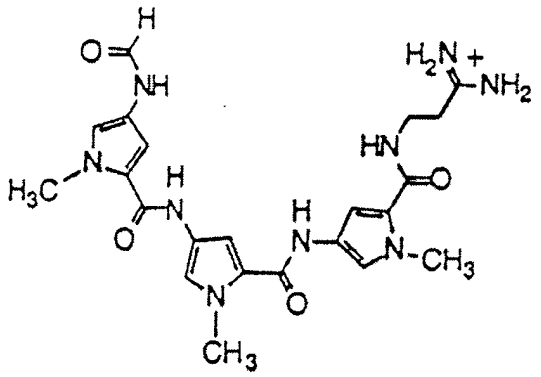

Distamycin

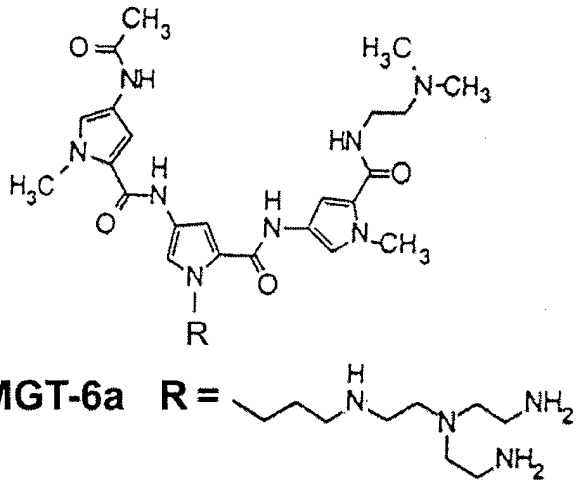

MGT-6a R =

FIGURE 1: Structures of distamycin and a first generation microgonotropen, MGT-6a.

Both agents bind selectively to A/T rich sequences in the minor groove, but the polyamine tail of MGT-6a allows it to electrostatically contact the phosphodiester backbone of DNA in the major groove.

Evaluation of the Effectiveness of DNA-Binding Drugs To Inhibit Transcription Using the c-fos Serum Response Element as a Target†

Christine M. White,‡ Olaf Heidenreich,§ Alfred Nordheim,§ and Terry A. Beerman*,‡

Department of Pharmacology and Therapeutics, Roswell Park Cancer Institute, Elm and Carlton Streets, Buffalo, New York 14263, and Institut für Zellbiologie, Abteilung Molekularbiologie, Universität Tübingen, D-72076 Tübingen, Germany

Received June 21, 2000; Revised Manuscript Received August 7, 2000

ABSTRACT: Previous work has demonstrated that sequence-selective DNA-binding drugs can inhibit transcription factors from binding to their target sites on gene promoters. In this study, the potency and effectiveness of DNA-binding drugs to inhibit transcription were assessed using the c-fos promoter's serum response element (SRE) as a target. The drugs chosen for analysis included the minor groove binding agents chromomycin A_3 and Hoechst 33342, which bind to G/C-rich and A/T-rich regions, respectively, and the intercalating agent nogalamycin, which binds G/C-rich sequences in the major groove. The transcription factors targeted, Elk-1 and serum response factor (SRF), form a ternary complex (TC) on the SRE that is necessary and sufficient for induction of c-fos by serum. The drugs' abilities to prevent TC formation on the SRE in vitro were nogalamycin > Hoechst 33342 > chromomycin. Their potencies in inhibiting cell-free transcription and endogenous c-fos expression in NIH3T3 cells, however, were chromomycin > nogalamycin > Hoechst 33342. The latter order of potency was also obtained for the drugs' cytotoxicity and inhibition of general transcription as measured by [^{3}H]uridine incorporation. These systematic analyses provide insight into how drug and transcription factor binding characteristics are related to drugs' effectiveness in inhibiting gene expression.

Drugs that bind to DNA can act as template poisons by inhibiting interactions between cellular proteins and their DNA targets. The activity of RNA polymerases, DNA polymerases, and topoisomerases I and II can all be affected by drug treatment of their DNA templates (*1*−*3*). Our studies focus on evaluating DNA reactive agents as inhibitors or disruptors of transcription factor (TF)[1] binding to target sequences in gene promoters and their resultant effects on gene expression. Successful initiation of transcription requires specific binding of TFs to their cognate promoter sequences (reviewed in *4*). Interfering with these specific TF/DNA interactions may therefore lead to decreased expression of a target gene of interest. The ability to selectively prevent TFs from binding to desired DNA targets has implications in the study of the molecular regulation of gene expression and, ultimately, in the development of therapeutics (reviewed in *5*).

DNA-binding agents can be classified according to both their mode of binding as well as their sequence preference. Members of the reversible minor groove binding family (MGBs), such as distamycin, netropsin, and the Hoechst compounds, exhibit preferential binding to A/T tracts at least 4 base pairs long (reviewed in *6*). Their curved structure allows them to interact favorably with base pairs on the floor and wall of the minor groove via hydrogen bonds and van der Waal forces. The sequence selectivity of these agents may be influenced by subtle, sequence-dependent variations in DNA structure. The inherent differences in groove width and flexibility that result from neighboring base pair effects are factors that influence these agents' ability to optimally recognize and bind to a particular sequence (reviewed in *7*). This generally holds true for other drugs as well. Anticancer antibiotics, such as chromomycin A_3 and mithramycin, are MGBs that prefer G/C-rich elements. Unlike the A/T-selective MGBs, which primarily widen the minor groove, chromomycin can unwind the double helix by about 11° and cause more extensive DNA structural alterations (*8*).

Intercalators, such as nogalamycin, doxorubicin, and hedamycin, possess aromatic moieties that are inserted between base pairs, resulting in unwinding and extension of the DNA helix. Their binding is therefore more disruptive to DNA structure than MGBs. While intercalators generally prefer binding to wider-grooved G/C-rich sequences, their binding selectivity may be influenced by surrounding base pairs, as has been demonstrated for nogalamycin (*9*). Footprinting studies have shown that this agent selectively binds to regions of alternating purines and pyrimidines, and notably prefers 5′TpG steps (*10*). Nogalamycin is also

† This study was supported in part by National Cancer Institute Grant CA16056 (to T.A.B.), American Cancer Society Grant RPG-96-034-04-CDD (to T.A.B.), US Army Medical Research Grant BC980100 (to C.M.W.), and DFG Grant 120/7-3 (to A.N.).

* To whom correspondence should be addressed. Phone: (716) 845-3443; Fax: (716) 845-8857; E-mail: Terry.Beerman@RoswellPark.org.

‡ Roswell Park Cancer Institute.

§ Universität Tübingen.

[1] Abbreviations: SRE, serum response element; SRF, serum response factor; TC, ternary complex; TF, transcription factor; MGB, minor groove binding drug; EMSA, electrophoretic mobility shift assay; bp, base pair(s).

10.1021/bi001427l CCC: $19.00
Published on Web 09/14/2000

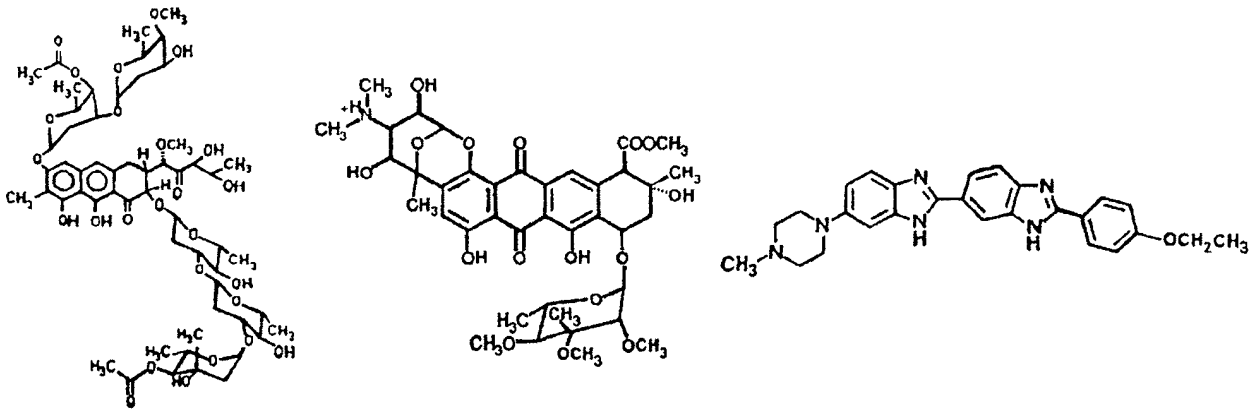

FIGURE 1: Structures of chromomycin A_3, nogalamycin, and Hoechst 33342.

somewhat unique because of its extremely slow dissociation kinetics, which likely stem from its characteristic threading mode of intercalation (*11*).

There has been considerable interest in targeting TFs using each of these drug classes. TFs can be classified into families according to their conserved DNA-binding domains. While TFs in each family can recognize and bind to specific consensus sequences, their precise recognition of promoter sites is often dependent on the composition and conformation of neighboring DNA base pairs. Electrophoretic mobility shift assays (EMSAs) using a variety of TF and DNA targets have established the potential of DNA-binding drugs as selective disruptors of target gene function. These previous studies have demonstrated that inhibition of TF/DNA complexes by DNA-binding drugs in vitro is more effective if the TFs and drugs analyzed share binding selectivities and characteristics. For example, the MGB distamycin is a potent inhibitor of TATA box binding protein (TBP) association with its A/T-rich target sequence in the minor groove (*12*). Distamycin's distortion of DNA groove conformation has also been implicated in its ability to disrupt TFs bound to A/T-rich sites in the major groove, such as homeodomain peptides (*13*).

Further investigations have suggested a relationship between the ability of drugs to disrupt TF binding to DNA in the simpler EMSAs and their ability to inhibit cell-free transcription under more complex conditions using a nuclear lysate. Distamycin was an effective inhibitor of both TBP complex formation in EMSAs as well as TBP-driven cell-free transcription (*14*). Mithramycin and chromomycin inhibited the binding of nuclear factors to G/C-rich Sp-1-binding sites on the long terminal repeat (LTR) of the HIV-1 promoter and were also able to inhibit HIV-1 LTR-directed transcription in a cell-free system (*15*). In such studies, higher drug concentrations were often needed to observe inhibition of transcription. In regards to novel drug development, these studies emphasize the need to maximize drug effectiveness in simpler systems before proceeding with testing in more complex assays or whole cells.

Evaluating DNA reactive compounds and developing paradigms for drug targeting in increasingly complex assay environments will help to improve drug specificity and potency. The c-fos promoter's serum response element (SRE) (reviewed in *16*) has characteristics that make it appropriate for this type of drug evaluation. The c-fos gene, which has been rigorously studied and characterized due to its importance in growth control, is an immediate-early response gene that is tightly regulated at the level of transcription (*17*). The SRE is necessary and sufficient for the rapid and transient induction of c-fos by serum (*18*). Two transcription factors bind to adjacent sites in this promoter sequence and mediate c-fos expression. A homodimer of SRF binds to the CArG box, an A/T-rich region (*19*). SRF binding is required for efficient recruitment of the ternary complex factor Elk-1 to its *ets* motif immediately upstream (*20*) (see Figure 2). Like other members of the *ets* family, Elk-1 binds to an invariant GGA core sequence in the major groove of DNA, but makes contacts with the phosphate backbone of unique flanking nucleotides in the minor groove (*21*). The TC, consisting of SRF and Elk-1, is constitutively bound to the SRE. Activation of this complex and upregulation of transcription are achieved as part of the cellular response to serum. Activation of signal transduction pathways by growth factors results in the phosphorylation of these factors by various kinases, most notably members of the mitogen-activated protein kinase (MAPK) family (*22, 23*).

The A/T-rich and mixed sequences present in the SRE are well suited for the study of a wide variety of DNA reactive agents. Also, the fact that Elk-1 contacts both grooves makes it an interesting target for drugs that bind in one groove or the other. Moreover, using this sequence as a target allows drug effects on more than one TF to be studied in a single system. Another advantage is that in addition to EMSAs and cell-free transcription assays, use of the c-fos SRE allows drug effects on endogenous c-fos mRNA production to be assessed. The rapid and transient expression of c-fos that follows serum induction provides a facile way of determining immediate or short-term drug effects on transcription in whole cells.

Here, we investigate the effectiveness of drugs as inhibitors of TF/DNA interactions in increasingly complex systems using the c-fos SRE as a target. Representative agents from the drug classes discussed above were chosen based upon their contrasting sequence preferences, and modes of DNA-binding (drug structures are shown in Figure 1). The MGBs chromomycin and Hoechst 33342, which do not radically distort DNA, have G/C- and A/T-rich preferences, respectively. They were compared to nogalamycin, which has less

sequence specificity but which causes greater helical distortion. The agents' abilities to affect TF/DNA interactions in vitro were evaluated in EMSAs, a simple system consisting of purified proteins and short oligonucleotides. The cell-free transcription assay, which uses a nuclear lysate to drive transcription from a plasmid, was used to analyze the drugs' effects in a more complicated environment. Finally, effects of these agents on endogenous c-fos expression in whole cells were assessed using Northern blots. Cytotoxicity and RNA synthesis assays also provided insight into how these agents were affecting cells in general.

MATERIALS AND METHODS

Drugs. Stocks of 5 mM chromomycin A_3 (Sigma, St. Louis, MO) and 5 mM nogalamycin (Pharmacia Upjohn Corp.) were prepared in dimethyl sulfoxide. A 20 mM stock of Hoechst 33342 (Aldrich Chemical Co.) was prepared in distilled water. All drugs were stored in the dark at −20 °C and diluted into water immediately before use.

Oligonucleotides. Two 24-mer oligonucleotides and their complementary strands were synthesized by the Biopolymer facility at Roswell Park Cancer Institute (Buffalo, NY) and purified on a Poly-Pak column. The first oligo (5′-ACACAGGATGTCCATATTAGGACA-3′), designated "SRE", contained the −301 to −324 sequence of the human c-fos promoter SRE. The second oligo (5′-GATACCGGAAGTCCATATTAGGAC-3′), designated "E74", was similar, but contained the high-affinity *ets*-binding site from the E74 *Drosophila* promoter (underlined), based on the consensus sequence published by Urness et al. (*24*). Oligos were reannealed according to Lee et al. (*25*). These double-stranded oligos were 5′-end-labeled with [γ-^{32}P]ATP (10 mCi/mL) and T4 Polynucleotide Kinase. Unincorporated nucleotides were removed using a Sephadex G-25 microspin column (Amersham Pharmacia Biotech).

Protein Purification. pILASRF, a plasmid encoding the SRF protein with an N-terminal His-tag, was developed in the Nordheim laboratory (Institut fuer Zellbiologie, Universitaet Tuebingen, Tuebingen, Germany). Expression of this protein and its purification were achieved following the protocol by Heidenreich et al. (*26*), but with two changes. First, the bacterial pellet was resuspended in PBS and lysed using three freeze/thaw cycles. The lysate was sonicated and pelleted at 10000*g* for 25 min at 4 °C before being combined with Ni−NTA beads (Qiagen, Inc.). Second, after transfer to a column, the beads were initially rinsed 4 times with 2 column volumes of PBS. pAS278, a plasmid encoding full-length Elk-1 with a C-terminal His-tag (*27*), was generously provided by Dr. Andrew Sharrocks (University of Newcastle, Newcastle upon Tyne, England). Following expression in BL21-pLysS bacteria, the protein was purified under native conditions using Ni−NTA beads, following manufacturer's instructions (Qiagen).

Electrophoretic Mobility Shift Assays. In general, experiments were performed as follows: drug, radioactively end-labeled oligo, and binding buffer were combined and allowed to incubate at room temperature for 30 min. Purified transcription factors were diluted into binding buffer. Following addition of purified protein(s), the reactions were allowed to incubate an additional 30 min at room temperature before being electrophoresed on a 5% polyacrylamide gel. These incubation times were based on time course experiments that established 30 min as sufficient time to achieve equilibrium of complex formation. Specifically, for the Elk-1 EMSAs, a binding buffer containing 25 mM Hepes−KOH, pH 7.9, 10 mM $MgCl_2$, 10 mM EDTA, 10 mM spermidine, 10 mM dithiothreitol, 7.5 μg/μL bovine serum albumin, and 20% glycerol was used. Ten nanograms of purified Elk-1 was added to 1 nM ^{32}P-end-labeled E74 oligo in these reactions. For the SRF EMSAs, the binding buffer contained 10 mM Tris-HCl, pH 7.5, 50 mM NaCl, 1 mM EDTA, 0.05% milk, 10 mM DTT, and 5% glycerol. Twenty-five nanograms of purified SRF was added to 1 nM ^{32}P-end-labeled SRE in these reactions. For ternary complex formation, the SRF binding buffer was used. Twenty-five nanograms of SRF and 6.25 ng of Elk-1 were added to 1 nM ^{32}P-end-labeled SRE. In samples containing chromomycin, Mg^{2+} was added to a final concentration of 10 mM in the binding reactions. For all EMSAs, a 5% native polyacrylamide gel was pre-run at room temperature at 200 V in 0.5× TBE buffer (44.6 mM Tris base, 44.5 mM boric acid, and 10 mM EDTA). Reactions were loaded onto the gel and electrophoresed for a maximum of 2 h. Adequate separation of free and complexed DNA on the Elk-1 and SRF MSAs was achieved by as little as 30 min of electrophoresis. Dried gels were exposed to Kodak Biomax Scientific Imaging film. Quantitation of free and complexed DNA was carried out by scanning the resulting autoradiogram on a computing laser densitometer (Molecular Dynamics) and analyzing the results with the manufacturer's ImageQuant program. Fifty percent inhibition of complex formation by the drugs (IC_{50}) was calculated by comparing drug-treated samples to controls. Where specified, purified proteins were added to the oligo before drug. These "reverse" experiments were electrophoresed as detailed above.

Cell Culture. Murine NIH3T3 fibroblast cells were obtained from the American Type Culture Collection and cultured in Dulbecco's modified Eagle's medium (DMEM) containing high glucose (4500 mg/mL) and sodium pyruvate (110 mg/mL) and supplemented with 10% calf serum. Cells were maintained at 37 °C and 5% CO_2.

NIH3T3 Nuclear Lysate Preparation for Cell-Free Transcription. NIH3T3 cells were grown in 175 cm^2 flasks until approximately 60% confluent before being starved overnight in starvation media (DMEM containing 0.5% calf serum). In general, a minimum of 10 flasks was needed to see adequate lysate activity. Cells were induced by adding induction media (DMEM with 15% calf serum) for 30 min, rinsed with room temperature PBS, and scraped into ice-cold PBS. Nuclear lysates were then prepared essentially as described by Blake et al. (*28*). All centrifugations were performed at 4 °C. In brief, cells were pelleted by centrifugation, washed, and repelleted in 5 pellet volumes of Buffer A [10 mM 4-(2-hydroxyethyl)-1-piperazineethanesulfonic acid (Hepes)/KOH, pH 7.9, 0.1 mM EDTA, 0.1 mM EGTA, 10 mM KCl, 0.75 mM spermidine, 0.15 mM spermine, 1 mM dithiothreitol (DTT)], and then allowed to swell on ice in the same volume of Buffer A for approximately 20 min. Cells were dounced on ice until 95% cell lysis was achieved, and then centrifuged until 31000*g* was reached. As soon as this speed was obtained, the centrifuge was turned off and the rotor was allowed to come to a halt. The pelleted nuclei were

resuspended in Buffer C [20 mM Hepes/KOH, pH 7.9, 20% glycerol, 0.2 mM EDTA, 2 mM EGTA, 0.75 mM spermidine, 0.15 mM spermine, 2 mM DTT, and 1 mM phenylmethanesulfonyl fluoride (PMSF)] to a final minimum concentration of 5×10^8 nuclei/mL. An equal volume of Buffer C + NaCl (same composition as buffer C, but with 0.75 M NaCl) was then added dropwise, with swirling. The lysate was rocked at 4 °C for 30 min, and then centrifuged at 214000*g* for 45 min. Supernatants were pooled, loaded into a Slide-A-Lyzer dialysis cassette (Pierce) with a 10 000 molecular weight cut-off, and dialyzed against 500 volumes of buffer D (20 mM Hepes/KOH, pH 7.9, 100 mM KCl, 20% glycerol, 0.2 mM EDTA, 0.2 mM EGTA, 12.5 mM $MgCl_2$, 2 mM DTT, and 1 mM PMSF) at 4 °C for 3 h, with a buffer change after the first 1.5 h. Dialyzed extract was cleared by a 15 min spin at 31000*g*. Aliquots of the resulting supernatant were immediately frozen on dry ice and stored at −80 °C.

Cell-Free Transcription Assay. The template, pFosLuc19, containing a human c-fos promoter fragment (−711 to −3) upstream of a luciferase reporter gene, was developed in the Nordheim laboratory. Digestion of this plasmid with *Sph*I prior to use in the assay yields a transcript approximately 750 bases in length. For drug studies, 0.5 μg of this plasmid was combined with drug and 5 μL of Buffer D for a total volume of 9 μL, and allowed to incubate 30 min at 30 °C. Approximately 15 μg of NIH3T3 nuclear lysate was added, the total volume was brought to 19 μL with Buffer D, and the reaction was allowed to incubate for 15 min at 30 °C. The subsequent reaction and transcript purification steps were carried out as described by Chiang et al. (*29*). A T3 transcript of pGEM4z (Promega), 250 bases long, was used as an internal control. Quantitation following autoradiography was as described for the EMSAs, and the visualized transcripts were normalized to the internal controls.

Whole Cell Drug Treatment and Northern Blot Analysis. For typical drug treatments prior to Northern blot analysis, 2.5×10^5 NIH3T3 cells were plated in 60 mm dishes and allowed to grow for 48 h until approximately 60% confluent. Growth medium was removed, the cells were rinsed with PBS, and starvation medium (DMEM containing 0.5% calf serum) was added. Appropriate dilutions of drugs were made into sterile water, and 20 μL of these dilutions was added directly to the plates. Solvent controls in which no drug was added were also prepared. Cells were generally starved for 16 h at the growth conditions detailed above. Induction of c-fos was accomplished by adding calf serum directly to the plates to a final concentration of 15%, followed by incubation at 37 °C for 30 min.

RNA Isolation/Northern Blot Analysis. Following serum induction of NIH3T3 cells, total RNA was isolated using TRIzol (GIBCO BRL). In brief, 20 μg of total RNA was loaded onto 1.5% denaturing agarose gel (2.2 M formaldehyde, 40 mM MOPS, pH 7.0, 10 mM sodium acetate, and 10 mM EDTA) and electrophoresed in 1× MOPS buffer (40 mM MOPS, 10 mM sodium acetate, and 10 mM EDTA) at 80 V for 4.5 h. The gel was rinsed in ddH_2O, and the RNA was transferred to GeneScreen (NEN Life Science Products) overnight. Following UV cross-linking of the RNA, the membrane was pre hybridized for 1 h at 60 °C in pre-hybe buffer [0.5 M sodium phosphate, pH 7.2, 7% SDS, 1 mM EDTA, 1% bovine serum albumin (BSA)]. A plasmid containing 4.8 kb of the murine c-fos coding sequence, pGEM4z-Fos (Loftstrand Labs, Ltd.), was linearized with *Hin*dIII before being radioactively labeled using a DecaPrime II kit (Ambion Inc.) and [α-^{32}P]dCTP (10 mCi/mL) for use as a probe. A phagemid containing the coding sequence for human glyceraldehyde-3-phosphate dehydrogenase (G3) (American Type Culture Collection) was also linearized with *Hin*d III and similarly labeled. Hybridization with the radiolabeled probes was overnight at 60 °C. Membranes were washed twice with wash buffer A (40 mM sodium phosphate, pH 7.2, 5% SDS, 1 mM EDTA, and 0.5% BSA) and twice with wash buffer B (20 mM sodium phosphate, pH 7.2, 1% SDS, and 1 mM EDTA) at 60 °C (each wash was for 20 min). The blot was exposed in a phosphorimager cassette (Molecular Dynamics) and scanned with a Molecular Dynamics phosphorimager.

Cytotoxicity Assay: Colony Formation Using NIH3T3 Cells. A total of 1×10^5 NIH3T3 cells were plated in 35 mm dishes and allowed to grow for 48 h until approximately 50% confluent. Growth medium was removed, and 1 mL of fresh medium containing the desired drug concentration was added. Following a 4 h drug exposure, the cells were trypsinized, serially diluted, and replated into 60 mm dishes. The total number of cells plated per dish ranged from 1×10^4 to 1×10^2. Cells were incubated at normal growth conditions for 10 days. The medium was then removed, and the cells were stained using 2 mL of methylene blue staining solution (7 mg/mL methylene blue in 70% EtOH) per dish for 30 min. Following removal of the staining solution, the dishes were rinsed in lukewarm water and air-dried. Colonies, designated as groups of 50 or more cells, were counted under a stereo microscope. Plating efficiencies were calculated by dividing the number of colonies by the total number of cells plated. Relative plating efficiencies for the drug treatments were then calculated by dividing the plating efficiencies of the drug-treated samples by the plating efficiencies of the controls.

RNA Synthesis ([^{3}H]Uridine Incorporation Assay). A total of 6.6×10^5 NIH3T3 cells were plated in 60 mm dishes and allowed to grow for 48 h until approximately 85% confluent. Drugs were diluted appropriately and added directly to the growth medium for a 4 h exposure under normal growth conditions. Then 2 μCi of [5-^{3}H]uridine (15 mCi/mmol) and unlabeled uridine to a final concentration of 50 μM were added to each dish. Following a 30 min pulse, the cells were rinsed with cold PBS, and then each dish was scraped into 1 mL of ice-cold 0.5 M perchloric acid (PCA) to begin precipitation of nucleic acids; 0.5 mL of the resuspension was transferred to prechilled eppendorf tubes, 1 mL of cold 0.5 M PCA was added, and the tubes were incubated on ice for 30 min. The samples were pelleted at 2800 rpm at 4 °C and washed 2 times in 0.4 M PCA before 0.5 mL 0.5 M PCA was added. The tubes were then heated to 70 °C for 1 h, and the counts in 0.5 mL were measured on a scintillation counter.

RESULTS

c-fos Components. The c-fos SRE sequence targeted in this study is shown in Figure 2A. This sequence is located approximately 300 bp upstream of the c-fos transcription

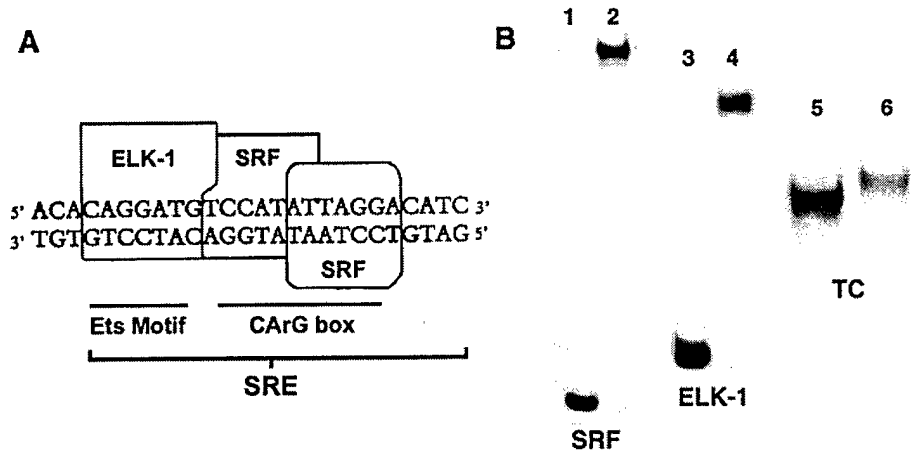

FIGURE 2: Components of the c-fos promoter. (A) TFs bound to the human c-fos promoter's SRE. Binding of the homodimer of SRF is required for the recruitment of Elk-1. Together, these TFs make up the ternary complex (TC). (B) Binding of SRF and Elk-1 to radiolabeled probes in EMSAs. ^{32}P-labeled oligonucleotides were incubated with purified proteins for 30 min at room temperature before being electrophoresed on a 4% polyacrylamide gel and autoradiographed. The 24 bp oligonucleotides contained sequences from the c-fos SRE or the *Drosophila* E74 promoter. Lane 1, free SRE probe; lanes 2 and 5, SRE plus SRF protein; lane 3, free E74 probe; lane 4, E74 plus Elk-1 protein; lane 6, SRE plus SRF and Elk-1 forms the TC. In lanes 5 and 6, the gel was electrophoresed longer to maximize shift differences. The free SRE probe ran off the gel under these conditions.

initiation site. Binding sites for the ternary complex factor Elk-1 and the homodimer of SRF are indicated. The TC is formed when binding of SRF to the CArG box recruits Elk-1 to the *ets* motif immediately upstream. SRF and Elk-1 were expressed as 6-Histidine-tagged proteins in bacteria and purified for use in the EMSAs as described in detail under Materials and Methods. While the SRE can be used to study drug effects on SRF binding and ternary complex formation on the SRE, it cannot be used to assess drug effects on Elk-1 binding alone, since this protein cannot bind to the SRE without SRF present (*30*). However, it can bind to the high-affinity *ets* motif in the *Drosophila* E74 promoter (*31*). Therefore, we made use of this promoter to study drugs' influence on Elk-1 association with DNA. Recombinant proteins were combined with 24 bp radiolabeled oligonucleotides containing the targeted promoter regions, and the complexes were electrophoresed on a polyacrylamide gel. Free SRE and E74 probe was successfully shifted by the addition of SRF or Elk-1 alone (Figure 2B, compare lanes 1 and 3 with lanes 2 and 4). In lanes 5 and 6, the gel was electrophoresed longer in order to maximize the difference in shift evident when SRF and Elk-1 were combined to form the TC (lane 6) as compared to SRF alone (lane 5). Under these conditions, the free probe ran off the gel. In subsequent experiments, where the complexes were electrophoresed under standard conditions as in Figure 2B (lanes 1−4), we noted that the TC was still distinguishable from the SRF complex on the basis of a slight difference in mobility (see Figure 3A, compare lanes 8 and 10 with lane 9).

Inhibition of TF Binding to the SRE in EMSAs. The ability of drugs to prevent TF binding to their specific promoter sites was assessed using the components of the SRE system. Three drugs were chosen on the basis of their different binding properties. The structures of chromomycin and Hoechst 33342, minor groove binding agents with G/C and A/T preferences, respectively, and nogalamycin, an intercalating drug that prefers G/C-rich regions, are shown in Figure 1. When incubated with the radiolabeled probes prior to protein addition, these drugs prevented TF binding in a dose-dependent manner. Representative results are shown in Figure 3A for chromomycin. As the amount of chromomycin added to the E74 promoter decreases in lanes 3−7, the amount of Elk-1 complexed with the probe increases back to control levels (lanes 1 and 2, no drug addition). Chromomycin also yields a dose-dependent inhibition of the TC as seen in lanes 11−15, as compared to controls in lanes 8 and 10. Similar inhibition was also achieved for SRF complex formation (data not shown).

Quantitation of the free and shifted DNA in drug-treated samples, and comparison to non-drug-treated controls, allowed percent inhibition of complex formation to be calculated. Representative dose−response curves for chromomycin (Figure 3B) show that this agent exhibits different potencies on the three TF complexes analyzed. The Elk-1 complex is by far the most sensitive to this drug, exhibiting a steep dose−response curve that plateaus by 10 μM. Formation of the SRF complex is less sensitive and yields a more gently sloping curve that starts to level off around 30 μM. When Elk-1 and SRF are combined to form the TC, the dose−response curve falls between those obtained for the individual factors, but retains the rather steep increase of the Elk-1 curve.

The drug concentration needed to inhibit complex formation by 50% (IC_{50}) was determined from dose−response curves plotted for each agent analyzed and used to compare the drugs' effectiveness in preventing TF binding (Figure 3C). Hoechst 33342 exhibited a trend similar to that observed for chromomycin: it was not particularly potent in preventing the SRF complex from forming, but was much more effective in inhibiting TC formation. Notably, Hoechst 33342 was approximately twice as potent as chromomycin in preventing TC formation. Unfortunately, the effects of Hoechst 33342 on Elk-1 complexes could not be determined, since binding of this drug to the E74 probe alone resulted in its retention in the well of the gel and excessive smearing, making quantitation impossible. Of the three drugs tested, nogalamycin was by far the most potent agent; IC_{50}s for all complexes fell well below 5 μM. Its inhibition profile differed from chromomycin in that SRF, rather than Elk-1, was the most sensitive target. Like chromomycin, however,

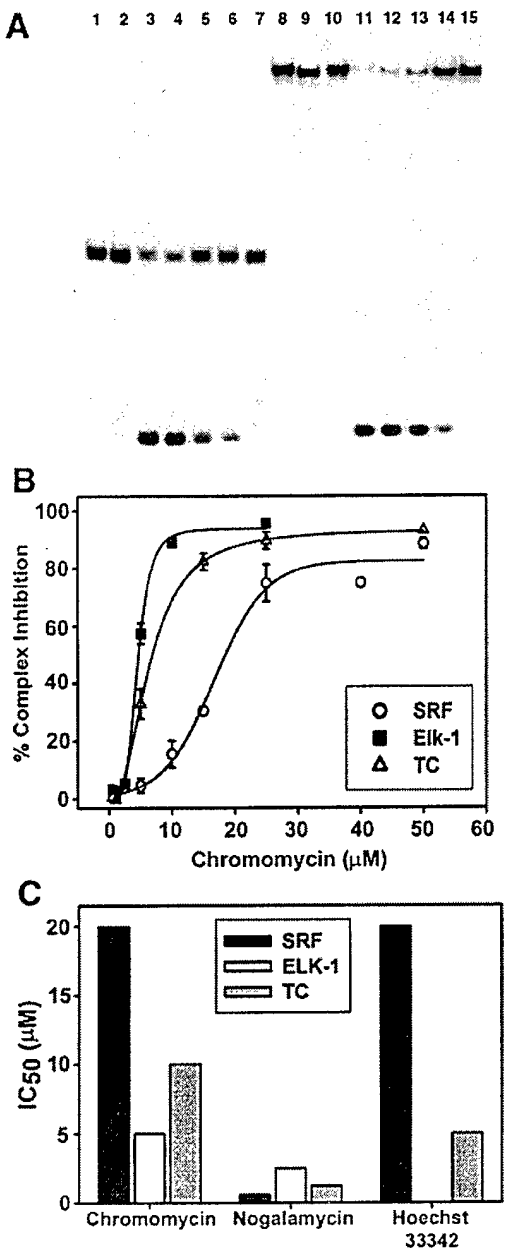

FIGURE 3: Effect of drugs on preventing complex formation in EMSAs. (A) Chromomycin's effect on Elk-1 and SRF complex formation. Increasing amounts of drug were incubated with the probes for 30 min before addition of purified proteins and electrophoresis as described in Figure 2. Lanes 1−7 contain Elk-1 complexes. Lanes 1−2, Elk-1 complex controls, no drug; lanes 3−7 contain 50, 25, 10, 5, and 1 μM chromomycin, respectively. Lanes 8 and 10−15 contain TC bound to the SRE. Lanes 8 and 10, TC controls, no drug; lane 9, SRF complex control, no drug; lanes 11−15 contain 100, 50, 25, 10, and 1 μM chromomycin, respectively. (B) Quantitation of chromomycin's inhibition of complex formation. Percent probe shifted in each drug treatment was compared to non-drug-treated controls to yield percent complex inhibition for SRF (○), Elk-1 (■), and TC (△). Results are the mean of four experiments (mean value ± standard error). (C) Comparison of drugs' potency in preventing complex formation in the EMSAs. Drug concentrations needed to prevent each complex formation by 50% (IC_{50}s) were calculated using graphs as shown in panel B.

the IC_{50} for TC inhibition fell between the IC_{50}s for the individual factors' complexes. In addition to its higher potency and unique inhibition profile in comparison to the MGBs, nogalamycin possessed another distinct characteristic. Reverse assays, in which each of the drugs was added after the TC was already formed on the SRE, demonstrated that only nogalamycin required significantly higher concentrations to disrupt complex formation (data not shown).

Drug Effects on c-fos Promoter-Driven Cell-Free Transcription. Upon observing different potencies among the drugs in the EMSAs, we wished to determine if similar levels of effectiveness could be maintained in a more complex, cell-free environment containing additional nuclear proteins and larger amounts of DNA with greater sequence complexity. The cell-free transcription assay makes use of a linearized plasmid containing the c-fos promoter. Upon addition of nuclear lysate from serum-induced NIH3T3 cells and the proper mix of nucleotides, the c-fos promoter drives the production of a transcript of a known length of 750 bp (Figure 4A, control lanes 3 and 8 marked by asterisks, top arrow). Preincubation of the plasmid with drug before nuclear lysate addition results in a dose-dependent inhibition of transcript production, as is seen for representative results following chromomycin treatment (lanes 1, 2, and 4−7). At 7.5 μM chromomycin (lanes 1 and 2), transcript appearance is abolished. At lower drug concentrations (5 and 2.5 μM in lanes 4−5 and 6−7, respectively), the intensity of the transcript is diminished, but there is no change in transcript size. The lack of detectable shorter transcripts suggests that transcriptional elongation is not being affected by the drug treatment. Quantitation of the bands followed by normalization to a 250 bp internal standard (Figure 4A, bottom arrow), and comparison to controls, yields percent inhibition of transcription. Dose−response curves, as seen in the representative graph for chromomycin in Figure 4B, were plotted for each drug treatment. The IC_{50}s for this assay were then used to compare the drugs in Figure 4C. Chromomycin and nogalamycin showed a level of potency that was only about 3 times higher than Hoechst 33342. The trend evident in the EMSAs, where an unusually high level of chromomycin was required to inhibit TC formation, therefore did not hold true in the cell-free transcription assays. While the IC_{50}s for nogalamycin and Hoechst 33342 increased approximately 4-fold from inhibition of the TC to inhibition of cell-free transcription, the respective IC_{50}s for chromomycin's inhibition actually decreased by a factor of 2.5.

Use of Northern Blots To Measure c-fos mRNA Induction. After observing that the drugs' potencies in the EMSAs and cell-free transcription assays were comparable, we next wished to assess the drugs' effectiveness in inhibiting c-fos expression in whole cells using Northern blots. The serum inducibility of the c-fos gene and its quick mRNA turnover (*17*) are advantageous in analyzing drug effects on endogenous c-fos transcription because complications arising from preexisting levels of c-fos mRNA are minimized. Optimal conditions established for c-fos induction in NIH3T3 cells are shown in Figure 5A. Unsynchronized, logarithmically growing cells have undetectable levels of c-fos mRNA (Figure 5A, lane 1). Inducing these cells with 15% serum for 30 min results in its detectable upregulation (lane 2). Starving the cells overnight (16 h) in media containing 0.5% serum downregulates c-fos (lane 3), and a subsequent 30 min induction of these cells with serum results in optimal expression (lane 4), as determined in time course studies (data not shown). The housekeeping gene, glyceraldehyde-3-

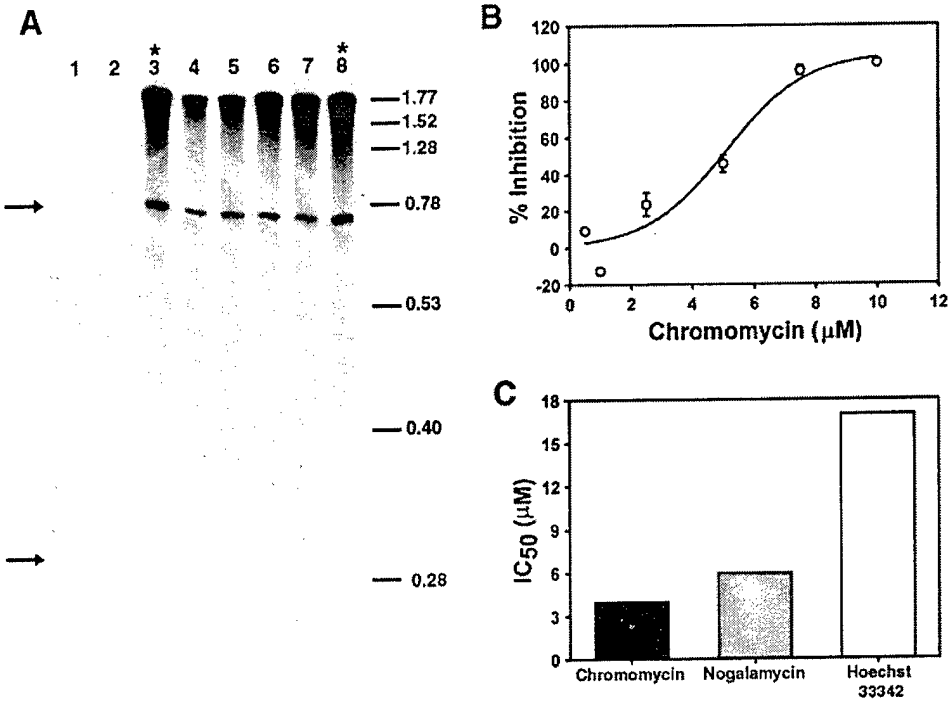

FIGURE 4: Effect of drugs on cell-free c-fos promoter-driven transcription (A) Chromomycin's effect on cell-free transcription. *Sph*I-linearized pFosLuc, a plasmid containing the human c-fos promoter upstream of a luciferase gene, was incubated with varying concentrations of drug for 30 min. Nuclear lysate from serum-induced NIH3T3 cells was then added for 15 min before the addition of nucleotides and [^{32}P]CTP. After a 1 h incubation, the resultant RNA transcripts were isolated and electrophoresed on a 4% denaturing polyacrylamide gel. Top arrow: the expected pFosLuc transcript at approximately 750 bases; lower arrow, internal control: a T3 transcript from pGEM4z at approximately 250 bases. Lanes 1−2, 4−5, and 6−7 contain 7.5, 5, and 2.5 μM chromomycin, respectively. Lanes 3 and 8, marked by asterisks: controls, with no drug treatment. Positions of size markers in a typical RNA ladder, in kilobases, are indicated. (B) Quantitation of chromomycin's inhibition of cell-free transcription. As in Figure 3B, comparison of drug-treated samples to controls yielded percent inhibition of transcription. Results are the mean of three experiments (mean ± standard error). (C) Comparison of drugs' effectiveness as inhibitors of cell-free transcription. IC_{50}s for each agent were calculated from graphs as shown in panel B.

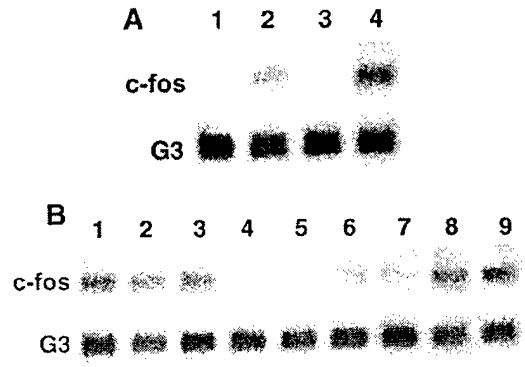

FIGURE 5: Representative Northern blot results. (A) Characteristics of c-fos expression in NIH3T3 cells. Following various treatments, 20 μg total RNA was electrophoresed on formaldehyde-containing agarose gels, transferred to a nylon membrane, and hybridized with radiolabeled probes for c-fos and G3. Lanes 1−2, normally growing cells; lanes 3−4, 16 h starvation in 0.5% serum; lanes 2 and 4, cells induced by raising serum concentration to 15% for 30 min. (B) Representative results on c-fos expression following exposure of NIH3T3 cells to chromomycin. After cells were starved for 16 h, drug was added for 1 h, and then cells were induced for 30 min as in (A). Lanes 1−3, controls, no drug treatment; lanes 4−5, 6−7, and 8−9 were exposed to 1, 0.5, and 0.25 μM chromomycin, respectively.

phosphate dehydrogenase (G3), is used in these blots as a loading control.

Analysis of Drug Effects on c-fos Expression in Whole Cells. For drug treatments, cells were starved for 16 h, exposed to varying drug concentrations for 1 h, and subsequently induced with serum. Chromomycin, as shown in Figure 5B, was capable of decreasing absolute c-fos mRNA levels in a dose-dependent manner (lanes 4−9), as compared to non-drug-treated controls (lanes 1−3). An approximately 30% decrease in c-fos expression is noted at only 0.5 μM (lanes 6 and 7), and the message is almost completely eliminated with a 1 μM treatment (lanes 4 and 5). There is no significant effect on G3 mRNA after a 1 h treatment at any drug concentration. In addition, as was noted in the cell-free transcription assay, there were no detectable levels of shorter transcripts following drug exposure.

Nogalamycin and Hoechst 33342 were analyzed in the above manner to see if they were also capable of inhibiting c-fos expression. Quantitation of the resulting hybridized signals allowed dose−response curves to be plotted (Figure 6). From these curves, it is evident that the drugs differ in their effectiveness: a 1 h exposure to 1 μM chromomycin results in 80% inhibition of c-fos expression, compared to no substantial inhibition for nogalamycin or Hoechst 33342 at the same concentration (compare panels A to B and C). At 2.5 μM Hoechst 33342 or nogalamycin, expression is inhibited approximately 40%, compared to greater than 95% inhibition for chromomycin. Chromomycin is therefore about an order of magnitude more potent than nogalamycin or Hoechst 33342 in inhibiting c-fos expression after a 1 h treatment. This is in contrast to the results obtained in the cell-free transcription assay, where chromomycin and nogala-

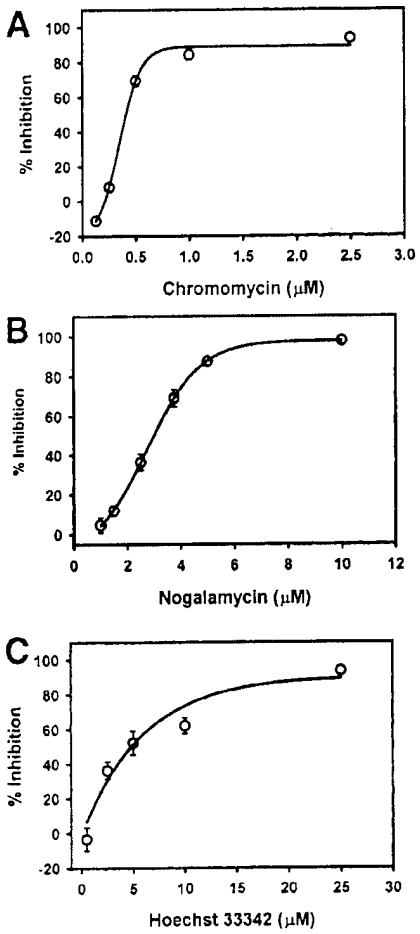

FIGURE 6: Quantitation of drugs' effects on endogenous c-fos expression in NIH3T3 cells following 1 h exposures. Cells were starved for 16 h before being exposed to a range of drug concentrations, in μM, for 1 h and induced with 15% serum for 30 min as described in Figure 5. Total RNA was analyzed in Northern blots through hybridization to radiolabeled c-fos and G3 probes, and the blots were visualized following autoradiography. Quantitation of the bands and comparison of the drug-treated lanes to controls yielded percent inhibition for each drug: (A) chromomycin; (B) nogalamycin; and (C) Hoechst 33342. Results are the mean of five experiments (mean ± standard error). The IC_{50}s calculated from these graphs are presented in Figure 8.

mycin exhibited similar potencies that were only 3 times greater than Hoechst 33342.

Chromomycin's Effects on c-fos Expression over a Shorter Time Course. After observing very effective inhibition of c-fos expression following exposure of cells to low levels of chromomycin after only 1 h, we wished to further characterize this drug's effect during shorter exposures. NIH3T3 cells were therefore starved for 16 h in low-serum media before being exposed to 1 μM chromomycin for various times (0−60 min). For the zero time point, drug was added to cells immediately before serum induction. Cells were then induced for 30 min before RNA isolation as discussed above. A concentration of 1 μM was chosen for this time course because of its substantial effect on c-fos expression (~80% inhibition after a 1 h exposure). As seen in Figure 7, there is a slight induction of c-fos mRNA after a 15 min exposure to chromomycin, but inhibition begins by 30 min and increases fairly rapidly to reach nearly 80% after an hour.

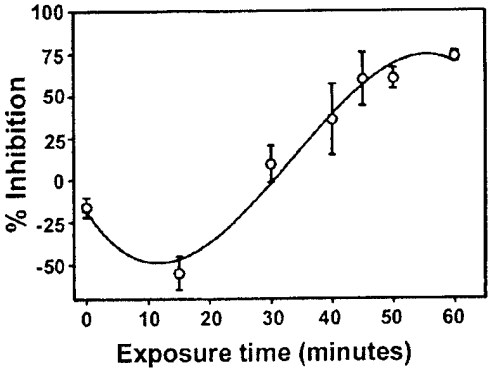

FIGURE 7: Chromomycin's inhibition of endogenous c-fos expression in NIH3T3 cells over time. Cells were starved for 16 h before being exposed to 1 μM chromomycin for various lengths of time. They were then induced with 15% serum for 30 min. Analysis using Northern blots and quantitation was carried out as previously described in Figure 6. Results are the mean of three experiments (mean ± standard error).

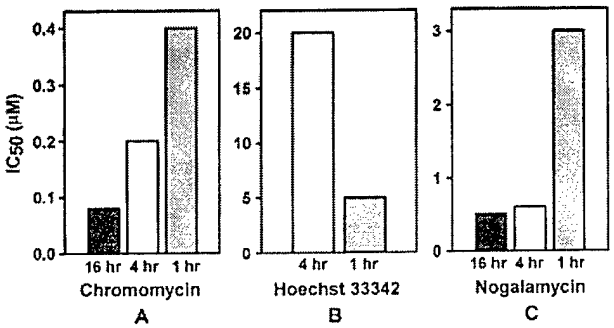

FIGURE 8: Effect of time on drug inhibition of endogenous c-fos expression. One hour drug exposures (gray bars) following 16 h starvation of NIH3T3 cells were performed as described in Figure 5. The 4 h exposures (white bars) were also performed after the cells were starved 16 h. For the 16 h exposures, (black bars), cells were starved and exposed to drug simultaneously. Northern blot analysis following hybridization to c-fos and G3 probes and subsequent quantitation yielded IC_{50} values. These values are plotted for each time point for (A) chromomycin, (B) Hoechst 33342, and (C) nogalamycin.

Drugs' Abilities To Inhibit c-fos Expression Over Time. Clearly, chromomycin is a rapid inhibitor of c-fos expression, but is this effect maintained over time to result in a continued decrease in expression? Longer exposures of 4 and 16 h were carried out to determine if each drug was able to maintain its effectiveness in the cellular environment. Like the 1 h time points, the 4 h drug exposures followed a 16 h overnight starvation period. However, for 16 h treatments, cells were starved and exposed to drug concurrently. The IC_{50} values were then used to compare the time course results as well as to compare drugs to one another. For chromomycin (Figure 8A), there was a continued increase in drug potency over time. That is, less drug was needed to obtain 50% inhibition of c-fos expression following a 16 h exposure compared to a 1 h exposure. Interestingly, Hoechst 33342 yielded a pattern of inhibition that was completely opposite. While a 16 h exposure to Hoechst 33342 yielded no consistent inhibition (not shown), the drug was more effective at shorter time points, with the IC_{50} dropping 4-fold between 4 and 1 h (Figure 8B). The pattern exhibited by nogalamycin (Figure 8C) was similar to that obtained for chromomycin. However, 5 times more drug was needed to obtain an

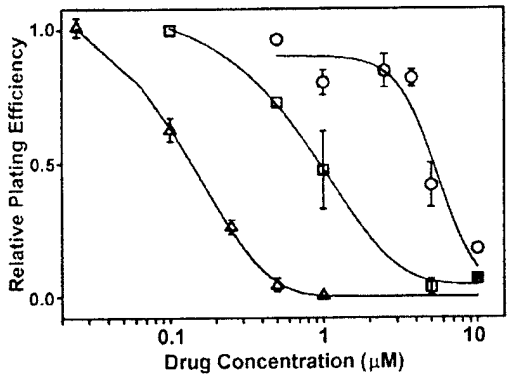

FIGURE 9: Cytotoxic effect of drugs on NIH3T3 cells. Cells were exposed to a range of drug concentrations for 4 h before being serially diluted, replated, and grown for 10 days. The cells were then stained and fixed in a solution of methylene blue and ethanol. Groups of more than 50 cells were deemed colonies and counted under a stereo microscope. Plating efficiencies were calculated by dividing the number of colonies by the number of cells plated. Relative plating efficiencies were then calculated by dividing the plating efficiency of each drug treatment by the control plating efficiency. The results shown for chromomycin (△), nogalamycin (□), and Hoechst 33342 (○) are the mean of three experiments (mean ± standard error).

equivalent level of inhibition at 1 h as compared to 4 h, after which more time did not result in any substantial further increases in drug effectiveness.

Drugs' Effects on Cell Survival and RNA Synthesis. The Northern blot results demonstrated that the drugs chosen are capable of affecting endogenous c-fos expression in a dose- and time-dependent manner. However, the complexity of the cellular environment necessitates that these results be interpreted in the context of the agents' other biological activities and whole cell effects. Therefore, to further characterize the drugs' effects in whole cells, NIH3T3 cells were exposed to a range of drug concentrations for 4 h before being plated in a colony formation assay. The colonies formed after 10 days of growth were counted and used to calculate relative plating efficiencies for each drug treatment as compared to non-drug-treated controls (Figure 9). Chromomycin was found to be the most toxic agent, causing 50% cell death at only 0.125 μM. The amount of Hoechst 33342 required to obtain the same level of toxicity (4.5 μM) was over an order of magnitude greater. Nogalamycin's toxicity fell between these values, with an IC_{50} of 1 μM. The cytotoxicity of these compounds may be reflected by their ability to shut down general transcription in cells, since they are capable of binding to many regions on DNA. To get a sense of how general transcription was being affected, RNA synthesis in NIH3T3 cells, as quantitated by [^{3}H]uridine incorporation, was measured following 4 h drug exposures (data not shown). The IC_{50}s from this assay are summarized in Table 1, along with IC_{50}s for the 4 h drug treatments in the cytotoxicity and Northern blot assays. The order of potency for drugs in the cellular assays was chromomycin > nogalamycin > Hoechst 33342. For all agents, similar drug concentrations were needed to achieve equivalent levels of activity in each assay.

Table 1: IC_{50} Values for Selected Whole Cell Assays[a]

drug	cytotoxicity	c-fos mRNA synthesis	total RNA synthesis
chromomycin	0.125	0.2	0.1
nogalamycin	1.0	0.6	0.5
Hoechst 33342	4.5	20	7.5

[a] Concentrations of drug, in μM, needed to inhibit the measured activity by 50%. The values for each assay, as described under Materials and Methods, were obtained after exposing NIH3T3 cells to drug for 4 h.

DISCUSSION

This study has compared and contrasted the ability of various classes of DNA-binding agents to inhibit TF/DNA interactions and resultant gene expression using a defined target gene promoter sequence, the c-fos SRE. To our knowledge, this is the first study that systematically analyzes the effectiveness of drugs possessing different sequence selectivities and modes of DNA binding to target two different TF-binding motifs in increasingly complex assays. The drugs' abilities to inhibit TF binding to target sequences in EMSAs were compared to their potencies in inhibiting cell-free transcription as well as their abilities to inhibit cellular gene expression. The drugs selected for analysis, chromomycin, nogalamycin, and Hoechst 33342, exhibited different potencies in each assay. Interesting differences were also noted when the drugs' effectiveness was compared between assays. These variations may stem from many factors including the DNA-binding characteristics of the compounds as well as their overall stability in cells.

In the EMSAs, the overall order of decreasing potency for inhibiting SRF and Elk-1 complexes was nogalamycin > Hoechst 33342 > chromomycin. Potential binding sites for nogalamycin, consisting of alternating purines and pyrimidines, are located near the *ets* motif of the Elk-1 binding site and in the CArG box of the SRF binding site. As an intercalator that makes contacts in both the major and minor grooves (*32*), and in comparison to the MGBs, nogalamycin dissociates from DNA very slowly (*11*), favoring more effective inhibition of TF binding under equilibrium conditions. It was anticipated that since SRF is required for Elk-1 binding, the IC_{50}s for inhibition of TC and SRF binding would be equivalent. However, 2 times more nogalamycin was needed to inhibit TC formation by 50% as compared to SRF binding. Structural studies and circular permutation analyses have shown that binding of a homodimer of SRF bends DNA 72° (*33*), while DNA bound to the TC has increased flexibility and is bent approximately 50° (*34*). This alteration in DNA conformation upon Elk-1 binding and its effects on neighboring DNA structure may therefore influence a drug's ability to optimally recognize and bind its target sequences.

In contrast to nogalamycin, chromomycin was more potent in inhibiting TC formation as compared to SRF binding but exhibited the highest potency in inhibiting Elk-1 complexes. While the E74 oligo used in the EMSAs contains four contiguous G/C base pairs in the *ets* motif that may be an appropriate chromomycin binding site (5′-CCGG-3′), the SRE lacks such a sequence. However, this drug was still able to prevent SRF and TC binding with lower potency, suggesting that if a consensus sequence is not available, the drug will associate with other sequences by default. Similar results have been obtained using chromomycin to inhibit TBP association with its A/T-rich binding site (*35*). The higher concentration of chromomycin required to inhibit TC forma-

tion as compared to Elk-1 complex formation may be due to SRF's stabilization of Elk-1 binding. Analogous results were seen in previous evaluations of drug effects on TBP binding. When TBP's binding was stabilized by addition of TFIIA, higher concentrations of distamycin were needed to disrupt complex formation (*12*).

Analysis of Hoechst 33342's inhibition of Elk-1 complexes was limited by well retention of the oligo when complexed to drug, regardless of whether protein was present (data not shown). This effect has been seen previously in our lab with other drug/oligonucleotide combinations. Despite its A/T preference, Hoechst 33342 was not a potent inhibitor of SRF binding to the A/T-rich CArG box on the SRE. Sequence selection studies have demonstrated that other bisbenzimidazole-based drugs, such as Hoechst 33258, greatly prefer some A/T sites over others, and surrounding sequences appear to influence the drug's affinity and optimal binding ability (*36*). In particular, the presence of 5′TpA steps greatly decreases the affinity of this Hoechst dye for DNA (*37*). The two 5′TpA steps present in the CArG box may therefore be contributing to the low potency observed in the SRF complex analysis. Given its high IC_{50} value, it is possible that Hoechst 33342 is binding to the target oligo by default, much like chromomycin.

When EMSA analyses using the TC were carried out, drugs never solely inhibited Elk-1 binding, which would have resulted in the appearance of the SRF complex. This suggests that these agents are generally disruptive and that they apparently alter the conformation of the DNA through bending or groove widening so that neither TF is able to bind. This is supported by previous studies that investigated long-range effects of drug binding on DNA. For example, the MGB distamycin can alter DNA allosterically up to 100 bp away from its binding site (*38*). Furthermore, the alterations in local DNA structure following binding of distamycin or the intercalator actinomycin produce changes in DNase I cleavage patterns at flanking sites (*39*).

In reverse EMSAs, where drug was added to preformed TF/DNA complexes, only nogalamycin required higher concentrations to achieve equivalent levels of TC inhibition. The equilibrium conditions required to inhibit complex formation were therefore altered, since more drug was needed to disrupt the TC if it was added after the proteins were bound. Dissociation studies carried out for the TC showed that this complex was stably bound for over 2 h under assay conditions (data not shown). SRF and Elk-1 primarily contact the SRE in the major groove. Since nogalamycin binds in a similar manner, the drug's association with DNA may be hindered by the presence of TFs at or near its binding site. In contrast, drugs such as chromomycin or Hoechst 33342 may be more effective in inhibiting TF binding to the major groove in reverse assays because they can approach DNA from the opposite, minor groove (*35*).

Drug activity was maintained in a more complex milieu of nuclear proteins and plasmid DNA in the cell-free transcription assay. IC_{50}s obtained in this assay were not substantially different from the EMSA IC_{50}s for TC inhibition, but the order of potency was chromomycin > nogalamycin > Hoechst 33342. As noted in Figure 4C, there was only a 4-fold decrease in potency for nogalamycin and Hoechst 33342 in this assay compared to the EMSA results. In contrast, chromomycin was about 2.5 times more effective in inhibiting transcription than in preventing TC formation. Overall, the presence of additional proteins and a higher amount of DNA with greater sequence complexity do not seem to greatly interfere with the ability of these drugs to inhibit cell-free transcription. This is in contrast to previous studies in which the MGB distamycin was used to inhibit the TF E2F from binding to the dihydrofolate reductaste (DHFR) promoter and to inhibit DHFR promoter-driven cell-free transcription (*29*). Here, 200 times more drug was needed to inhibit transcription as compared to inhibition of E2F/DHFR promoter complex formation. However, studies carried out using mithramycin (which is chemically related to chromomycin) demonstrated that similar levels of drug were needed to inhibit both TF complex formation and cell-free transcription from the c-myc promoter (*40*). The ability of any given drug to inhibit TF complex formation and to maintain an equivalent level of activity in a cell-free environment may therefore be dependent on the particular TFs studied and the DNA sequence used as a target. The results obtained here may also stem from the drugs' effects on other sequences in the c-fos promoter. By interfering with the binding of other TFs, recruitment of a functional RNA polymerase complex may be inhibited and levels of transcription will drop. The TFs bound to the c-fos promoter may be more sensitive to chromomycin than the other drugs analyzed. This may explain chromomycin's greater potency in inhibiting cell-free transcription and endogenous c-fos expression, as discussed below. None of the drugs tested resulted in the detectable production of shorter transcripts, which suggests that these agents are acting on the level of transcription initiation, rather than elongation. This is supported by previous work where transcriptional elongation inhibition was not observed except at high drug concentrations in some systems (*14, 41*).

The serum inducibility of the c-fos promoter and the rapid turnover of its mRNA facilitated assessment of immediate or short-term drug effects on gene expression in NIH3T3 cells. In Northern blots, the order of the drugs' potency in inhibiting endogenous c-fos transcription following serum induction was chromomycin > nogalamycin > Hoechst 33342. The time course study, which demonstrated an approximately 40% inhibition after only 40 min of treatment with 1 μM chromomycin, demonstrates the fast-acting nature of this drug and suggests that it is able to enter cells quickly and effectively. These rapid effects, in addition to the cell-free transcription data discussed above, suggests that this drug is acting on the level of DNA by inhibiting TF association with the c-fos promoter. Higher concentrations of chromomycin were needed at shorter time points in order to achieve an equivalent level of inhibition. This drug's effects may therefore depend, at least in part, on accumulation within the cell. The fact that the drug still exhibits inhibitory effects after 16 h in cells suggests that it is relatively stable. Similar results were obtained in studies using mithramycin and chromomycin to inhibit the expression of a stably transfected c-myc gene in NIH3T3 cells (*41*). Here, expression of an exogenous gene was very effectively inhibited after a 24 h exposure to 1 μM of either drug.

Nogalamycin's pattern of inhibition of gene expression was similar to that obtained using chromomycin. Hoechst 33342, however, was more effective at shorter time points as evidenced by a lower IC_{50} for 1 h exposures. The

inhibition seen following 16 h exposures, although variable, was marginal at best (data not shown). Hoechst 33342 may therefore become unstable or inactivated in these cells over time. Because there are undetectable levels of c-fos mRNA prior to serum induction and because shorter transcripts cannot be detected, the presence of drug is likely preventing the initiation of transcription. No decrease in absolute G3 mRNA levels was noted after any drug treatment. In short-term drug exposures, this may be due to G3's longer mRNA half-life (8 h for G3 compared to 30 min for c-fos) (*42*). In addition, the lack of detectable shorter G3 transcripts following drug treatment of cells is again consistent with the drugs' inhibition of transcription initiation. If the drugs were causing transcript degradation or inhibition of transcription elongation, partial transcripts or smearing of the RNA samples would have been visible.

The IC_{50}s for drug inhibition of c-fos expression as measured in the Northerns were less than the IC_{50}s calculated for the cell-free transcription assay. The largest difference of an order of magnitude was obtained for chromomycin. The process of transcription is far more complex on an endogenous promoter, where many other proteins and long-range changes in DNA conformation come into play to provide an intricately regulated cellular response. These drugs' abilities to bind to many other regions on the c-fos promoter is likely contributing to their increased potency in the whole cell environment. The complexity of the drugs' effects is further evidenced by the results obtained in the other whole cell analyses. The similarity in IC_{50}s for the cytotoxicity, RNA synthesis, and Northern blot assays following 4 h drug exposures suggests that the toxicity of these agents is reflected by their inhibition of general transcription.

Drug association with many sequences in the genome and the resultant toxic effects could potentially be avoided by developing more specific DNA-binding compounds. Designing more effective and potent DNA-binding drugs with the goal of disrupting specific TF/DNA complexes is an essential step in developing potentially therapeutic compounds. Our results demonstrate how the properties and DNA-binding characteristics of classical DNA-binding compounds are related to their biological consequences on a particular gene. Structural modification of classical drugs has yielded novel agents, such as microgonotropens and polyamides (*43, 44*). These agents will next be analyzed using the c-fos SRE target to determine which modifications result in potent and specific DNA-binding drugs with significant cellular activity.

ACKNOWLEDGMENT

We gratefully thank Drs. David Kowalski and Deborah Kramer for their comments and advice in preparing the manuscript.

REFERENCES

1. Phillips, D. R., White, R. J., Trist, H., Cullinane, C., Dean, D., and Crothers, D. M. (1990) *Anticancer Drug Des. 5*, 21–29.
2. McHugh, M. M., Woynarowski, J. M., Mitchell, M. A., Gawron, L. S., Weiland, K. L., and Beerman, T. A. (1994) *Biochemistry 33*, 9158–9168.
3. Beerman, T. A., McHugh, M. M., Sigmund, R., Lown, J. W., Rao, K. E., and Bathini, Y. (1992) *Biochim. Biophys. Acta 1131*, 53–61.
4. Latchman, D. S. (1997) *Int. J. Biochem. Cell Biol. 29*, 1305–1312.
5. Hurst, H. C. (1996) *Eur. J. Cancer. [A] 32A*, 1857–1863.
6. Geierstanger, B. H., and Wemmer, D. E. (1995) *Annu. Rev. Biophys. Biomol. Struct. 24*, 463–493.
7. Yang, X. L., and Wang, A. H. (1999) *Pharmacol. Ther. 83*, 181–215.
8. Utsuno, K., Kojima, K., Maeda, Y., and Tsuboi, M. (1998) *Chem. Pharm. Bull. (Tokyo) 46*, 1667–1671.
9. Fox, K. R., and Alam, Z. (1992) *Eur. J. Biochem. 209*, 31–36.
10. Fox, K. R., and Waring, M. J. (1986) *Biochemistry 25*, 4349–4356.
11. Fox, K. R., Brassett, C., and Waring, M. J. (1985) *Biochim. Biophys. Acta 840*, 383–392.
12. Chiang, S. Y., Welch, J., Rauscher, F. J., III, and Beerman, T. A. (1994) *Biochemistry 33*, 7033–7040.
13. Dorn, A., Affolter, M., Muller, M., Gehring, W. J., and Leupin, W. (1992) *EMBO J. 11*, 279–286.
14. Bellorini, M., Moncollin, V., D'Incalci, M., Mongelli, N., and Mantovani, R. (1995) *Nucleic Acids Res. 23*, 1657–1663.
15. Bianchi, N., Passadore, M., Rutigliano, C., Feriotto, G., Mischiati, C., and Gambari, R. (1996) *Biochem. Pharmacol. 52*, 1489–1498.
16. Treisman, R. (1992) *Trends Biochem. Sci. 17*, 423–426.
17. Greenburg, M. E., and Ziff, E. B. (1984) *Nature 311*, 433–438.
18. Treisman, R. (1985) *Cell 42*, 889–902.
19. Norman, C., Runswick, M., Pollock, R., and Treisman, R. (1988) *Cell 55*, 989–1003.
20. Shaw, P. E., Schroter, H., and Nordheim, A. (1989) *Cell 56*, 563–572.
21. Shore, P., Bisset, L., Lakey, J., Waltho, J. P., Virden, R., and Sharrocks, A. D. (1995) *J. Biol. Chem. 270*, 5805–5811.
22. Gille, H., Sharrocks, A. D., and Shaw, P. E. (1992) *Nature 358*, 414–417.
23. Janknecht, R., Ernst, W. H., Pingoud, V., and Nordheim, A. (1993) *EMBO J. 12*, 5097–5104.
24. Urness, L. D., and Thummel, C. S. (1990) *Cell 63*, 47–61.
25. Lee, D. K., Horikoshi, M., and Roeder, R. G. (1991) *Cell 67*, 1241–1250.
26. Heidenreich, O., Neininger, A., Schratt, G., Zinck, R., Cahill, M. A., Engel, K., Kotlyarov, A., Kraft, R., Kostka, S., Gaestel, M., and Nordheim, A. (1999) *J. Biol. Chem. 274*, 14434–14443.
27. Yang, C., Shapiro, L. H., Rivera, M., Kumar, A., and Brindle, P. K. (1998) *Mol. Cell. Biol. 18*, 2218–2229.
28. Blake, M. C., Jambou, R. C., Swick, A. G., Kahn, J. W., and Azizkhan, J. C. (1990) *Mol. Cell. Biol. 10*, 6632–6641.
29. Chiang, S. Y., Azizkhan, J. C., and Beerman, T. A. (1998) *Biochemistry 37*, 3109–3115.
30. Hipskind, R. A., Rao, V. N., Mueller, C. G., Reddy, E. S., and Nordheim, A. (1991) *Nature 354*, 531–534.
31. Rao, V. N., and Reddy, E. S. (1992) *Oncogene 7*, 65–70.
32. Smith, C. K., Davies, G. J., Dodson, E. J., and Moore, M. H. (1995) *Biochemistry 34*, 415–425.
33. Pellegrini, L., Tan, S., and Richmond, T. J. (1995) *Nature 376*, 490–498.
34. Sharrocks, A. D., and Shore, P. (1995) *Nucleic Acids Res. 23*, 2442–2449.
35. Welch, J. J., Rauscher, F. J., III, and Beerman, T. A. (1994) *J. Biol. Chem. 269*, 31051–31058.
36. Spink, N., Brown, D. G., Skelly, J. V., and Neidle, S. (1994) *Nucleic Acids Res. 22*, 1607–1612.
37. Abu-Daya, A., and Fox, K. R. (1997) *Nucleic Acids Res. 25*, 4962–4969.
38. Hogan, M., Dattagupta, N., and Crothers, D. M. (1979) *Nature 278*, 521–524.
39. Fox, K. R., and Waring, M. J. (1984) *Nucleic Acids Res. 12*, 9271–9285.

40. Snyder, R. C., Ray, R., Blume, S., and Miller, D. M. (1991) *Biochemistry 30*, 4290−4297.
41. Ray, R., Thomas, S., and Miller, D. M. (1990) *Am. J. Med. Sci. 300*, 203−208.
42. Dani, C., Piechaczyk, M., Audigier, Y., El Sabouty, S., Cathala, G., Marty, L., Fort, P., Blanchard, J. M., and Jeanteur, P. (1984) *Eur. J. Biochem. 145*, 299−304.
43. Dervan, P. B., and Burli, R. W. (1999) *Curr. Opin. Chem. Biol. 3*, 688−693.
44. Bruice, T. C., Sengupta, D., Blasko, A., Chiang, S. Y., and Beerman, T. A. (1997) *Bioorg. Med. Chem. 5*, 685−692.

BI001427L

Double-Stranded DNA Binding Characteristics and Subcellular Distribution of a Minor Groove Binding Diphenyl Ether Bisbenzimidazole†

Alexander L. Satz,‡ Christine M. White,§ Terry A. Beerman,*,§ and Thomas C. Bruice*,‡

Department of Chemistry and Biochemistry, University of California at Santa Barbara, Santa Barbara, California 93106, and Department of Pharmacology and Therapeutics, Roswell Park Cancer Institute, Elm and Carlton Streets, Buffalo, New York 14263

Received February 16, 2001; Revised Manuscript Received March 23, 2001

ABSTRACT: The interactions of Hoechst 33377 (H1) with 20 different oligomeric duplexes have been investigated via spectrofluorometric titrations and/or thermal denaturation experiments. H1 is shown to form 2:1 complexes with dsDNA binding sites of at least four contiguous A/T base pairs. H1 is also shown to possess the rare ability to meaningfully distinguish between different A·T rich sequences. For example, the combined equilibrium constants for complexation of the oligomeric duplex 5′-GCAATTGC-3′ (**15**) by H1 are found to be 110-fold greater than for the duplex 5′-GCTTAAGC-3′ (**16**). It is believed that the 5′-TpA-3′ dinucleotide step in **16** disrupts the rigid "A-tract" conformation of **15** and discourages minor groove binding by agents capable of recognizing longer dsDNA sequences. Molecular models are presented which elucidate the structure of the $(H1)_2$−dsDNA minor groove complex. The two H1 molecules bind to an A/T rich sequence of 6 bp in a slightly staggered, side-by-side, and antiparallel arrangement. Evidence suggests that the piperazine rings of the H1 side-by-side complex are capable of resting in the minor groove of G/C base pairs. Fluorescence microscopy studies using NIH3T3 cells indicate that H1 is capable of traversing the cytoplasmic membrane and selectively localizing to nuclear DNA. H1 also demonstrated the ability to inhibit endogenous transcription of the c-fos gene in NIH3T3 cells at micromolar concentrations. Cytotoxicity studies employing the same cell type show H1 to possess an LD_{50} of 3.5 μM.

Interest in the control of transcription at the molecular level has spurred efforts toward the development of new minor groove binding agents with greater sequence selectivity (*1*−*7*). Increased selectivity can be achieved by increasing the number of base pairs recognized by a DNA-binding agent. An alternative is to develop agents capable of distinguishing among all four DNA bases (*1*). Recently, we reported a novel tripyrrole peptide−bisbenzimidazole conjugate capable of recognizing 9 bp in the minor groove of dsDNA[1] (*8*). In a continuing effort to develop bisbenzimidazole-type compounds with increased specificity, we investigated the dsDNA binding characteristics of a diphenyl ether bisbenzimidazole H1 (*9*). H1 held the potential for recognizing dsDNA sequences longer than other bisbenzimidazole-type compounds such as H2 due to its increased length while still maintaining a crescent-shaped curvature. A crescent shape is a characteristic of bisbenzimidazoles that allows them to maintain optimal contact in the minor groove.

Although H3 is the most widely investigated of the bisbenzimidazole-type compounds, both H1 and H2 are known to be significantly more cytotoxic (*10*, *11*). It has been suggested that these agents exhibit greater cytotoxicity due to their greater cellular permeability (*11*). Minor groove binding agents can inhibit the binding of regulatory proteins to their DNA consensus sites in cell-free studies (*7*, *12*, *13*). This may be the mechanism by which H1 and H2 contribute to cell death. The cytotoxicity of H1 suggests that it possesses some type of biological activity. Previous studies did not investigate the ability of H1 to traverse the cell membrane and reach its nuclear DNA target. Quantitative determination of its ability to inhibit gene transcription in whole cells, in combination with the knowledge that it selectively localizes in nuclear DNA, would provide a much stronger link between its ability to bind DNA and its cytotoxicity.

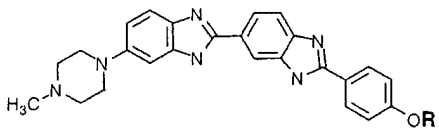

Hoechst 33377 (H1) R = -phenyl
Hoechst 33342 (H2) R = -ethyl
Hoecsht 33258 (H3) R = -H

Here we employ a combination of cell-free and cellular assays to determine if H1 would make a good lead compound for the pursuit of new minor groove binding agents with increased binding selectivity and potency. We have investigated the binding of H1 to the 18 bp oligomeric duplex 5′-GCGGTATAAAATTCGACG-3′ (**1**) and nine other related duplexes (**2**−**10**) in an effort to characterize H1's

† This work was supported by grants from the National Institutes of Health to T.C.B. (5R37DK09171-36) and the American Cancer Society to T.A.B. (RPG-96-034-04-CDD).

‡ University of California at Santa Barbara.

§ Roswell Park Cancer Institute.

[1] Abbreviations: H1, Hoechst 33377; H2, Hoechst 33342; H3, Hoechst 33258; dsDNA, double-stranded DNA; HPLC, high-pressure liquid chromatography; DMSO, dimethyl sulfoxide; Ar, aromatic; ssDNA, single-stranded DNA; TF, transcription factor; SRE, serum response element; SRF, serum response factor; EMSA, electrophoretic mobility shift assay; oligo, oligonucleotide.

10.1021/bi0103415 CCC: $20.00
Published on Web 00/00/0000 PAGE EST: 9.8

Table 1: Stoichiometries and Equilibrium Association Constants for (Ligand)$_x$−dsDNA Complexes and Relative Fluorescence Intensities[a]

oligomeric duplex[b]	H1	H2	H3
5′-GCGACTGCAATTTCGACGTCC-3′ (**11**)			
(ligand)$_x$−**11** stoichiometry	2:1	1:1	1:1
fluorescence intensity	5400	6400	6900
equilibrium association constant[d]	$K_1K_2 = 8.4 \times 10^{16}$ M^{-2}	$K_1 = 1.2 \times 10^{9}$ M^{-1}	$K_1 = 4.2 \times 10^{8}$ M^{-1}
5′-GCGACTGCAATTCGACGTCC-3′ (**12**)			
(ligand)$_x$−**12** stoichiometry	2:1	1:1	1:1
fluorescence intensity	4400	5600	6400
equilibrium association constant[d]	$K_1K_2 = 2.6 \times 10^{16}$ M^{-2}	$K_1 = 1.5 \times 10^{8}$ M^{-1}	$K_1 = 1.8 \times 10^{8}$ M^{-1}
5′-GGACGTCGATTGCAGTCGTC-3′ (**13**)			
(ligand)$_x$−**13** stoichiometry	no clear binding[c]	2:1	2:1
fluorescence intensity	140−190	4000	2500
equilibrium association constant[d]	no clear binding	$K_1K_2 = 2.3 \times 10^{14}$ M^{-2}	$K_1K_2 = 4.7 \times 10^{14}$ M^{-2}
5′-GGACGTCGTTGCAGTCGTCG-3′ (**14**)	no binding	no binding	no binding
fluorescence intensity	22	35	150
buffer only (no DNA)	22	23	160

[a] Stoichiometries determined by spectrofluorometric titration (10 mM potassium phosphate pH 7.0 buffer, 150 mM NaCl, 26 °C). Relative fluorescence intensities stated in arbitrary fluorescence units (450 nm) × M^{-1}. [b] Potential A·T rich binding sites are underlined. [c] The relative fluorescence intensity of the ligand−**13** complex is too weak to accurately measure the level of complex formation. [d] Determined by nonlinear least-squares fitting of an isothermal binding curve. Isothermal binding curves were generated using 10 mM potassium phosphate pH 7.0 buffer and 150 mM NaCl at 26 °C. Equilibrium constants are given as the product K_1K_2 for 2:1 ligand:DNA stoichiometries since separation of individual equilibrium constants is not possible. The stated equilibrium constants have a standard deviation of ±80%.

Table 2: Melting Temperatures for Ligand−18-mer Complexes (°C)[a]

18 bp oligomeric duplex	t^0_m	Δt_m H1	H2	H3
5′-GCGGTATAAAATTCGACG-3′ (**1**)	57	6	5	3
5′-GCGGCATAAAATTCGACG-3′ (**2**)	62	4	4	2
5′-GCGGTGTAAAATTCGACG-3′ (**3**)	60	5	5	1
5′-GCGGTACAAAATTCGACG-3′ (**4**)	60	5	5	1
5′-GCGGTATGAAATTCGACG-3′ (**5**)	58	6	6	1
5′-GCGGTATAGAATTCGACG-3′ (**6**)	57	5	6	2
5′-GCGGTATAAGATTCGACG-3′ (**7**)	57	2	2	1
5′-GCGGTATAAAGTTCGACG-3′ (**8**)	58	1	0	1
5′-GCGGTATAAAACTCGACG-3′ (**9**)	58	3	2	1
5′-GCGGTATAAAATCCGACG-3′ (**10**)	58	5	3	2

[a] t_m values for complexes were determined by first-derivative analysis. t^0_m values are melting temperatures of oligomeric duplexes (0.15 μM) in 10 mM potassium phosphate pH 7.0 buffer containing 150 mM NaCl in the absence of ligand. Δt_m values are differences in melting temperatures for oligomeric duplexes in the absence and presence (0.3 μM = 2 equiv) of ligand. The standard deviation for Δt_m values is ±1 °C.

Table 3: Melting Temperatures for Oligomeric Duplexes of the Type d(-A$_x$T$_x$-) and d(-T$_x$A$_x$-) and Their Ligand Complexes (°C)[a,b]

oligomeric duplex[c]	t^0_m	Δt_m H1	H2	H3	netropsin
5′-GCAATTGC-3′ (**15**)[b]	40	12	11	8	6
5′-GCTTAAGC-3′ (**16**)[b]	30	0	11	9	4
Δt_m(**15**) − Δt_m(**16**)		12	0	−1	2
5′-GAAAATTTTC-3′ (**17**)	29	19	18	14	14
5′-GTTTTAAAAC-3′ (**18**)	24	12	16	13	12
Δt_m(**17**) − Δt_m(**18**)		7	2	1	2
5′-GAAAAAATTTTTTC-3′ (**19**)	42	15	16	13	10
5′-GTTTTTTAAAAAAC-3′ (**20**)	39	16	15	13	9
Δt_m(**19**) − Δt_m(**20**)		−1	1	0	1

[a] t_m values for oligomer complexes were determined by first-derivative analysis. All t_m values were determined by employing 1.5 μM oligomeric duplex and 3 μM ligand. t^0_m values are melting temperatures of oligomeric duplexes in the absence of ligand. Δt_m values are differences in melting temperatures for oligomeric duplexes in the absence and presence of ligand. The standard deviation for Δt_m values is ±1 °C. [b] All experiments employed 10 mM potassium phosphate pH 7.0 buffer and 150 mM NaCl except for those involving **15** and **16**, for which equivalent buffer of 1 M NaCl was used. [c] 5′-TpA-3′ dinucleotide steps are underlined.

sequence selectivity (Table 2). The oligomeric duplex **1** contains the TATA box, which in eukaryotes consists of the consensus sequence 5′-TATAAAA-3′, and is recognized by the TATA binding protein (TBP) subunit of TFIID of the RNA polymerase II transcription initiation complex. One benefit of studying bisbenzimidazoles such as H1 is that they form highly fluorescent dsDNA complexes. This makes it possible to determine dsDNA complex stoichiometries and equilibrium association constants via spectrofluorometric titrations (*8*, *14*−*16*). (H1)$_x$−dsDNA complex stoichiometries and equilibrium association constants are reported for a series of oligomeric duplexes which differ in the size of their A/T rich binding sites (Table 1). The ability of H1 to distinguish among different A/T rich oligomeric duplexes of the type d(-A$_x$T$_x$-) versus d(-T$_x$A$_x$-) (x = 2, 4, and 6) is discussed (Tables 3 and 4). Comparisons are made between H1, H2, H3, and netropsin. Additionally, we report the ability of H1 to inhibit endogenous transcription of the c-fos gene in NIH3T3 cells and describe the use of fluorescence microscopy in determining the subcellular distribution of the agent.

To determine if H1 is able to bind to nuclear DNA, the subcellular localization of H1 was explored using fluorescence microscopy. Localization to the nucleus may be connected to an agent's ability to affect DNA-related functions. Recently, H2 was demonstrated to inhibit the endogenous expression of the c-fos gene in NIH3T3 cells at micromolar concentrations (*17*). The c-fos gene, an immediate-early response gene, is tightly regulated at the level of transcription (*18*, *19*). The expression of c-fos requires a functional serum response element (SRE), a promoter region containing an A/T rich site, to which a dimer of the serum response factor (SRF) binds (*20*, *21*). This A/T rich site in the SRE is a potential target for binding by H1 and disruption of normal gene expression. Consequently, we investigate the ability of H1 to inhibit endogenous transcription of the c-fos gene in NIH3T3 cells. Finally, because the DNA binding activity of H1 may contribute to its ability to cause cell death, its cytotoxicity profile is compared to those of H2 and H3.

Table 4: Comparison of Equilibrium Association Constants for Complexation of d(GCA_2T_2GC) versus d(GCT_2A_2GC) for H1 and H3[a]

	H1	H3
5′-GCAATTGC-3′ (**15**)		
equilibrium constant	$K_1K_2 = 1.6 \times 10^{16}\ M^{-2}$	$K_1 = 2.4 \times 10^{8}\ M^{-1}$
(ligand)$_x$−**15** stoichiometry	2:1	1:1
fluorescence intensity (λ_{max} = 450 nm)	4260	7200
5′-GCTTAAGC-3′ (**16**)		
equilibrium constant	$K_1K_2 = 1.4 \times 10^{14}\ M^{-2}$	$K_1 = 1.1 \times 10^{8}\ M^{-1}$
(ligand)$_x$−**16** stoichiometry	2:1	1:1
fluorescence intensity (λ_{max} = 480 nm)	1280	500
factor change in equilibrium constant given as K_{15}/K_{16}	110	2

[a] Determined by nonlinear least-squares fitting of an isothermal binding curve. Isothermal binding curves were generated using 10 mM potassium phosphate pH 7.0 buffer and 1 M NaCl at 16.5 °C. Equilibrium constants are given as the product K_1K_2 for 2:1 ligand:DNA stoichiometries since separation of individual equilibrium constants is not possible. The stated equilibrium constants have a standard deviation of ±80%. Complex stoichiometries were determined via spectrofluorometric titrations. Fluorescence intensities are provided in arbitrary fluorescence units × M^{-1} (oligomeric duplex). Fluorescence emission was monitored at 450 or 480 nm depending on the wavelength of maximum signal intensity for the ligand−dsDNA complex (λ_{max}).

MATERIALS AND METHODS

Organic Synthesis. ^{1}H NMR spectra were obtained on a Varian Unity Inova 400 spectrometer. Fast atom bombardment mass spectra were obtained on a VG analytical, VG-70E double-focusing mass spectrometer, with an Ion Tech Xenon Gun FAB source, and an OPUS/SIOS data interface and acquisition system. High-pressure liquid chromatography was carried out using a Hewlett-Packard series 1050 HPLC system equipped with a diode array detector. For preparative separations, an Alltech Macrosphere 300A, C8, silica, 7 μm, 250 mm × 10 mm reverse phase column was used. For analytical separations, an Alltech Macrosphere 300A, C18, silica, 7 μm, 250 mm × 4.6 mm reverse phase column was used.

H1. 2-(3-Nitro-4-aminophenyl)-6-(4-methyl-1-piperazinyl)-benzimidazole (222 mg, 0.63 mmol) was hydrogenated according to literature procedure to form the reactive diortho amine 2-(3,4-diaminophenyl)-6-(4-methyl-1-piperazinyl)benzimidazole (*22*). The diortho amine was dried under vacuum for 30 min and then without purification added to 5 mL of nitrobenzene and 1 equiv of 4-phenoxybenzaldehyde (125 mg). The solution was stirred at 140 °C for 23 h. The product was precipitated out with hexanes and collected by filtration. The crude product was then purified by flash chromatography (silica, 70:30:1 ethyl acetate/methanol/triethylamine mixture). The product was then further purified via HPLC reverse phase chromatography (0.1% aqueous trifluoroacetic acid, acetonitrile mobile phase) to yield 9.25 × 10^{-6} mol of product. Quantification of product quantity was achieved via NMR spectroscopy using an internal standard. Product purity was shown by analytical HPLC analysis: R_f = 0.1 (silica, 70:30:1 ethyl acetate/methanol/triethylamine mixture); ^{1}H NMR (D_2O + DMSO-d_6) δ 2.85 (s, 3H, CH_3-NR_2), 3−3.1 and 3.14−3.26 [two multiplets, 4H, (-CH_2)$_2$NMe, piperazine], 3.54 and 3.84 [two doublets, 4H, -(CH_2)$_2$N-Ar, piperazine], 7.04 (m), 7.1 (m), 7.18 (m), 7.23 (m), 7.28 (m), 7.4 (m), 7.66 (m), 7.84 (m), 7.93 (m), 8.1 (m), 8.32 (m) (signals detected between 7 and 8.4 ppm are due to Ar protons); LRMS (FAB) 501 $(M + H)^+$.

DNA Binding Investigations. Purified DNA oligomers were purchased from the Biomolecular Resource Center, University of California at San Francisco (San Francisco, CA). H2, H3, 0.05 wt % 3-(trimethylsilyl)propionic-2,2,3,3-d_4 acid, sodium salt in D_2O, solvents, and other reagents were purchased from Aldrich Chemical Co. Oligomeric duplexes were formed by annealing complementary oligomers by heating equal molar mixtures to 95 °C for 10 min and slowly cooling them to ambient temperature. In the case of less thermally stable oligomeric duplexes, ssDNA oligomers were heated to 90 °C and slowly cooled to 5 °C at a rate of 2 °C/min by employing a temperature programmable cell block. Molar extinction coefficients for oligomeric duplexes were approximated using an A_{260} of 16 800 M^{-1} (G·C base pair)$^{-1}$ and an A_{260} of 13 600 M^{-1} (A·T base pair)$^{-1}$. Solutions of known ligand concentrations were prepared via peak integration of the ligand's NMR spectrum where the ligand samples that were used contained a known quantity of the internal standard 3-(trimethylsilyl)propionic-2,2,3,3-d_4 acid, sodium salt (*15*). UV−vis spectra were acquired on a Cary 100 Bio UV−vis spectrophotometer equipped with a temperature programmable cell block. Data points were taken every 1 °C with a temperature ramp of 0.5 °C/min. Thermal melting temperatures were calculated by first-derivative analysis. Fluorescence spectra were obtained on a Perkin-Elmer LS50B fluorimeter equipped with a constant-temperature water bath. Solutions were excited at 345 nm. Spectrofluorometric titrations were carried out by titrating a constant concentration of DNA, usually between 2 and 100 nM, with a relatively concentrated solution of ligand. All experiments were carried out in 10 mM potassium phosphate pH 7.0 buffer and 150 mM NaCl unless specifically stated otherwise. Buffer solutions were treated with Chelex and filtered (0.22 μm).

Following determination of ligand−dsDNA complex stoichiometries, equilibrium constants for dsDNA complexation were determined by generating isothermal binding curves via spectrofluorometric titrations (titration of a dilute dsDNA solution with ligand). Equilibrium constants for ligand−dsDNA stoichiometries were calculated by fitting isothermal binding curves using either eq 1 or 2 with eq 3 (Figure 1C) (*8*, *15*). Equations 1 and 2 were employed to fit plots of fluorescence versus concentration of unbound ligand ($[L]_f$) for cases of 1:1 and 2:1 binding stoichiometries, respectively. The $[L]_f$ is calculated using eq 3. The derivation and use of eqs 1−3 have been discussed previously (*8*, *15*, *16*).

$$F = \sum \Phi_f \left(\frac{K_1[L]_f}{1 + K_1[L]_f} \right) \quad (1)$$

$$F = \sum \Phi_f \left(\frac{0.5K_1[L]_f + K_1K_2[L]_f}{1 + K_1[L]_f + K_1K_2[L]_f} \right) \quad (2)$$

where $\sum\Phi_f$ is the total fluorescence intensity upon saturation of dsDNA binding sites with ligand while K_1 and K_2 are the equilibrium association constants for the first and second binding events, respectively.

$$F = \sum \Phi_f \frac{[L]_{bound}}{n[DNA]_T} \quad (3)$$

where $[L]_{bound}$ is the concentration of ligand bound to dsDNA, n is the stoichiometry of binding, and $[DNA]_T$ is the total concentration of duplex DNA in the sample. Equation 4 was only employed for investigation of the H3−**13** and H3−**16** complexes. It was used to calculate the fluorescence signal of the ligand−dsDNA complexes adjusted for background emission of the uncomplexed ligand (F_{adj}).

$$F_{adj} = F - [L]_f \Phi_{buffer} \quad (4)$$

where $[L]_f$ is calculated using eq 3 and Φ_{buffer} is the relative fluorescence intensity of ligand in buffer as listed in Table 1 in units of fluorescence × M^{-1}.

Model Building. The molecular modeling program SYBYL was used to construct plausible ligand−dsDNA complexes. For $(H1)_2$−dsDNA and $(H3)_2$−dsDNA complexes, ligand molecules were docked into the A/T rich minor groove of a model B-DNA helix. The 1:1 H2−, H3−, and netropsin−dsDNA complex models were derived from X-ray crystal structure coordinates (*23*, *24*). Estimates of binding site size were made by measuring the length of the bound ligand along the helix axis (angstroms) and dividing that value by 3.4 Å, the average distance that separates bases along the helix axis of B-DNA.

Cell Culture. Murine NIH3T3 fibroblasts [American Type Culture Collection (ATCC)] were passaged in Dulbecco's modified Eagle's medium (DMEM) containing high levels of glucose (4500 mg/L) and sodium pyruvate (110 mg/L), supplemented with 10% calf serum. Cells were maintained at 37 °C in 5% CO_2.

Drug Handling and Storage. H1 samples were stored as lyophilized, 10 nmol aliquots at −20 °C in a light-tight box. Samples were resuspended in dH_2O (pH 3) to a final working concentration of 1 mM and stored at −20 °C until they were used. Resuspended drug was warmed to room temperature and mixed well before further dilutions into dH_2O as noted below. H2 (Aldrich Chemical Co.) was prepared in dH_2O and treated similarly.

Fluorescence Microscopy and Visualization of Drug Localization in Live NIH3T3 Cells. A total of 3.7 × 10^4 NIH3T3 cells were seeded onto 18 mm round coverslips in flat-bottomed 12-well plates and allowed to grow for 48 h. The growth medium was replaced with 0.8 mL of starvation medium (0.5% calf serum in DMEM), to which was added 10 μL of drug appropriately diluted in sterile dH_2O. After 16 h, the coverslips were pried from their wells and dip-rinsed in phosphate buffered saline. They were placed onto glass slides and observed immediately using an Olympus BX40 epifluorescence microscope equipped with a universal reflected light fluorescence vertical illuminator (Olympus, Inc.). An Olympus U-MNU filter cube was chosen to visualize the cells. Images were captured using an RT-SPOT color digital camera (Diagnostic Instruments, Inc.). Initially, the exposure time was manually set to 100 ms to accommodate the best visualization of the brightest image, and all subsequent images were captured using this exposure for any given experiment. Monochrome and color fluoromicrographs and their respective phase contrast images were captured. Duplicate coverslips for each drug exposure were evaluated in three separate experiments, and three images of different fields in each coverslip were captured to obtain representative results. Semiquantitative assessment of comparative drug intensity in the monochrome images was achieved using Diagnostic Instrument's ImagePro Plus program. The integrated optical density (IOD) of the cells was quantified and expressed per cell number in the field of view. IOD values for the three images captured per coverslip were then averaged.

Northern Blot Analysis. A total of 2.5 × 10^5 NIH3T3 cells were seeded into 60 mm plates and allowed to grow for 48 h. Following removal of growth medium and a PBS rinse, starvation medium was added. Drug dilutions were made into sterile dH_2O, and 20 μL of these dilutions was added to duplicate plates. At least three controls, which received dH_2O only, were used in each experiment. After 16 h, the cells were induced for c-fos by adding calf serum directly to the plates to a final concentration of 15% and incubating the cells at 37 °C for 30 min (previously determined to be optimal for c-fos mRNA expression). Total RNA was then isolated using TRIzol (GIBCO BRL) and electrophoresed in 1× MOPS buffer [40 mM MOPS (pH 7.0), 10 mM sodium acetate, and 10 mM EDTA] on a 1.5% denaturing agarose gel (2.2 M formaldehyde and 1× MOPS) for 4.5 h at 80 V. RNA was transferred and UV cross-linked to a GeneScreen membrane (NEN Life Science Products), incubated at 60 °C for 1 h in pre-hybe buffer [0.5 M sodium phosphate (pH 7.2), 7% SDS, 1 mM EDTA, and 1% bovine serum albumin (BSA)], and then hybridized to radiolabeled probes under the same conditions overnight. The plasmid pGEM4z-Fos (Loftstrand Laboratories, Ltd.), containing the murine c-fos coding sequence, and a phagemid containing the coding sequence for glyceraldehyde-3-phosphate dehydrogenase (G3) (ATCC) served as the probes. Each was linearized with *Hin*dIII and radiolabeled with [α-^{32}P]dCTP using Ambion's DecaPrime II kit. Blots were given two 20 min washes each in buffer A [40 mM sodium phosphate (pH 7.2), 5% SDS, 1 mM EDTA, and 0.5% BSA] and buffer B [20 mM sodium phosphate (pH 7.2), 1% SDS, and 1 mM EDTA] before being exposed to a Molecular Dynamics phosphorimaging screen and scanned with the company's STORM phosphorimager. Quantitation using the company's ImageQuant program allowed percent growth inhibition to be calculated by comparing drug-treated samples to solvent controls.

Cytotoxicity Assay. A total of 1 × 10^4 NIH3T3 cells were seeded into each well of a 24-well plate and allowed to grow for 24 h. Growth medium was removed and replaced with 0.4 mL of fresh growth medium. Drug was diluted into sterile dH_2O, and 10 μL of appropriate dilutions was added to each well. Triplicate samples for each drug concentration per experiment were carried out. In total, three experiments were performed. Cells were allowed to grow for 72 h before being trypsinized and counted using a automated particle counter (Beckman Coulter, Inc.). Percent cell survival was calculated by comparing drug-treated samples to solvent controls.

RESULTS

Synthesis of H1. H1 was originally synthesized via two consecutive reactions of diortho amines with imino ethers

to form the molecule's two benzimidazole rings (*9*). Our slightly modified approach took advantage of a reaction pioneered by Lown and co-workers that involves condensation of a diortho amine with an aldehyde in nitrobenzene solvent to give the final product (*25*). The ^{1}H NMR data for H1, previously unreported, are included in Materials and Methods.

*Spectrofluorometric Titrations of Oligomeric Duplexes **11**−**14** (15).* Similar to that of H3 (*14*, *15*), the fluorescence emission intensities of H1 and H2 greatly increase upon complexation with dsDNA. When excited at 345 nm, H1− and H2−dsDNA complexes emit a broad fluorescence signal centered at 450 nm. Table 1 lists stoichiometries of (ligand)$_x$−dsDNA complexes and their relative fluorescence intensities at 450 nm.

H1 forms 2:1 ligand−dsDNA complexes with oligomeric duplexes **11** and **12**. H2 and H3 form complexes with the same oligomers with 1:1 stoichiometries. The fluorescence spectra of H1 and H2 in pH 7.0 buffer (no DNA present) consist of a featureless straight line between 410 and 490 nm. In contrast, the uncomplexed fluorescence spectrum of H3 has a broad plateau or peak which begins to increase at ~460 nm and reaches a maximum at wavelengths of ≥480 nm.

The fluorescence spectrum of H1 in the presence of **13** contains a broad peak centered at 450 nm, characteristic of an (H1)$_x$−dsDNA complex. However, the instability and weak fluorescence of the (H1)$_x$−**13** complex prevented its stoichiometry from being determined accurately. H2− and H3−**13** complexes were found to have 2:1 stoichiometries. Titration of **13** with 1 equiv of H3 effects a pronounced peak centered at 450 nm within the fluorescence spectrum, which is characteristic of H3−dsDNA complexes. Later in the titration, at points with >1 equiv of H3, the solution's fluorescence spectrum shifts to the red and begins to resemble that expected for uncomplexed H3. As shown in Figure 1A, the high background fluorescence of uncomplexed H3 obscures the fluorescence emission of the (H3)$_2$−**13** complex. The later part of the titration (Figure 1A) describes a straight line with a slope of 1.76×10^8 M^{-1}, roughly equivalent to the value of 1.6×10^8 M^{-1} determined for uncomplexed H3 in pH 7.0 buffer. The magnitude of the fluorescence signal due to uncomplexed H3 was subtracted from each data point (eq 4) to yield a plot of $F_{adjusted}$ versus $[H3]_0$ from which the stoichiometry of the complex was determined (Figure 1B). Additionally, an isothermal binding curve was plotted and the equilibrium constant for complexation of **13** calculated (Figure 1C). Relative fluorescence intensities for ligands in the presence of oligomeric duplex **14** are equivalent to those observed in buffer only (Table 1).

*Equilibrium Association Constants for Complexation of Oligomeric Duplexes **11**−**13**.* All three ligands formed complexes with **11** and **12** at near-nanomolar concentrations (Table 1). Comparison between equilibrium constants determined in units of M^{-2} and M^{-1} can be made by calculating the square root of K_1K_2 values to give approximate equilibrium constants for individual binding events in units of M^{-1}. By this approximation, the equilibrium constant for complexation of **12** by H1 (K_1) is $\sim 1.6 \times 10^8$ M^{-1}, equivalent to the K_1 values for H2 and H3. Using this same method, K_1 values for complexation of **13** by H2 and H3 are $\sim 1.5 \times 10^7$ and 2.2×10^7 M^{-1}, respectively. Hence, binding of H2 and H3 to the oligomeric duplex **13** yields a K_1 value that is 10-fold lower than that obtained with duplex **12**.

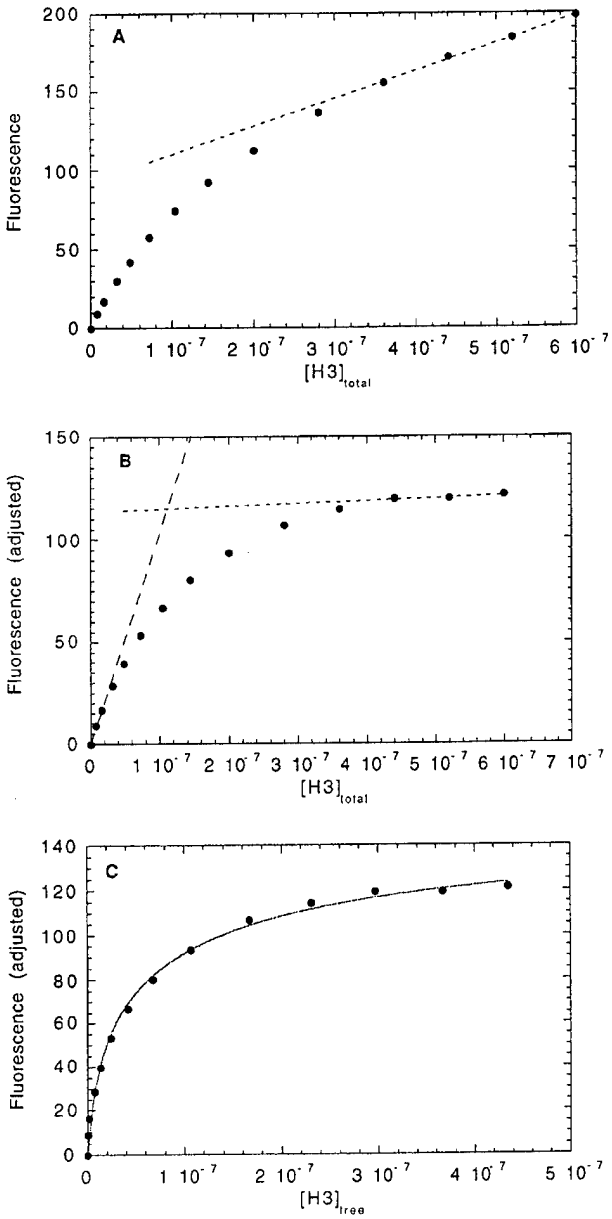

FIGURE 1: (A) Titration of 50 nM **13** with H3. The plot shows the relative fluorescence intensity at 450 nm in arbitrary units vs $[H3]_{total}$. The straight line was generated by linear least-squares fitting of data points late in the titration ($y = 92.51 + 1.77 \times 10^8$). (B) The fluorescence data from panel A have been adjusted to account for fluorescence due to uncomplexed (free) H3 using eq 4. The straight lines were generated by linear least-squares fitting of data points early and late in the titration. The two lines intersect at 100 nM, indicating formation of an (H3)$_2$−**13** complex. (C) The fluorescence data from panel B have been plotted vs $[H3]_{free}$ as calculated by eq 3. The data have been fit by a nonlinear least-squares fitting routine by employing eq 2 to determine the equilibrium association constant for complexation (for the fit shown in panel C, $R^2 = 0.99$).

The effects of ligands on the thermal stabilities of oligomeric duplexes **11**−**14** were investigated in an attempt to compare the effects with values ascertained via spectrofluorometric titrations. However, ligands had little effect on the thermal stabilities of **11**−**14** even when employing low-

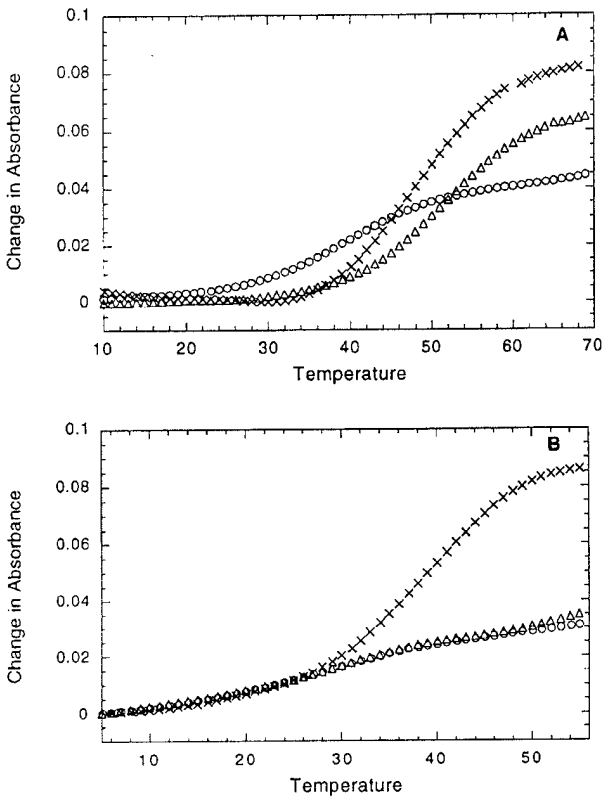

FIGURE 2: Thermal melting curves for oligomeric duplexes **15** (A) and **16** (B) and their ligand (2 equiv) complexes. Plots are shown as the change in absorption units vs degrees Celsius. Experiments were carried out using 1.5 μM duplex and 3 μM ligand, 10 mM potassium phosphate pH 7.0 buffer, and 1 M NaCl: DNA with H1 (△), DNA with H3 (×), and DNA with no ligand (○).

salt buffer (10 mM NaCl) due to intrinsically large t^0_m values (otherwise, thermal melting experiments employing **11**−**14** were carried out under the conditions provided in Table 2). H1−H3 each raised the melting point of **11** from 59 to 64 °C. Ligand Δt_m values were 1 °C or less for oligomeric duplexes **12**−**14**.

Thermal Stability of Ligand−18-mer Complexes. The thermal stabilities of (ligand)$_x$−dsDNA complexes for H1 are little affected by base pair changes of the type A/T → G/C within the TATAA region of **1** (Table 2). In contrast, H1 is very sensitive to A/T → G/C base pair changes in several other positions within **1** as illustrated by the small Δt_m values for oligomeric duplexes **7**−**9**. Thus, the increased thermal stability of the (H1)$_x$−**1** complex is attributed to complex formation between H1 and the duplex's AAATT region. Binding of **1**'s TATAA region by H1 appears to be so weak that A·T → G·C mutations have little effect on the overall thermal stability of the complexes. The Δt_m values for H2 show a similar trend to those for H1. Overall, The Δt_m values for H3 are too small to assess the ligand's sequence selectivity.

*Thermal Stability of Oligomeric Duplexes **15**−**20** and Their Ligand Complexes.* Thermal melting temperatures for a series of oligomeric duplexes are listed in Table 3 (Figure 2). Each pair contains an oligomeric duplex lacking a 5′-TpA-3′ step (**15**, **17**, and **19**) and a duplex containing a 5′-TpA-3′ dinucleotide in the middle of its A/T rich binding site (**16**, **18**, and **20**). H1 shows a tremendous preference for **15** over **16** and a significant preference for **17** over **18**. The (H1)$_2$−**15** complex has a Δt_m of 12 °C, and its melting curve shows a large increase in the hyperchromicity of the duplex. In contrast, the (H1)$_2$−**16** complex has a Δt_m of 0 °C and its melting curve shows no enhancement of the hyperchromicity of the duplex (Figure 2B). The Δt_m values for H1 complexes of **19** and **20** are equivalent. As shown in Table 3, neither H2, H3, nor netropsin demonstrates the selectively exhibited by H1.

*Equilibrium Constants for Complexation of **15** and **16** by H1 and H3.* As for oligomeric duplexes **11** and **12**, H1 formed 2:1 complexes with both **15** and **16** while H3 formed 1:1 complexes (Table 4). The K_1K_2 value for complexation of **15** by H1 was found to be 110-fold greater than for **16**. The fluorescence emission of the H3−**16** complex was found to be relatively weak. As was seen for the H3−**13** complex, the fluorescence signal of uncomplexed H3 obscured that of the H3−dsDNA complex such that it had to be subtracted out by employing eq 4. Fluorescence spectra for both H1 and H3 complexes with **16** displayed a peak with its maxima centered at ~480 nm, red-shifted approximately 30 nm compared to spectra of "normal" ligand−DNA complexes such as those for **11** and **12**. Spectrofluorometric titrations were conducted under conditions of high salt (1 M NaCl) and low temperature (16.5 °C) to stabilize the short oligomeric duplex **16**.

Estimation of Binding Site Size via Model Building. A plausible structure of a side-by-side (H1)$_2$−dsDNA complex was constructed, and its binding site size was measured to be 6.2 bp (Figures 3 and 4). With the piperazine rings not being counted, the side-by-side dimer was estimated to extend 14 Å along the helix axis and cover 4.1 bp. Binding site sizes for several other types of ligand−dsDNA complexes were also estimated (Figure 4).

Localization of H1 in Cells. To determine if H1 is able to enter nuclei, NIH3T3 cells were plated onto coverslips and exposed to the agent for 16 h in starvation medium (DMEM with 0.5% calf serum). Starvation conditions were chosen so that appropriate comparisons could be made to subsequent Northern blot experiments, which require starving NIH3T3 cells overnight in preparation for evaluation of drug effects on c-fos gene expression. Since H1 is a Hoechst analogue, cells were exposed to H2 under the same conditions to compare localization of the two compounds. The cells were not fixed or mounted following exposure to drug. Rather, the coverslips were simply transferred to glass slides and viewed immediately, when the cells were still alive. Representative fluoromicrographs (Figure 5A′,B′) of cells exposed to 1 μM H1 or 0.5 μM H2 show that both compounds localize exclusively to nuclei with similar staining patterns. While diffuse nuclear staining is observed, small regions of high drug concentrations exist as evidenced by areas of high fluorescence intensity. This speckled pattern for either drug does not always correspond to nucleoli, visible in the corresponding phase contrast micrographs. Overall, treatment of cells with 0.5 μM H2 yields nuclei that are slightly brighter than those treated with 1 μM H1. The staining on any given coverslip was fairly even, with little variation between viewing fields. These and additional images captured using a range of drug concentrations as well as semiquantitative analysis of the resulting fluoromicrographs (data not shown) demonstrated that approximately 4 times more H1 was

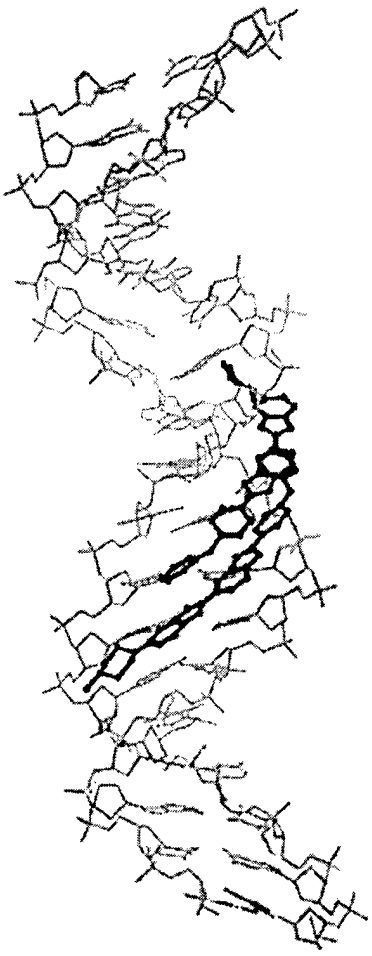

FIGURE 3: Computer-generated model of a plausible $(H1)_2$–dsDNA side-by-side antiparallel staggered complex.

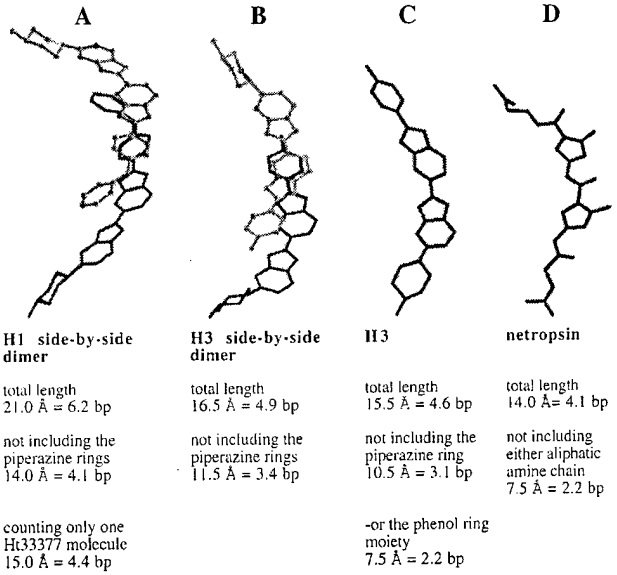

FIGURE 4: Ligands were extracted from computer-generated $(ligand)_x$–dsDNA models and are pictured in their dsDNA-bound conformations (DNA atoms are not shown so that ligand curvature can be better displayed). Estimated binding site sizes of $(ligand)_x$–dsDNA complexes are provided below the pictured ligands. Also generated but not pictured was the 1:1 H2–dsDNA complex whose binding site size was estimated to be 17.5 Å (5.1 bp).

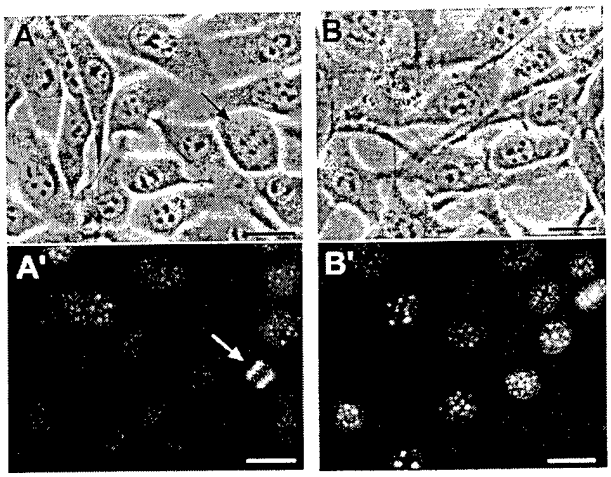

FIGURE 5: Localization of H2 and H1 to nuclei in live NIH3T3 cells. (A and A′) Representative phase contrast and fluoromicrographs, respectively, of NIH3T3 cells exposed to 1 μM H1 for 16 h. (B and B′) Representative phase contrast and fluoromicrographs, respectively, of NIH3T3 cells exposed to 0.5 μM H2 for 16 h. Images were captured immediately following transfer of coverslips of live cells to glass slides. H1 localizes to nuclear material, even in actively dividing cells (arrows). The bars are 10 μm in length.

required to attain the same level of H2 fluorescence intensity. A cell captured in the process of mitosis (Figure 5A,A′, arrows) shows that H1 associates with nuclear material even during division.

Effects of H1 on Endogenous c-fos mRNA Expression. The presence of H1 in the nucleus suggested that it may have DNA template effects in whole cells. The c-fos promoter has been established in the Beerman lab as a model system for evaluating the effect of DNA-binding drugs on transcription (*17*). Therefore, H1's effects on endogenous transcription of the c-fos gene in whole cells were evaluated. NIH3T3 cells were exposed to H1 for 16 h under starvation conditions before being serum induced for 30 min, which was previously determined to be an optimal time course for c-fos mRNA production. Control cells upregulate c-fos in response to serum stimulation, as detected in Northern blots (Figure 6A, first two lanes). Glyceraldehyde-3-phosphate dehydrogenase (G3), a constitutively expressed housekeeping gene, was used here as a loading control. The half-lives of G3 and c-fos mRNA are 8 h and 30 min, respectively. Therefore, drug effects on the total amount of G3 mRNA are expected to be minimal after only 16 h. Treatment of cells with H1 led to a dose-dependent inhibition of c-fos transcription, as evidenced by the loss in signal intensity (Figure 6A, lanes 3–6). There was no detectable drug effect on G3 expression, nor was there detection of shorter transcripts for either c-fos or G3. Quantitation of the Northern blot autoradiographs allowed drug-treated samples to be compared to controls, yielding a measurement of percent inhibition of c-fos expression (Figure 6B). A maximum concentration of 10 μM H1 was used, resulting in approximately 70% inhibition of expression. Inhibition of expression by 50% (the IC_{50} value) occurred at approximately 4 μM. To note, H2 had very little effect on c-fos expression at this time point, although inhibition was seen for shorter exposures of 1 and 4 h (*17*). In contrast, H1 had no effect on c-fos expression after these shorter exposures (data not shown).

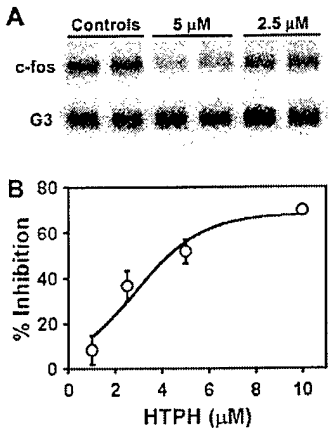

FIGURE 6: Effect of H1 on c-fos mRNA expression. (A) Representative Northern blot results from NIH3T3 cells exposed to H1 at the concentrations shown for 16 h under starvation conditions (0.5% serum). Following induction of c-fos by increasing the serum concentration to 15% for 30 min, 20 μg of total RNA was isolated and electrophoresed on a denaturing agarose gel. Subsequent blots were hybridized with radiolabeled probes for c-fos or G3. (B) Quantitation of H1's effects on c-fos cellular transcription was achieved through densitometric analysis of blots as shown in panel A. Comparison of drug-treated lanes to controls yielded percent inhibition for each treatment. The results are the means of four experiments (mean ± standard error).

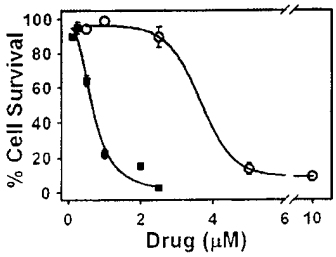

FIGURE 7: Cytotoxicity of H1 in NIH3T3 cells. Cells were allowed to grow in the presence of either H1 (○) or H2 (■) for 3 days before being trypsinized and counted. Percent cell survival was calculated by comparing the total cell number in drug-treated samples to solvent controls. The results are the means of triplicate samples in three separate experiments (mean ± standard error).

Cytotoxic Effects of H1. NIH3T3 cells were continuously exposed to a range of H1 or H2 concentrations for 3 days before being trypsinized and counted. Total cell numbers from each treatment were compared to appropriate solvent controls to yield percent cell survival. As shown in Figure 7, the concentration of H1 needed to kill 50% of the cells (LD_{50}) was 3.4 μM. By 10 μM H1, more than 90% cell death was observed. In comparison, the LD_{50} of H2 was 0.6 μM, and more than 95% of the cells died by 2.5 μM. Treatment of cells with 100 μM H3 over the same time period effected approximately 50% cell death.

DISCUSSION

Spectrofluorometric titrations were employed in an effort to determine the dsDNA binding characteristics of H1 (Table 1). H1 is shown to form $(H1)_2$–dsDNA complexes and to require a minimum binding site of 4 A/T bp. In contrast, H2 and H3 will form complexes with 3 A/T bp, although both ligands do prefer larger sites. The requirement of only 3 A/T bp for strong binding is an interesting observation since it is commonly reported that these agents require at least 4 A/T bp (*1*, *26*). Additionally, the $(H3)_2$–**13** complex stoichiometry of 2:1 is rather uncommon since such a stoichiometry has been previously reported only once for H3 (*16*). The difference in binding stoichiometries between H1 and H3 for normal size binding sites (4–5 bp) is not unexpected. It has been previously noted by this laboratory that changes in the terminal phenyl ring of H3 can alter the stoichiometries of its dsDNA complexes (*15*). The possibility that ligand–dsDNA stoichiometries determined via spectrofluorometric titrations might be misleading due to alternative modes of ligand binding has also been considered. H3 is know to interact with dsDNA by a secondary form of binding [probably intercalation (*27*)] which occurs at relatively high ligand:base pair ratios, shows no apparent base pair specificity, and is weakened considerably with increasing ionic strength (*28*). Relative fluorescence intensities for ligands in buffer with and without **14** were compared to determine if secondary forms of binding could be affecting our fluorescence measurements. The relative fluorescence intensities of H1–H3 were found to be unaffected by the addition of **14**. Thus, either no secondary form of dsDNA binding occurs at the concentrations of dsDNA that are employed, or they occur but are not detected by fluorescence spectroscopy. Either way, secondary forms of binding by H3 can only affect the observed stoichiometries if they occur in competition with H3's primary form of dsDNA binding (minor groove binding of A/T rich sites). This is unlikely since H3's secondary form of binding is roughly 100–1000-fold weaker than its primary form (*28*, *29*). Additionally, our observed stoichiometries (Table 1) are inconsistent with a competitive but nonspecific secondary form of binding.

A plausible $(H1)_2$–dsDNA complex constructed via model building illustrates the curvature of the two H1 molecules when placed in a slightly staggered, side-by-side, and antiparallel arrangement within the minor groove (Figure 3). This type of side-by-side arrangement within the minor groove has precedence since monocationic minor groove binders such as distamycin-based compounds have a propensity to complex dsDNA in this manner (*2*, *30–32*). When the molecules are staggered, the placement of the phenoxy ether ring of one H1 molecule adjacent to the bulky piperazine ring of the other is avoided. Structural investigations of side-by-side complexes of other minor groove binders such as polyamides with dsDNA consistently show the two polyamide molecules of the trimeric complex to be both antiparallel and staggered (*2*, *30–32*).

Inspection of the $(H1)_2$–dsDNA model suggests a binding site size of 6.2 bp versus an experimentally determined minimum binding site of 4 A/T bp (Figure 4). The 2 bp difference is interpreted as a lack of binding specificity on the part of H1's piperazine rings. Some X-ray crystal structures of H3–dsDNA complexes show the bisbenzimidazole rings of H3 bound to an A/T rich binding site while the piperazine ring rests against an adjacent G·C base pair (*24*, *33*). When the piperazine rings are excluded, the H1 side-by-side complex covers 4.1 bp, in agreement with the experimentally determined minimum A·T rich binding site size.

If the piperazine rings of $(H1)_2$–dsDNA complexes are capable of resting in the wider minor groove of G/C base pairs, it stands to reason that the piperizine rings of H2 and H3 might also. The binding site size of an $(H3)_2$–dsDNA

side-by-side complex was estimated to be 4.9 bp versus an experimentally determined minimum binding site size of 3 A/T bp. When the piperazine rings are excluded, the H3 side-by-side complex covers ~3.4 bp, roughly equivalent to the experimentally determined minimum A/T rich binding site size. The side-by-side $(H3)_2$–dsDNA complex was constructed in a manner similar to that of the $(H1)_2$–dsDNA complex with the two H1 molecules placed in a slightly staggered, side-by-side, and antiparallel arrangement within the minor groove.

As shown in Table 2, H1 selectively stabilizes those oligomeric duplexes which contain 4 bp A/T rich binding sites free of a 5′-TpA-3′ dinucleotide step (i.e., 4 bp "A-tracts"). A similar trend was observed for H2. It has been suggested that the 5′-TpA-3′ step produces a DNA structural alteration which discourages minor groove binding (*23*, *34*). Dickerson and co-workers have reported that A/T rich regions of dsDNA usually adopt poly(dA)/poly(dT)-like structures (termed A-tracts) (*35*, *36*). A-tracts consist of successive adenine bases which stack in a rigid and unbent column. Dickerson and co-workers emphasize that the A-tract structure can incorporate 5′-ApT-3′ steps, but is broken by 5′-TpA-3′ steps.

It was previously reported that the terbenzimidazole 5PTB was capable of selectively stabilizing **17** relative to **18** (*37*). The duplex **17** (5′-GA_4T_4C-3′) contains an uninterrupted 8 bp A tract, assumes a rigid A-tract conformation, and exhibits an anomalously slow migration in a polyacrylamide gel (*38*). The other duplex, **18** (5′-GT_4A_4C-3′), contains two 4 bp A tracts separated by a TpA dinucleotide, assumes a normal "B-like" conformation, and, on the basis of its molecular weight, migrates normally. The duplexes have also been shown to possess differential thermodynamic properties (**17** possesses a larger t^0_m than **18**) (*37*). These complexes have identical base compositions, yet evidence suggests that **17** is conformationally distinct from **18**. It was argued that the origin of 5PTB's selectivity was an entropically driven preference for highly solvated A-tracts such as those found within **17** (*37*). We have found that H1 also selectively stabilizes **17** relative to **18** (Table 3). We have also employed two additional pairs of oligomeric duplexes differing in the lengths of their A·T tracts: the pair **15** (5′-GCA_2T_2GC-3′) and **16** (5′-GCT_2A_2GC-3′), and the pair **19** (5′-GA_6T_6C-3′) and **20** (5′-GT_6A_6C-3′). Both previously uncharacterized pairs of duplexes exhibit differential thermodynamic properties similar to those of **17** and **18**. As shown by the values listed in Table 3, those duplexes containing a 5′-TpA-3′ dinucleotide have lower t^0_m values than those without. The $\Delta\Delta t_m$ values listed in Table 4 are unimpressive for all the ligands investigated except for H1 which selectively stabilizes **15** and **17** over **16** and **18** with $\Delta\Delta t_m$ values of 12 and 7 °C, respectively. The equilibrium constants for complexation of **15** with H1 were determined to be 110-fold larger than those for **16** (Table 4).

The selectivities of the different ligands can be explained in terms of the number of bases covered by their sequence selective moieties. As discussed earlier, the piperazine rings of the H1 side-by-side dimer are incapable of differentiating between A/T and G/C base pairs. Presumably, they are also incapable of selecting against 5′-TpA-3′ steps. When the piperazine rings are excluded, the H1 side-by-side dimer is estimated to have a sequence selective binding region which covers about 4.2 bp and prefers A-tracts over A/T rich sites containing 5′-TpA-3′ steps. H1 does not selectively stabilize **19** over **20** since H1 side-by-side complex formation may occur with an A-tract on either side of the dinucleotide 5′-TpA-3′ located within the middle of **20**. When the piperazine ring is not included, H2 is estimated to cover roughly 3.7 bp. The lack of selectivity of H2 for **17** over **18** can perhaps be explained in that the ligand can bind an A-tract on either side of the dinucleotide 5′-TpA-3′ located in the middle of **18**. However, this same rationale fails to explain H2's lack of selectivity between the shorter duplexes **15** and **16** unless the sequence selective moieties of H2 cover significantly less than 3.7 bp. The phenolic group of H3 has been shown by NMR spectroscopic investigations to rapidly rotate (at a rate of $>10^3$ s^{-1}) while the molecule is still bound within the minor groove (*39*, *40*). We propose that the phenol ring of H1 may not significantly contribute to the ligand's sequence selectivity. Alone, the bisbenzimidazole rings of H2 and H3 cover roughly 2.2 bp. Thus, H2 may complex **16** with its bisbenzimidazole rings on one side or the other of the 5′-TpA-3′ step. Netropsin's lack of selectivity between duplexes **15** and **16** can also be rationalized in terms of the size of its sequence selective binding site. When the agent's highly flexible aliphatic moieties are not included, netropsin is also estimated to recognize roughly 2.2 bp.

The subcellular distribution of H1 was investigated in an effort to determine if H1 was capable of associating with DNA in live cells (Figure 5). Visualization of H1 by fluorescence microscopy shows that this compound selectively localizes in the nucleus. H1 is therefore capable of traversing both the cytoplasmic and nuclear membranes and accumulating in the nucleus in a pattern suggestive of DNA binding. As previously mentioned, DNA binding agents such as H1 have the potential to act as template poisons by preventing the binding of various nuclear proteins to their DNA target sites (*7*, *41*). However, the ability of a ligand to bind DNA in vitro does not ensure its cellular activity. We demonstrate here that H1 inhibits endogenous transcription of the c-fos gene in whole cells at micromolar concentrations (Figure 6). These results suggest that H1 possesses the ability to reach its cellular target and is capable of inhibiting the binding of regulatory proteins. Our finding that H1 causes cell death at micromolar concentrations demonstrates that it is capable of disrupting normal cell function. The results of our cellular investigations for H1 and H2 were fairly similar. H3 showed little cellular activity in accord with literature reports (*10*, *11*). Apparently, alkylation of the terminal phenoxy moiety of H3 imparts upon both these molecules a superior ability to traverse the cell membrane and reach its DNA target.

CONCLUSIONS

The formation of a side-by-side complex with dsDNA appears to impart upon H1 a rare degree of sequence specificity. This may be due to the aromatic rings of the H1 side-by-side complex being held more rigidly in comparison to a 1:1 complex as for H2 or H3. Only two other types of minor groove binding agents are capable of distinguishing between different A/T rich sequences, and of the three, the mechanism by which H1 achieves its specificity is unique. The previously mentioned terbenzimidazole 5PTB forms only 1:1 complexes with **15** and **16** (*37*). Dervan and co-workers

have investigated a series of heteropolyamide hairpin-type molecules which contain various combinations of pyrrole, imidazole, and hydroxypyrrole subunits (*42*, *43*). These types of heteropolyamide molecules have, in some cases, demonstrated the ability to distinguish between A·T and T·A base pairs. However, the mechanism of heteropolyamide specificity is intrinsically different from that for H1 since heteropolyamide specificity is not related to the presence of A-tracts (heteropolyamides target sites which contain both A/T and G/C base pairs).

Evaluation of H1's biological potential revealed that it possesses many characteristics that are desirable for a DNA-reactive drug, including cellular permeability and nuclear localization, and an ability to decrease the level of gene expression. We believe that the unique mechanism of H1's specificity, combined with its ability to localize in nuclear DNA and inhibit RNA transcription, makes it a valuable starting point for the development of other sequence selective agents.

REFERENCES

1. Reddy, B. S. P., Sondhi, S. M., and Lown, J. W. (1999) *Pharmacol. Ther. 84*, 1−111.
2. Sharma, S. K., Tandon, M., and Lown, J. W. (2000) *J. Org. Chem. 65*, 1102−1107.
3. Xuereb, H., Maletic, M., Gildersleeve, J., Pelczer, I., and Kahne, D. (2000) *J. Am. Chem. Soc. 122*, 1883−1890.
4. Zimmer, C., and Wähnert, U. (1986) *Prog. Biophys. Mol. Biol. 47*, 31−112.
5. Boger, D. L., and Johnson, D. S. (1996) *Angew. Chem., Int. Ed. 35*, 1438−1474.
6. Bailly, C., and Chaires, J. B. (1998) *Bioconjugate Chem. 9*, 513−538.
7. Chiang, S. Y., Bruice, T. C., Azizkhan, J. C., Gawron, L., and Beerman, T. A. (1997) *Proc. Natl. Acad. Sci. U.S.A. 94*, 2811−2816.
8. Satz, A. L., and Bruice, T. C. (2001) *J. Am. Chem. Soc. 123*, 2469−2477.
9. Loewe, V. H., and Urbanietz, J. (1974) *Arzneim.-Forsch. 24*, 1927−1933.
10. Harapanhalli, R. S., Howell, R. W., and Rao, D. V. (1994) *Nucl. Med. Biol. 21*, 641−647.
11. Finlay, G. J., and Baguley, B. C. (1990) *Eur. J. Cancer 26*, 586−589.
12. Bruice, T. C., Sengupta, D., Blasko, A., Chiang, S. Y., and Beerman, T. A. (1997) *Bioorg. Med. Chem. 5*, 685−692.
13. Dorn, A., Affolter, M., Muller, M., Gehring, W. J., and Leupin, W. (1992) *EMBO J. 11*, 279−286.
14. Loontiens, F. G., Regenfuss, P., Zechel, A., Dumortier, L., and Clegg, R. M. (1990) *Biochemistry 29*, 9029−9039.
15. Satz, A. L., and Bruice, T. C. (2000) *Bioorg. Med. Chem. 8*, 1871−1880.
16. Browne, K. A., He, G. X., and Bruice, T. C. (1993) *J. Am. Chem. Soc. 115*, 7072−7079.
17. White, C. M., Heidenreich, O., Nordheim, A., and Beerman, T. A. (2000) *Biochemistry 39*, 12262−12273.
18. Nigg, E. A., and Treisman, R. (1994) *Curr. Opin. Cell Biol. 6*, 333−334.
19. Inada, K., Okada, S., Phuchareon, J., Hatano, M., Sugimoto, T., Moriya, H., and Tokuhisa, T. (1998) *J. Immunol. 161*, 3853−3861.
20. Treisman, R. (1985) *Cell 42*, 889−902.
21. Norman, C., Runswick, M., Pollock, R., and Treisman, R. (1988) *Cell 55*, 989−1003.
22. Ebrahimi, S. E. S., Bibby, M. C., Fox, K. R., and Douglas, K. T. (1995) *Anti-Cancer Drug Des. 10*, 463−479.
23. Ward, B., Rehfuss, R., Goodisman, J., and Dabrowiak, J. C. (1988) *Biochemistry 27*, 1198−1205.
24. Carrondo, M., Coll, M., Aymami, J., Wang, A. H. J., Vandermarel, G. A., Vanboom, J. H., and Rich, A. (1989) *Biochemistry 28*, 7849−7859.
25. Yadagiri, B., and Lown, J. W. (1990) *Synth. Commun. 20*, 955−963.
26. Harshman, K. D., and Dervan, P. B. (1985) *Nucleic Acids Res. 13*, 4825.
27. Moon, J. H., Kim, S. K., Sehlstedt, U., Rodger, A., and Norden, B. (1996) *Biopolymers 38*, 593−606.
28. Jorgenson, K. F., Varshney, U., and van de Sande, J. H. (1988) *J. Biomol. Struct. Dyn. 5*, 1005−1023.
29. Rao, K. E., and Lown, J. W. (1991) *Chem. Res. Toxicol. 4*, 661−669.
30. Kopka, M. L., Goodsell, D. S., Han, G. W., Chiu, T. K., Lown, J. W., and Dickerson, R. E. (1997) *Structure 5*, 1033−1046.
31. Wemmer, D. (1998) *Nat. Struct. Biol. 5*, 169−171.
32. Kielkopf, C. L., Baird, E. E., Dervan, P. B., and Rees, D. C. (1998) *Nat. Struct. Biol. 5*, 104−109.
33. Pjura, P. E., Grzeskowiak, K., and Dickerson, R. E. (1987) *J. Mol. Biol. 197*, 257−271.
34. Chen, F. M., and Sha, F. (1998) *Biochemistry 37*, 11143−11151.
35. Goodsell, D. S., Kaczorgrzeskowiak, M., and Dickerson, R. E. (1994) *J. Mol. Biol. 239*, 79−96.
36. Dickerson, R. E., Goodsell, D., and Kopka, M. L. (1996) *J. Mol. Biol. 256*, 108−125.
37. Pilch, D. S., Xu, Z. T., Sun, Q., LaVoie, E. J., Liu, L. F., and Breslauer, K. J. (1997) *Proc. Natl. Acad. Sci. U.S.A. 94*, 13565−13570.
38. Chen, J.-H., Seeman, N. C., and Kallenbach, N. R. (1988) *Nucleic Acids Res. 16*, 6803−6815.
39. BostockSmith, G. E., Laughton, C. A., and Searle, M. S. (1998) *Nucleic Acids Res. 26*, 1660−1667.
40. Embrey, K. J., Searle, M. S., and Craik, D. J. (1993) *Eur. J. Biochem. 211*, 437−447.
41. Mote, J., Ghanouni, P., and Reines, D. (1994) *J. Mol. Biol. 236*, 725−737.
42. Urbach, A. R., Szewczyk, J. W., White, S., Turner, J. M., Baird, E. E., and Dervan, P. B. (1999) *J. Am. Chem. Soc. 121*, 11621−11629.
43. Melander, C., Herman, D. M., and Dervan, P. B. (2000) *Chem. Eur. J. 6*, 4487−4497.

BI0103415

Title: Inhibiting transcription factor/DNA complexes using Hoechst-based fluorescent microgonotropens (FMGTs)

Christine M. White[a], Alexander L. Satz[b], Loretta S. Gawron[a], Thomas C. Bruice[b], and Terry A. Beerman[a]*

From the [a]Department of Pharmacology and Therapeutics, Roswell Park Cancer Institute, Elm and Carlton Streets, Buffalo, New York 14263, and the [b]Department of Chemistry, University of California, Santa Barbara, California 93106

*To whom correspondence should be addressed: Terry Beerman, Department of Pharmacology and Therapeutics, Roswell Park Cancer Institute, Elm and Carlton Streets, Buffalo, New York 14263. Tel: (716) 845-3443; Fax: (716) 845-8857; E-mail: Terry.Beerman@Roswellpark.org

Abbreviations: TF, transcription factor; MGT, microgonotropen; FMGT, fluorescent microgonotropen; SRE, serum response element; SRF, serum response factor; TC, ternary complex; EMSA, electrophoretic mobility shift assay; bp, base pair(s); oligo, oligonucleotide; topo II, topoisomerase II.

Keywords: DNA-binding drug, Hoechst 33342, Hoechst 33258, transcription factor, minor groove, microgonotropen

ABSTRACT:

The fluorescent microgonotropens (FMGTs) are A/T selective, minor groove-binding ligands based upon the bisbenzimidazole structure of Hoechst compounds. Polyamine tails extending from these agents electrostatically interact with the phosphodiester backbone of DNA in the major groove, endowing them with high binding affinity. Here, we assess the ability of these agents to inhibit transcription factor (TF) binding to DNA and explore whether their ability to contact both grooves enhances the effectiveness of classical minor groove-binders. A series of FMGTs (FMGTs 1, 2, 3, and 5), with polyamine tails of varying lengths and degrees of branching, were compared to their parent analogs, Hoechst 33342 and Hoechst 33258, for effects on TF complex formation on the c-fos serum response element (SRE). The FMGTs were up to 50 times more potent than the Hoechst compounds in inhibiting TF/SRE interactions in electophoretic mobility shift assays. The FMGTs also inhibited c-fos promoter-driven cell-free transcription and topoisomerase II mediated activity in nuclei. These studies establish the potential of FMGTs as TF/DNA complex inhibitors in cell-free systems and provide insight into the relationship between their chemical structure and their biological activities.

INTRODUCTION:

The design, synthesis and evaluation of DNA-binding agents as inhibitors of biologically relevant activities continue to be areas of intense research. Small molecule DNA-binding ligands are capable of interfering with the function of proteins that interact with DNA, including transcription factors (TFs) and topoisomerases (topos) [1, 2]. For example, the activity of TFs, proteins that play an integral role in the coordinated and regulated expression of genes by recognizing and binding to specific sequences in gene promoters, can be inhibited by a variety of DNA-binding drugs [3, 4]. Increasing focus has been made on using drugs to interfere with TF recognition of target sites in order to inhibit gene expression.

Drugs that bind reversibly to DNA can be categorized according to their mode of binding, their groove selectivity and their sequence preference. For example, the minor groove-binding drug family includes the naturally occurring oligopeptide distamycin and the synthetic bisbenzimidazole Hoechst compounds, both of which show preference for A/T rich sites. Previous work has demonstrated that these agents effectively inhibit TF/DNA interactions in cell-free systems [2]. Such studies indicated that the sequence and groove preferences of both TFs and drugs are important factors to consider when designing novel agents to disrupt desired TF/DNA complexes. This is reflected by the ability of distamycin to inhibit the TATA binding protein from binding to its A/T rich target sequence in the minor groove in cell-free assays but its ineffectiveness in preventing complex formation between early growth response factor and its G/C rich target sequence in the major groove [5]. However, distamycin successfully inhibits the binding of other major groove binding proteins, such as homeodomain peptides, to their A/T rich target sites [6].

The majority of DNA-binding proteins interact with the major groove, presumably because it bears most of the recognizable nucleotide functional groups [7]. Many other proteins utilize both grooves [8, 9]. Because of limited success at creating compounds targeting both grooves, many drug design strategies have focused on improving the specificity and affinity of minor groove-binding drugs [10]. Their ability to approach DNA from the opposite groove and to change the conformation of the double helix upon binding allows them to inhibit TF complex formation in the major groove as discussed above. While drugs that bind solely to the minor groove are successful in inhibiting various TF/DNA complexes, drugs that extend into both grooves with increased affinity might have the potential to be more effective inhibitors of a wider range of TFs.

Microgonotropens (MGTs), developed by the Bruice laboratory, are novel agents that bind selectively to A/T rich sequences in the minor groove, but make electrostatic contact with the phosphodiester backbone in the major groove through polyamine tails [11]. This allows these ligands to bind DNA with very high affinity ($K_a = 10^9\ M^{-1}$ or greater) and results in significant bending of the helix [12]. The structures of the first generation of MGTs were based upon a tripyrrole moiety similar to distamycin, with polyamine tails of varying lengths and degrees of branching extending from the central pyrrole. Cell-free experiments revealed that the most successful ligand, MGT-6a, was several orders of magnitude more potent than distamycin in preventing the TF E2F1 from binding to its target sequence [13]. E2F1 contacts both grooves of DNA at a mixed A/T and G/C rich site, a mode of binding that proved to be a uniquely sensitive target for the action of these ligands. While the inhibitory potencies of the MGTs primarily correlated with their DNA-binding affinities, their effectiveness was also dependent

upon the structure and length of their polyamine tails, suggesting that both factors are important determinants to consider when designing such agents to interfere with TF complex formation.

The success of first generation MGT design led to modification of alternative minor groove-binding "anchors" in order to improve their effectiveness as inhibitors of TF binding. The ease of synthesis of the Hoechst compounds made this class of agents a convenient starting point for the covalent attachment of major groove-binding functional groups. Additionally, members of this family, such as Hoechst 33342 or Hoechst 33258 (Fig. 1A), have been shown to inhibit TF/DNA complex formation in a variety of systems [14, 15]. Attaching polyamine tails to the *meta* position of the terminal benzene ring of the Hoechst structure resulted in fluorescent microgonotropens (FMGTs) (Fig. 1B) [16, 17]. As Hoechst analogues, the FMGTs bind to A/T rich sequences in the minor groove, but like their MGT predecessors are capable of contacting the phosphate backbone of DNA in the major groove. Moreover, the FMGTs can bind DNA in 2:1 stoichiometries at some A/T rich sites. Association constants determined by fluorescent spectroscopy indicate that FMGT-1, with a K_a of $4.8 \times 10^9\ M^{-1}$, has a five-fold higher affinity for DNA than Hoechst 33258 [16]. This new application of the MGT design concept therefore has the potential to enhance the ability of Hoechst-based structures to inhibit certain TF/DNA associations.

A model system using the serum response element (SRE) of the human c-fos promoter as a target was established to analyze the abilities of DNA reactive ligands to inhibit TF binding to their target sites [18]. The transcriptional upregulation of c-fos depends upon the activation of TFs constitutively bound to the SRE in a ternary complex (TC) (reviewed in [19]). The binding of a homodimer of serum response factor (SRF) to an A/T rich CArG box is required for

recruitment of Elk-1 to a GGA-containing *ets* motif (see Fig. 2). Activation of the TC through phosphorylation of Elk-1 is necessary and sufficient for c-fos transcription [20]. The mode of binding of SRF and Elk-1 makes these factors amenable for targeting by FMGTs. Both factors primarily contact their consensus sequences in the major groove, but also make contact with surrounding base pairs and the phosphodiester backbone in the minor groove [21, 22]. Occupation and deformation of the A/T rich SRF binding site in the minor groove by FMGTs combined with the extension of their polyamine tails into the neighboring major groove may therefore lead to effective disruption of both SRF and Elk-1 binding.

While the concept of equipping minor groove-binding ligands with major groove-associating functional groups proved useful in improving the ability of the polypyrrole-based MGTs to inhibit TF/DNA interactions, biological analysis of these novel class of compounds has been somewhat limited [13, 23], and the biological activities of the FMGTs have not yet been tested. Our lab has therefore undertaken to further analyze and characterize the FMGTs in order to determine whether the above concept can also enhance the inhibitory ability of other minor groove binders. The c-fos model was used to evaluate and compare the effects of FMGT-1, FMGT-2, FMGT-3 and FMGT-5 with those of their parent compounds, Hoechst 33342 and Hoechst 33258. This model allowed us to evaluate the FGMTs in a more rigorous fashion compared to previous MGT evaluations, since it involves assessing drug effects on more than one TF in increasingly complex assays. The ability of the drugs to inhibit SRF and Elk-1 complex formation on the SRE were determined using electrophoretic mobility shift assays. Their effects on c-fos promoter-driven cell-free transcription assay were also analyzed. Since the cellular activity of the novel FMGTs have never been investigated, we determined their effects

on endogenous c-fos expression in whole cells using Northern blots. Our lab previously showed that minor groove-binding agents, including Hoechst analogues, are capable of decreasing topo II mediated activities in isolated nuclei. This system allowed us to examine the general effects of FMGTs on DNA template function without the complications of cellular uptake. Our findings can potentially be used as a basis for future FMGT structural modifications that may improve their potency and effectiveness. Additionally, these studies suggest that this drug design concept may be extended to other classes of minor groove-binding drugs as a means to enhance their potential as TF/DNA inhibitors.

MATERIALS AND METHODS:

Drugs – Stocks of 20 mM Hoechst 33342 or Hoechst 33258 (Aldrich Chemical Co., Milwaukee, WI) were prepared in distilled water. FMGT synthesis is described elsewhere [16, 17]. Aliquots of FMGTs were stored lyophilized at –20°C and resuspended in 25% dimethyl sulfoxide to 1 mM in distilled water before use. All drug solutions were stored in the dark at –20°C and diluted into distilled water immediately before use.

Electrophoretic mobility shift assays (EMSAs) – Oligonucleotide (oligos) and protein preparation and reaction conditions were as described elsewhere [18]. Briefly, for the forward EMSAs, 1 nM radiolabeled oligo and varying concentrations of drug were incubated in binding buffer (see below) at room temperature for 30 min before purified TFs were added. The double stranded oligo sequences were designated SRE (5'-ACACAGGATGTCCATATTAGGACA-3') and E74 (5'-GATACCGGAAGTCCATATTAGGAC-3'). After a subsequent 30 min incubation,

the complexes were electrophoresed at 200 V in 0.5x TBE (44.6 mM Tris base, 44.5 mM boric acid, and 10 mM EDTA) on a 5% polyacrylamide gel for up to 2 h, with adequate separation of complexed and free DNA occurring by a minimum of 30 min. The dried gels were exposed to a phosphorimager cassette (Molecular Dynamics, Sunnyvale, CA) and scanned with a Molecular Dynamics phosphorimager. Autoradiographs were quantitated using the manufacturer's ImageQuant program.

Cell culture – NIH3T3 cells were maintained as described previously [18]. Logarithmically growing HeLa cells were maintained in suspension cultures in Joklik-modified minimal essential medium (S-MEM) supplemented with 5% fetal bovine serum and 5% horse serum at 37°C.

Cell-free transcription – Nuclear extracts were prepared from NIH3T3 cells and stored at –80°C until use [18]. In brief, the reaction was carried out by combining 0.5 μg of an Sph-1 digested plasmid containing the full length human c-fos promoter (pFosLuc19) with drug and 5 μL buffer D (20 mM Hepes/KOH, pH 7.9, 100 mM KCL, 20% glycerol, 0.2 mM EDTA, 0.2 mM EDTA, 12.5 mM $MgCl_2$, 2 mM DTT, and 1 mM PMSF) to a final volume of 9 μL. After 30 min at 30°C, 15 μg of NIH3T3 nuclear lysate was added, the final volume was adjusted to 19 μL with buffer D and the reaction was incubated an additional 15 min. Addition of a reaction mixture containing α-[^{32}P]CTP and the subsequent purification and electrophoresis of the resulting radiolabeled 750 base transcript were accomplished using the protocol by Chiang, et al. [24]. A radiolabeled, 250 base T3 transcript of pGEM4z (Promega) was used as an internal control. Autoradiography and quantitation were as described for the EMSAs. The c-fos transcript was

normalized to the internal control in each lane before comparisons between drug-treated samples and controls were made.

Northern blot assay – Analysis of drug effects on endogenous c-fos expression in NIH3T3 cells, including drug treatment, RNA isolation, electrophoresis and hybridization to radiolabeled probes, was according to published procedure [18]. Keeping with this protocol, NIH3T3 cells were exposed to the FMGTs for 16 h under starvation conditions (low serum media) before subsequent serum induction and isolation of total RNA.

Topo II activity assay – Nuclei isolation and subsequent topo II assays were carried out as described by Beerman, et al., and Woynarowski, et al., respectively, with some modification [25, 26]. In brief, HeLa suspension cultures were radiolabeled with [^{14}C]thymidine (0.03 μCi/ml) for 24 h. All subsequent centrifugations were done at 4°C. Cells were pelleted for 4 min at 100 x g and rinsed with cold nuclei isolation buffer (NIB: 2 mM KH_2PO_4, 150 mM NaCl, 1 mM EGTA, and 5 mM $MgCl_2$, pH 6.9). After repelleting as above, cells were resuspended in NIB containing 0.3% Triton X-100 and incubated on ice for 20 min. Following centrifugation at 300 x g for 10 min, the pellet was resuspended in NIB to 10^6 nuclei/mL. In each reaction, 20 μM drug was incubated with 0.5 mL of prepared nuclei for 10 min at 37°C. VM-26 to a final concentration of 20 μM was added, followed by a 15 min incubation at the same temperature. No drug was added to controls. Reactions were carried out in the absence of VM-26 in order to test the ability of the agents themselves to induce precipitable complex formation. The reaction volume was brought to 1 mL with NIB, then 1 mL of 2X buffer (3% SDS, 40 mM EDTA, and 0.4 mg/mL salmon

sperm DNA) was added. After a 15 min incubation at 65°C, the samples were cooled to room temperature and vortexed for 30 sec. Addition of 0.5 mL 0.325 M KCl, followed by a 30 min incubation on ice, began precipitation of the topo II/DNA complexes. Following centrifugation at 1570 x g for 15 min, 4 ml wash solution (10 mM Tris, 1 mM EDTA, 0.1 mg/ml salmon sperm DNA and 100 mM KCl) was added to each pellet and they were heated to 65°C for 5 min, cooled on ice for 15 min, then centrifuged at 1570 x g as above. This washing step was repeated twice before the final pellet was hydrolyzed in 2 M perchloric acid for 1 h at 70°C. Precipitated complexes were quantitated through liquid scintillation counting and results were expressed as percent of total DNA co-precipitable with protein. Percent inhibition was then calculated by comparing drug treated samples to controls.

RESULTS:

Components of the c-fos model: The binding sites for SRF and Elk-1 on the c-fos SRE are shown in Fig. 2A. These TFs were purified following expression as 6-histidine tagged proteins in bacteria and combined with radiolabeled DNA oligos to establish optimal binding conditions in electrophoretic mobility shift assays (EMSAs). SRF alone can bind to the SRE (Fig. 2B: compare free SRE in lane 1 with the shifted SRF complex in lanes 2 and 3). While Elk-1 cannot bind to the SRE on its own, it can bind to the high affinity *ets* motif on the *Drosophila* E74 promoter [27], as seen in Fig. 3B, lanes 1 and 2. Combining SRF and Elk-1 on the SRE in lanes 3 and 4 forms the TC, which can be distinguished from the SRF complex on the basis of its slight difference in mobility. This difference can be maximized by electrophoresing the complexes longer than illustrated, a condition that results in free probe running off the gel (not shown).

Drug effects on complex formation in EMSAs: The TF/DNA complexes of the c-fos system were targeted using the six minor groove-binding agents shown in Fig. 1. The FMGTs share many basic structural characteristics with parent compounds Hoechst 33342 and Hoechst 33258. To determine if the presence of the polyamine tails attributes different properties to the novel agents, their ability to inhibit complex formation in EMSAs was first evaluated. Increasing concentrations of drug and radiolabeled oligos were co-incubated for 30 min. After addition of purified TFs, the samples were incubated for an additional 30 min to allow complex formation to reach equilibrium. Representative results of subsequent electrophoresis and autoradiography are shown for FMGT-2 in Fig. 3A and 3B. The TC bound to the radiolabeled SRE is evident as a shifted complex in the untreated control (Fig. 3B, lane 1). 10 μM FMGT-2 in lane 2 fully prevents complex formation while decreasing drug concentrations in lanes 3-6 results in the return of TC complex formation to near control levels. Similar results were obtained in the same concentration range of FMGT-2 for inhibition of SRF complex formation (Fig. 3A, lanes 7-12).

To determine if the FMGTs or their Hoechst parent compounds inhibited Elk-1 binding alone, EMSA evaluations were repeated using purified Elk-1 and a radiolabeled E74 probe (Fig. 3B). No inhibition of Elk-1 complexes occurred at low drug levels up to 1 μM (lane 5). However, at 5 μM FMGT-2 or higher (lanes 3 and 4), the probe smeared and became retained in the well of the gel, prohibiting accurate analysis at or above this concentration. This occurred regardless of the presence of Elk-1 protein (data not shown).

Densitometric analysis of autoradiograms as shown in Fig. 3A and 3B allowed the relative amounts of free and complexed DNA to be quantitated. After calculating percent

complex formation for each sample, these values were expressed relative to non-drug treated controls to yield percent inhibition of complex formation. Graphing these values against drug concentration produced inhibition curves for FMGT-2 effects on each complex (Fig. 3C). FMGT-2 inhibited SRF and TC complex formation nearly equivalently, with maximal inhibition of 80% at about 1 μM. For Elk-1 complexes, only those lanes that clearly lacked visible smearing were analyzed. As seen in the representative gel in Fig. 3B, FMGT-2 concentrations up to 1 μM could be successfully quantitated. As noted above, there is no measurable effect of FMGT-2 on Elk-1 complex formation up to this concentration.

Comparing drug inhibition of TF/DNA complex formation in EMSAs: The effectiveness of FMGT-2 as an inhibitor of TF complex formation was compared to that of the remaining compounds. Inhibition curves for the effects of FMGTs on TC formation are shown in Fig. 4A. Since the effects of Hoechst 33342 and Hoechst 33258 were extremely similar in this assay, only Hoechst 33342 results are plotted as a dotted line for reference.

Overall, the FMGTs were more potent inhibitors of TC formation when compared to their Hoechst parents. The most potent agent, FMGT-2, was over an order of magnitude more effective than Hoechst 33342 in this assay and about twice as potent as either FMGT-1 or FMGT-3. At 1 μM, the latter was able to effect 60% complex inhibition. In contrast, Hoechst 33342 was only able to achieve 20% inhibition at this concentration. Although FMGT-1 was not the most potent compound, it was the only agent analyzed to completely abolish complex formation by about 2 μM. In comparison, FMGT-2 and FMGT-3 reached a plateau of

approximately 80% inhibition by 1 μM and 5 μM, respectively. At the highest concentration of Hoechst 33342 tested (10 μM), complex formation was inhibited by 75%.

Analysis of FMGT-5 demonstrated that it was a far less effective inhibitor of TC formation. Even at 10 μM FMGT-5, only 40% inhibition was attained. Above this concentration, FMGT-5 caused oligo smearing similar to that observed in the earlier Elk-1 EMSAs, prohibiting further analysis. To note, FMGT-3 and FMGT-5 differ in length and complexity by two branched polyamine tail units attached to an amide-bonded backbone. This increased length therefore seems to reduce the ability of FMGT-5 to inhibit TC formation on the SRE.

The inhibition of SRF complex formation by the FMGTs and Hoechst parents were similar to the profiles just discussed for TC inhibition (data not shown). None of the compounds inhibited Elk-1 complex formation and all caused well retention of the oligo at micromolar concentrations, as seen for FMGT-2 (Fig. 3B).

The concentration of each agent required to inhibit complex formation by 50% (its IC_{50} value) was calculated from inhibition curves and used to compare drug potencies (Fig. 4B). FMGT-2 was the most potent inhibitor of SRF or TC formation with IC_{50} values of 0.4 μM and 0.5 μM, respectively. The other novel agents, FMGTs 1 and 3, also had submicromolar IC_{50} values. In contrast, approximately an order of magnitude more Hoechst 33342 or Hoechst 33258 was required for the same level of SRF complex inhibition. With an IC_{50} of 20 μM, Hoechst 33342 was two times less potent than Hoechst 33258 in inhibiting SRF complex formation. Notably, whereas the FMGTs were equipotent in inhibiting TC or SRF complex formation, the Hoechst compounds were slightly more effective inhibitors of TC formation. However, despite

their improved performance in the TC EMSAs, Hoechst 33342 and Hoechst 33258 were still between 5 and 10 times less potent than FMGTs 1, 2, or 3.

Drug effects on c-fos promoter-driven cell-free transcription: Previous studies of DNA-binding drugs have demonstrated that agents often lose potency as assay conditions become more complex [18, 24, 28]. We therefore next wished to evaluate whether the FMGTs would also be able to inhibit c-fos promoter-driven transcription in cell-free assays and whether their ability to do so correlated with their EMSA potencies. Here, a more complex environment is achieved by placing the SRE into a longer piece of DNA with greater sequence variation and by adding a nuclear extract that contains cellular transcriptional machinery and an extensive array of additional proteins. The assay can therefore be carried out without nuclear uptake of the agents becoming a complicating factor. A plasmid containing the human c-fos promoter was linearized and incubated with drug for 30 min before being combined with nuclear extract from serum stimulated NIH3T3 cells, α-[^{32}P]CTP, and a mix of nucleotides to drive the production of a radiolabeled transcript. This 750 base transcript was subsequently purified, electrophoresed on a denaturing polyacrylamide gel, and visualized following autoradiography (Fig. 5A, upper arrow). Quantitation of the transcript and normalization to the internal control (lower arrow) allowed accurate comparisons between drug-treated and control samples.

Representative results for FMGT-2 (Fig. 5A) show dose dependent inhibition of transcription. A concentration of 30 μM FMGT-2 nearly abolished transcript formation (lanes 1-2). As drug concentrations decrease to 10 μM in lane 7, transcripts are restored to near control levels (lanes 8-9). No change in transcript size was noted in any samples, indicating that

inhibition of transcriptional elongation is unlikely. The disappearance of transcripts as drug concentrations increase therefore suggests that transcription initiation is primarily being affected.

FMGTs 1 and 2, the most potent agents in the EMSA analyses, were compared to the Hoechst compounds for their effectiveness in inhibiting cell-free transcription. Following densitometric quantitation of autoradiographs, transcript levels in drug treated samples were expressed relative to controls and graphed against drug concentration (Fig. 5B). As in the EMSAs, the inhibition profile of both Hoechst compounds in this assay were similar and their IC_{50} values were equal, so the results for Hoechst 33342 are presented as a dotted line. In contrast to the inhibition of TF complex formation in the EMSAs, there were no differences in potencies between the FMGTs and Hoechst 33342. All had IC_{50} values of approximately 17 μM. The pattern of transcript disappearance upon Hoechst treatment was similar to the FMGT results in that no shortened transcripts were observed (data not shown). However, like the EMSAs, slightly lower levels of the FMGTs compared to Hoechst 33342 were needed to achieve complete inhibition of transcription. Over 90% inhibition of transcript formation was achieved at 30 μM FMGT-1 or 2, while more than 50 μM Hoechst 33342 was needed for equivalent inhibition.

Since the FMGTs could inhibit cell-free transcription, their effect on endogenous c-fos expression in whole cells was subsequently investigated. Use of whole cells provides the additional complexity of cellular uptake and distribution of drug. In previous studies, exposure of NIH3T3 cells to 10 μM Hoechst 33342 for just 1 h resulted in a 60% decrease in c-fos gene expression [18]. In contrast, treatment with Hoechst 33258 concentrations as high as 50 μM up to 16 h did not result in any detectable inhibition of c-fos mRNA production (data not shown),

corroborating earlier studies that found similar differences in these cellular effects of these compounds [29, 30]. The chemistry of the Hoechst structure itself can obviously have a significant influence on the cellular activity of these compounds, and the addition of polyamine tails to this structure may further modulate their whole cell activity. However, similar to Hoechst 33258, exposing NIH3T3 cells to 10 μM FMGTs for up to 16 h failed to decrease c-fos mRNA levels (data not shown).

Evaluation of drug effects on topo II activity: While the FMGTs could inhibit TF complex formation on the SRE and resultant transcription when more DNA and proteins are present, their inability to inhibit endogenous c-fos expression in cells prevented further evaluation of their effects on the DNA template in more complex environments. We wished to determine if the FMGTs were still effective at disrupting other DNA-associated activities in a cell-free environment, and whether this activity could be correlated to their performance in the simpler EMSAs. As an enzyme responsible for maintaining correct DNA topology, topo II associates with the helix and nicks both strands, becoming covalently bound to the DNA ends formed in the process [31]. The DNA-topo II crosslink in this "cleavable complex" can be induced by drugs such as the epipodophyllotoxins (i.e. VM-26 or VP-16) [32]. In the presence of minor-groove binding drugs such as netropsin or Hoechst 33258, the formation of these crosslinks in isolated nuclei is inhibited [26, 33].

Nuclei isolated from ^{14}C-thymidine treated HeLa cells were co-incubated with VM-26 and 20 μM of each of the FMGTs and the Hoechst compounds. The DNA-topo II crosslinks were then precipitated and quantitated. The percent inhibition calculated for each compound is

listed in Table 1. Hoechst 33342 proved to be more potent than Hoechst 33258 in this assay. The FMGTs varied greatly in their ability to inhibit crosslink formation, and this inhibition did not correlate to their observed potencies in inhibiting TF/DNA complex formation. Although these agents exhibited EMSA potencies in the order FMGT-2 > FMGT-1 > FMGT-3 > Hoechst 33258 > Hoechst 33342 > FMGT-5, their potencies in the topo II assay ranked FMGT-5 > FMGT-2 > Hoechst 33342 > FMGT-3 > Hoechst 33258 > FMGT-1. Formation of crosslinks did not occur in the presence of any of these agents alone, in the absence of VM-26 (data not shown), demonstrating that they lacked the ability to induce cleavable complex formation themselves. Although no correlation between the EMSAs and the topo II assay was noted, the FMGTs were able to inhibit topo II activity in the more complex environment of isolated nuclei.

DISCUSSION:

The novel approach of adding polyamine tails to Hoechst compounds proved to be an effective method for enhancing their ability to inhibit TF complex formation on the c-fos SRE in cell-free assays. The potencies of FMGT-1, FMGT-2 and FMGT-3 in inhibiting TF complex formation in EMSAs were 50 fold higher than those of their parent compounds, Hoechst 33342 and 33258. FMGTs 1 and 2 also inhibited cell-free c-fos promoter-driven transcription. Additionally, the FMGTs affected general DNA template function as demonstrated by their ability to inhibit the formation of the topo II cleavable complex in isolated nuclei.

The previously determined chemical characteristics of the FMGTs can be related to their abilities to inhibit TF/DNA complexes [16, 17]. FMGTs 1, 3 and 5 can bind dsDNA in higher order complexes with 1:1 or 2:1 stoichiometries, while cooperative binding may even result in

FMGT-2:DNA stoichiometries of 3:1. The binding stoichiometries of these agents as well as their equilibrium constants were dependent on the number of contiguous A/T bases at the binding site, but were also modulated by surrounding bp composition. The binding affinities of the FMGTs for A/T rich sites up to 5 contiguous A/T base pairs are in the order FMGT-2 > FMGT-5 = FMGT1 ~ FMGT-3 >> Hoechst 33258 . A similar ranking was obtained for the stabilization of DNA as measured by increases in DNA melting temperatures.

The success of FMGT design is highlighted by their superior performance in the EMSAs as summarized in Fig. 4B. FMGT-2 was about 50 times more potent in inhibiting SRF complex formation than Hoechst 33342. Notably, while the Hoechst compounds were more potent in inhibiting TC formation than SRF complex formation, the FMGTs were nearly equipotent on either complex. Thus, while the presence of Elk-1 in the TC may affect the ability of the Hoechst compounds to prevent complex formation on the SRE, it appears to have little effect on the inhibitory activities of the FMGTs. Recruitment of Elk-1 to the TC alters helical conformation and bending [34]. This DNA conformational change may increase the affinity of the Hoechst compounds for their binding site on the SRE, perhaps by altering groove width or shape. The fact that FMGT potency does not change may be due to their higher affinity and their ability to clamp onto DNA by interacting with both grooves. This affinity may therefore be maintained regardless of the presence of a second TF.

The rank of potencies of the FMGTs in inhibiting TF binding overall (FMGT-2 > FMGT-1 ~ FMGT-3 > FMGT-5 >> Hoechst compounds) may be based in part on the order of their DNA-binding affinities, but these alone fail to explain the EMSA results. For example, FMGTs 1, 5 and 3 bound an oligo containing 5 contiguous A/T bp with nearly equal affinities, supporting

a prediction of nearly equal potencies in the EMSAs. Although FMGTs 1 and 3 were nearly equipotent, FMGT-5 failed to reach even 50% inhibition of TC formation. As noted earlier, the polyamine tail of FMGT-5 is longer and contains two more branch points than FMGT-3. While these characteristics may increase the affinity of FMGT-5 for isolated DNA, they fail to impart an improved ability to inhibit TF binding to the A/T rich site on the SRE.

Extending this analysis to the remaining FMGTs, the polyamine tail of FMGT-2 is about two times longer than that on FMGT-1 and the observed potencies of these compounds in the EMSAs were similar. The additional branching on the polyamine tail of FMGT-1 did not appear to improve the inhibitory potential of this agent. FMGT-3 was nearly as long as FMGT-2, but more highly branched, and the former was slightly less potent in the EMSAs. It may be that a minimum tail length is required for these compounds to make adequate contact with the phosphodiester backbone. Increasing the length or complexity of branching, as found on FMGT-5, may interfere with the ability of these novel agents to inhibit TF/DNA association.

The sequence and conformation of the SRE may also influence the ability of the FMGTs to optimally bind. The SRF binding site on the EMSA oligos consists of 6 contiguous A/T bp, a site large enough for potential FMGT binding in higher order complexes. However, Hoechst compounds show distinct preferences for some A/T rich sites, and the presence of a 5'-TpA-3' step may interfere with their proper binding [35]. Since this step is found near the middle of the SRF binding site, it may greatly diminish the binding ability of the FMGT bisbenzimidazole moiety. Calculations of FMGT binding affinities were carried out using oligos that lacked such a step. Targeting TFs that bind to other A/T rich sites may therefore reveal that the FMGTs are even more superior to their Hoechst parents than demonstrated herein.

The effect of DNA sequence on FMGT binding is also exemplified by the Elk-1 EMSA results. The E74 oligo sequence differs from the SRE near its 5' end, a factor that may alter its inherent flexibility. The smearing of E74 in the presence of the FMGTs may have resulted from their bending of the oligo, a conformational change that can affect gel migration. MGTs with varying polyamine tail structures were able to effect such visible changes in other systems [36, 37]. Interestingly, their ability to cause migration changes did not directly correlate with their binding affinities [36]. Although the FMGTs have not been analyzed in this manner, their polyamine tails likely endow them with analogous bending capabilities, and this distortion could prevent proper TF/DNA contacts. Qualitative differences in these capabilities may help explain their potency differences. The inability of the Hoechst compounds to cause extreme structural changes may make these agents comparatively less effective inhibitors [38, 39]. Furthermore, the contacts FMGTs make with the major groove and their ability to cooperatively bind DNA in greater than 1:1 stoichiometries, other characteristics that Hoechst compounds lack, may provide more extensive steric hindrance to TF binding.

The FMGTs, like the Hoechst compounds, inhibited c-fos promoter-driven cell-free transcription in a more complex environment. Based solely upon the differences in potencies between the two classes of agents in the EMSAs, one would predict that the FMGTs would be more potent transcriptional inhibitors. As noted earlier, a decrease in the potency of DNA-binding drugs as assay conditions become more complex has been observed in many systems [18, 24, 28]. Additionally, previous studies of the polypyrrole-based MGTs focused mainly on their inhibition of TF/DNA complex formation in EMSAs. However, when evaluated in cell-free transcription assays, their potency was significantly reduced and became comparable to

classical minor groove binders such as distamycin (S.Y. Chiang and T.A. Beerman, unpublished observations). Similar results were even obtained with selected polyamides, pyrrole and imidazole-based synthetic minor groove-binding agents that can be designed to bind specific DNA sequences [40]. Moreover, the level of improvement of the polyamides over the classical minor groove-binder distamycin in the transcription assay compared to the EMSAs was not maintained. Although the polyamides were 100 fold better than distamycin in the EMSAs, the improvement was reduced to a 5 fold difference in inhibiting cell-free transcription. While the drop in potency for novel minor groove binders in cell-free transcription assays was expected due to higher DNA amount, the relative decrease in potency compared to distamycin was not. In general, it appears that the ratio of improvement between drugs in simple EMSAs is not easily maintained in more complex environments.

While we hoped that the addition of major groove-associating tails to minor groove binding agents would overcome these limitations, the FMGTs were equipotent to their Hoechst parents in the cell-free transcription assay. Similar to the results described above for other minor groove-binding agents, 5 times more Hoechst 33342 was needed for 50% inhibition in the cell-free transcription assay as compared to complex formation in the EMSAs, while 20 times more FMGTs were needed. The increased amount of DNA in the transcription assay likely contributed in part for this decrease in potency by acting as a "sink" and lowering the levels of drug available for binding to the SRE, which is rate-limiting for transcription. Since Hoechst 33342 and the FMGTs presumably target the same sequences, the need for higher relative levels of the FMGTs may indicate that the DNA conformation or presence of additional proteins is interfering with their optimal binding. If prevented from making contact in the major groove,

these agents may perform at the same level of effectiveness as the Hoechst compounds, resulting in similar IC_{50} values.

While the primary purpose of this study was to determine if the ability of Hoechst-based drugs to disrupt TF complexes could be enhanced using the novel MGT design approach, we had also hoped that these agents would behave similar to Hoechst 33342 and exhibit cellular activity. However, the FMGTs acted more like Hoechst 33258 since they could not inhibit endogenous c-fos expression. This probably stems from factors unrelated to DNA-binding abilities, including cellular permeability and the ability to localize to and be retained in the nucleus. These findings suggest that, ultimately, further modifications of the FMGTs are needed to keep their TF complex inhibitory activity high but also endow them with improved cellular properties similar to Hoechst 33342.

Encouragingly, the ability of the FMGTs to function in a more complex environment and inhibit other DNA template-associated processes was demonstrated by their inhibition of topo II activity in isolated nuclei. In this system, barriers to cellular or nuclear uptake do not exist and DNA template effects can be measured directly. Here, the order of potency of the compounds correlated with neither their DNA binding affinities nor their TF/DNA complex inhibitory potencies in the EMSAs.. However, some similarities were noted between the levels of drug needed to inhibit topo II activity and those needed to inhibit cell-free transcription. For FMGT-2 and Hoechst 33342, 20 μM was sufficient to cause nearly equal levels of inhibition in both assays. However, 20 μM FMGT-1 resulted in four-fold higher inhibition of cell-free transcription. The characteristics that make the FMGTs good inhibitors of TF/DNA interactions may therefore differ from those needed to inhibit other DNA related activities. This initial

finding may suggest that with additional modification, it may be possible to design an FMGT that selectively inhibits transcription over other DNA-related activities.

The potential of adding major-groove binding constructs to minor-groove binding compounds to enhance inhibition of TF/DNA complex formation is apparent from these studies, although further improvement is needed to attain more potent effects on transcription. Adding a polyamine tail to a Hoechst-based bisbenzimidazole improves its ability to inhibit TF binding to DNA in cell-free systems. The FMGTs, with their high DNA-binding affinity and ability to interact with both grooves in higher order complexes, were more effective and potent inhibitors of TF/DNA interactions than their Hoechst parent compounds. Moreover, these studies provide some initial insight into how polyamine tail length and branching can affect the inhibitory activity of these novel agents. We plan to further pursue whether additional changes to drug structure and polyamine tail configuration may improve drug activity in cell-free assays as well as whole cells. In the field of drug design, minor groove-binding agents are playing increasingly significant roles in developing agents with improved abilities to distinguish between sequences. Achieving selective inhibition of desired TF/DNA complexes has potentially far-reaching implications in the molecular study of gene regulation as well as therapeutics. Perhaps most significantly, then, this study confirms that the novel drug design concept first employed in enhancing the DNA-binding qualities of the polypyrrole based MGTs can be applied to other sequence selective minor groove-binding agents and actually improves their ability to inhibit TF/DNA complexes.

Acknowledgments:

We graciously thank Dr. Alfred Nordheim for providing the SRF expression vector (pILA-SRF) and pFosLuc19 plasmid. We also thank Dr. Andrew Sharrocks for providing the Elk-1 expression vector (pAS278). This study was supported in part by National Cancer Institute Grant CA16056 (to T.A.B.), American Cancer Society Grant DHP 158 (to T.A.B.), US Army Medical Research Grant BC980100 (to C.M.W), and National Institutes of Health Grant 5R37DK0917136 (to T.C.B.)

REFERENCES:

1 Chen, A.Y., Yu, C., Gatto, B. and Liu, L.F. (1993) Proc Natl Acad Sci USA 90, 8131-8135.
2 Turner, P.R. and Denny, W.A. (1996) Mutat Res 355, 141-69.
3 Hurst, H.C. (1996) Eur J Cancer [A] 32A, 1857-1863.
4 Welch, J.J., Rauscher, F.J., 3rd and Beerman, T.A. (1994) J Biol Chem 269, 31051-8.
5 Chiang, S.Y., Welch, J.J., Rauscher, F.J., 3rd and Beerman, T.A. (1996) J Biol Chem 271, 23999-24004.
6 Dorn, A., Affolter, M., Muller, M., Gehring, W.J. and Leupin, W. (1992) The EMBO Journal 11, 279-286.
7 Schleif, R. (1988) Science 241, 1182-7.
8 Feng, J.A., Johnson, R.C. and Dickerson, R.E. (1994) Science 263, 348-55.
9 Schumacher, M.A., Choi, K.Y., Zalkin, H. and Brennan, R.G. (1994) Science 266, 763-70.
10 Hélène, C. (1998) Nature 391, 436-438.
11 Bruice, T.C., Houng, Y.M., Gong, X.H. and Lopez, V. (1992) Proc Natl Acad Sci USA 89, 1700-1704.
12 Browne, K.A., Gong, X.H. and Bruice, T.C. (1993) J Am Chem Soc 115, 7072-7079.
13 Chiang, S.Y., Bruice, T.C., Azizkhan, J.C., Gawron, L. and Beerman, T.A. (1997) Proc Natl Acad Sci USA 94, 2811-6.
14 Zhang, X.B. and Kiechle, F.L. (1998) Biochem Biophys Res Commun 248, 18-21.
15 Wong, S., Sturm, R.A., Michel, J., Zhang, X.M., Danoy, P., McGregor, K., Jacobs, J.J., Kaushal, A., Dong, Y., Dunn, I.S. and Parsons, P.G. (1994) Biochem Pharmacol 47, 827-837.
16 Satz, A.L. and Bruice, T.C. (1999) Bioorg Med Chem Lett 9, 3261-6.
17 Satz, A.L. and Bruice, T.C. (2000) Bioorg Med Chem 8, 1871-80.
18 White, C.M., Heidenreich, O., Nordheim, A. and Beerman, T.A. (2000) Biochemistry 39, 12262-73.
19 Treisman, R. (1992) Trends Biochem Sci 17, 423-6.
20 Marais, R., Wynne, J. and Treisman, R. (1993) Cell 73, 381-93.
21 Mo, Y., Vaessen, B., Johnston, K. and Marmorstein, R. (2000) Nat Struct Biol 7, 292-7.
22 Pellegrini, L., Tan, S. and Richmond, T.J. (1995) Nature 376, 490-8.
23 Bruice, T.C., Sengupta, D.D., Blasko, A., Chiang, S.-Y. and Beerman, T.A. (1997) Bioorg Med Chem 5, 685-692.
24 Chiang, S.Y., Azizkhan, J.C. and Beerman, T.A. (1998) Biochemistry 37, 3109-3115.
25 Woynarowski, J.M., Sigmund, R.D. and Beerman, T.A. (1988) Biochim Biophys Acta 950, 21-9.
26 Beerman, T.A., McHugh, M.M., Sigmund, R., Lown, J.W., Rao, K.E. and Bathini, Y. (1992) Biochim. Biophys. Acta 1131, 53-61.
27 Rao, V.N. and Reddy, E.S. (1992) Oncogene 7, 65-70.
28 Chiang, S.Y., Burli, R.W., Benz, C.C., Gawron, L., Scott, G.K., Dervan, P.B. and Beerman, T.A. (2000) J Biol Chem.
29 Harapanhalli, R.S., Howell, R.W. and Rao, D.V. (1994) Nucl Med Biol 21, 641-7.

30 Zhang, X. and Kiechle, F.L. (1998) Ann Clin Lab Sci 28, 104-14.
31 Burden, D.A. and Osheroff, N. (1998) Biochim Biophys Acta 1400, 139-54.
32 Chen, G.L., Yang, L., Rowe, T.C., Halligan, B.D., Tewey, K.M. and Liu, L.F. (1984) J Biol Chem 259, 13560-6.
33 Beerman, T.A., Woynarowski, J.M., Sigmund, R.D., Gawron, L.S., Rao, K.E. and Lown, J.W. (1991) Biochim. Biophys. Acta 1090, 52-60.
34 Sharrocks, A.D. and Shore, P. (1995) Nucleic Acids Res 23, 2442-9.
35 Portugal, J. and Waring, M.J. (1988) Biochim Biophys Acta 949, 158-68.
36 Sengupta, D., Blasko, A. and Bruice, T.C. (1996) Biorganic and Med. Chem. 4, 803-813.
37 He, G.X., Browne, K.A., Groppe, J.C., Blaskó, A., Mei, H.Y. and Bruice, T.C. (1993) J Am Chem Soc 115, 7061-7071.
38 Pjura, P.E., Grzeskowiak, K. and Dickerson, R.E. (1987) The Journal of Molecular Biology 197, 257-271.
39 Utsuno, K., Maeda, Y. and Tsuboi, M. (1999) Chem Pharm Bull (Tokyo) 47, 1363-8.
40 Dervan, P.B. and Burli, R.W. (1999) Curr Opin Chem Biol 3, 688-93.

TABLE 1: Comparison of drug effects on topoisomerase II activity in HeLa nuclei.

Agent	Percent reduction in DNA-protein crosslinks
Hoechst 33342	49.3%
Hoechst 33258	21.6%
FMGT-1	15.3%
FMGT-2	60.1%
FMGT-3	36.1%
FMGT-5	65.8%

HeLa cells were labeled with ^{14}C-thymidine prior to nuclei isolation. The crosslinking agent VM-26 was co-incubated with radiolabeled nuclei in the presence of 20 μM of each agent for 10 min at 37°C. DNA-protein crosslinks were quantitated following sodium dodecyl sulfate precipitation. Results are from three experiments.

FIGURE LEGENDS:

FIGURE 1: Chemical structures of the agents analyzed. (A) The commercially available Hoechst compounds. (B) The novel, rationally designed fluorescent microgonotropens (FMGTs). Polyamine tails of varying lengths and degrees of branching extend from a Hoechst-based structure.

FIGURE 2: Components of the c-fos promoter. (A) Binding of TFs to the human c-fos SRE. A homodimer of SRF must be bound before recruitment of Elk-1 can occur to form a ternary complex (TC). (B) Complex formation between purified TFs and radiolabeled probes in EMSAs. TFs and ^{32}P-labeled oligonucleotides are co-incubated 30 min before being electrophoresed on a polyacrylamide gel and autoradiographed. The 24 bp oligonucleotides contain sequences from the c-fos SRE or the *Drosophila* E74 promoter. Lane 1, free SRE probe; lanes 2-3, SRE plus SRF; lanes 4-5, SRE plus Elk-1 and SRE yields the TC; lane 6, free E74 probe; lanes 7-8, Elk-1 plus E74 probe.

FIGURE 3: Drug effects on complex formation in EMSAs. For (A) and (B), FMGT-2 was co-incubated with radiolabeled probe for 30 min before purified TFs were added. Electrophoresis and autoradiography followed as described in Fig. 2. In each panel, upper arrows: TF/DNA complexes; lower arrows, free DNA. (A) Inhibition of complex formation on the SRE by FMGT-2. Lanes 1-6: Inhibition of TC formation. Lanes 7-12: Inhibition of SRF complex formation. Lanes 1 and 7, control, no drug; lanes 2 and 8, 10 μM; lanes 3 and 9, 1 μM; lanes 4, 5 ,10 and 11, 0.5 μM; lanes 6 and 12, 0.1 μM. (B) Inhibition of complex formation on E74.

Lanes 1-2, control; lane 3, 10 μM; lane 4, 5 μM, lane 5, 1 μM; lane 6, 0.5 μM; lane 7, 0.1 μM. (C) Quantitation of FMGT-2 inhibition. The percent DNA shifted in each drug treated lane was compared to controls to calculate percent inhibition of SRF (●), Elk-1 (□) or TC (○) formation. Results are from four experiments (mean value ± standard error).

FIGURE 4: Comparison of drug effects on TF complex formation in EMSAs. (A) Drug inhibition of TC formation. Inhibition curves for each compound were plotted and quantitated as described in Fig. 3. Data for FMGT-1 (●), FMGT-2 (○), and FMGT-3 (□), and FMGT-5 (Δ) are compared to Hoechst 33342 (dotted line). Results are from four experiments (mean value ± standard error). (B) Summarized comparison of drug potencies in EMSAs. Drug concentrations required for 50% inhibition of complex formation (IC_{50}s) were calculated from inhibition curves as shown in panel (A) for TC and SRF complexes.

FIGURE 5: Drug effects on c-fos promoter-driven cell-free transcription. (A) Effect of FMGT-2 on cell-free transcription. A plasmid containing the human c-fos promoter was linearized and incubated with drug for 30 min before nuclear extracts from serum-induced NIH3T3 cells were added. Following the reaction in the presence of [^{32}P]CTP, the radiolabeled, 750 base transcript (top arrow) is electrophoresed on a denaturing polyacrylamide gel. A radiolabeled 250 base transcript, used as an internal control (lower arrow), is added to each sample prior to loading. Positions of size markers, in kb, are indicated. Lanes 1-2, 30 μM; lanes 3-4, 20 μM; lanes 5-6, 15 μM; lane 7, 10 μM, lanes 8-9, controls, no drug added. (B) Quantitation of drug effects in this assay. All c-fos transcripts were normalized to internal controls before quantitation as in

Fig. 4. Results from four experiments (mean value ± standard error) are shown for FMGT-1 (●), FMGT-2 (○), and Hoechst 33342 (dotted line).

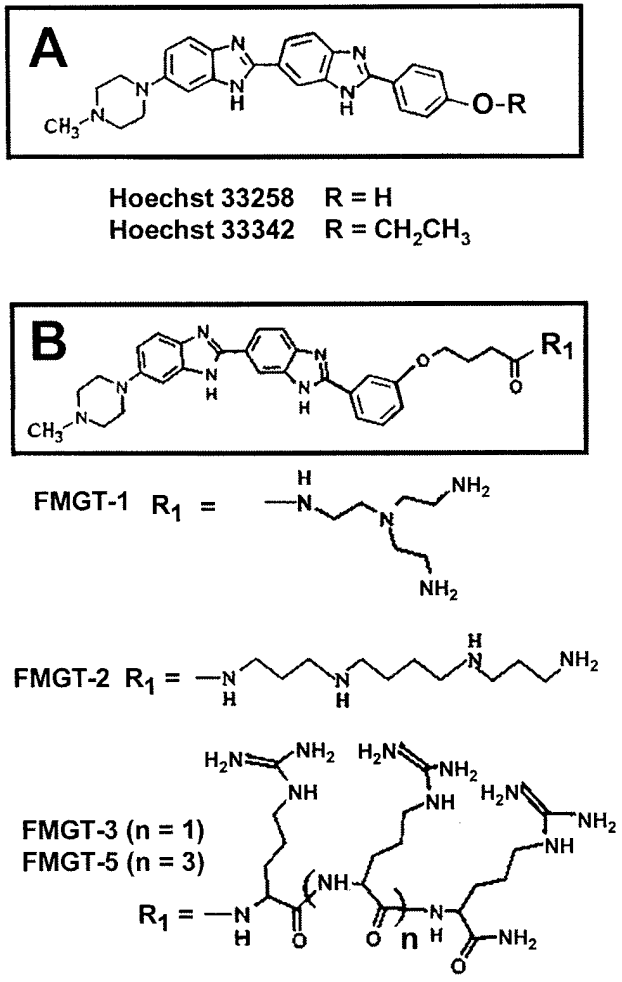
A
O-R
Hoechst 33258 R = H
Hoechst 33342 R = CH2CH3
B
R1
FMGT-1 R1 =
FMGT-2 R1 =
FMGT-3 (n = 1)
FMGT-5 (n = 3)
R1 =
n

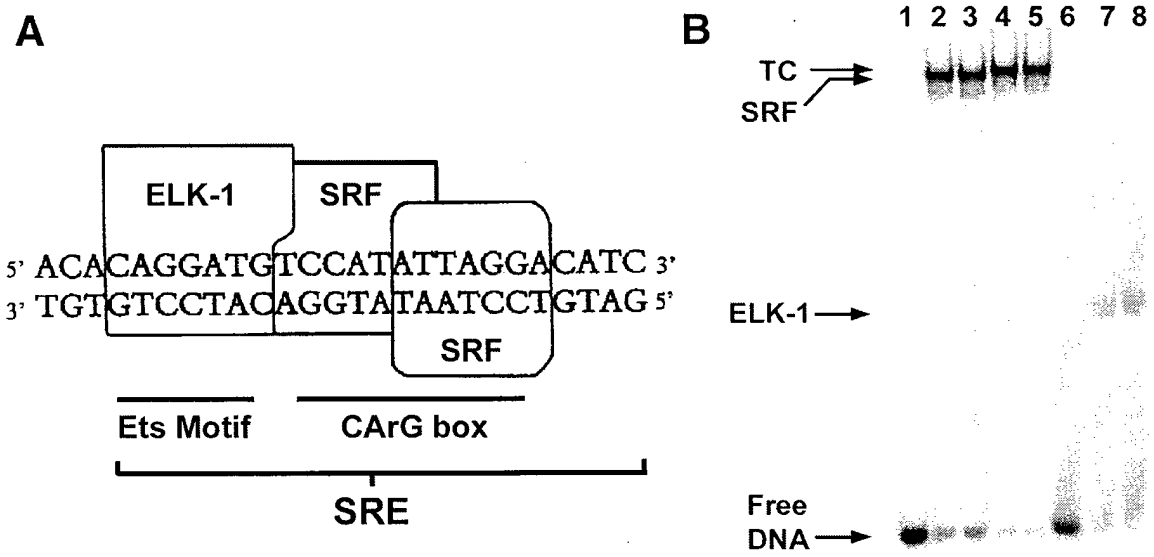
A
ELK-1
SRF
5' ACACAGGATGTCCATATTAGGACATC 3'
3' TGTGTCCTACAGGTATAATCCTGTAG 5'
SRF
Ets Motif
CArG box
SRE
B
1 2 3 4 5 6 7 8
TC
SRF
ELK-1
Free
DNA

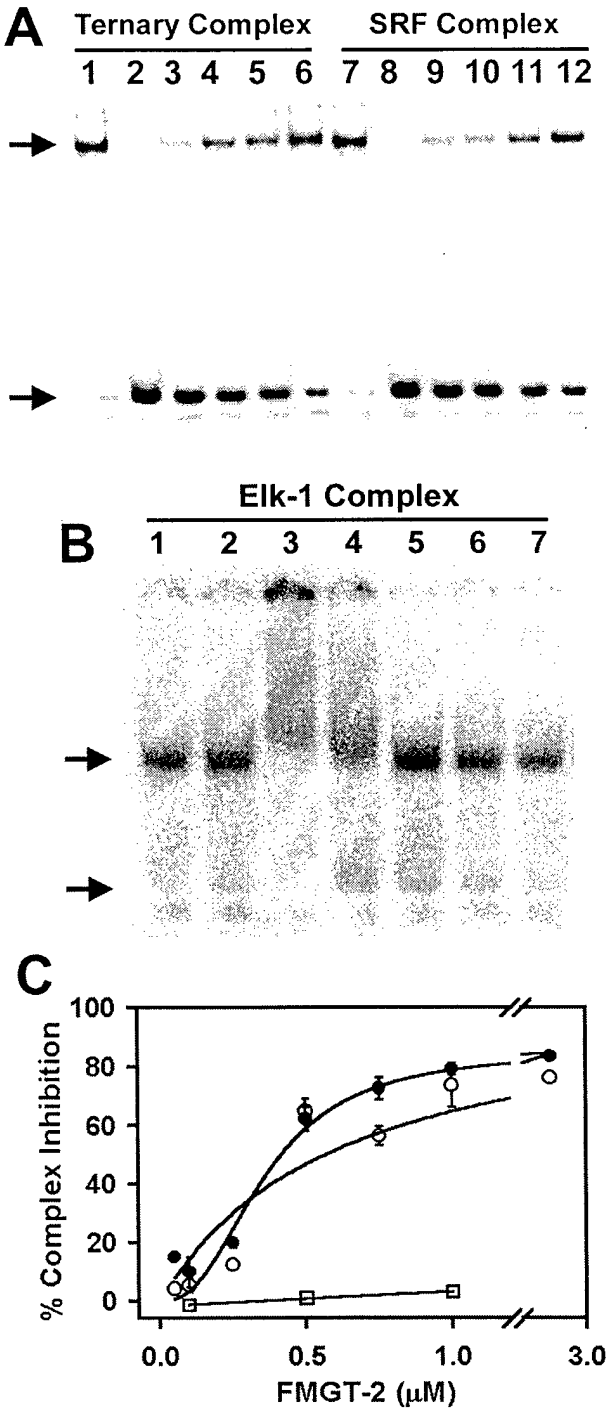
A
Ternary Complex
SRF Complex
1 2 3 4 5 6 7 8 9 10 11 12
B
Elk-1 Complex
1 2 3 4 5 6 7
C
% Complex Inhibition
100
80
60
40
20
0
0.0
0.5
1.0
3.0
FMGT-2 (μM)

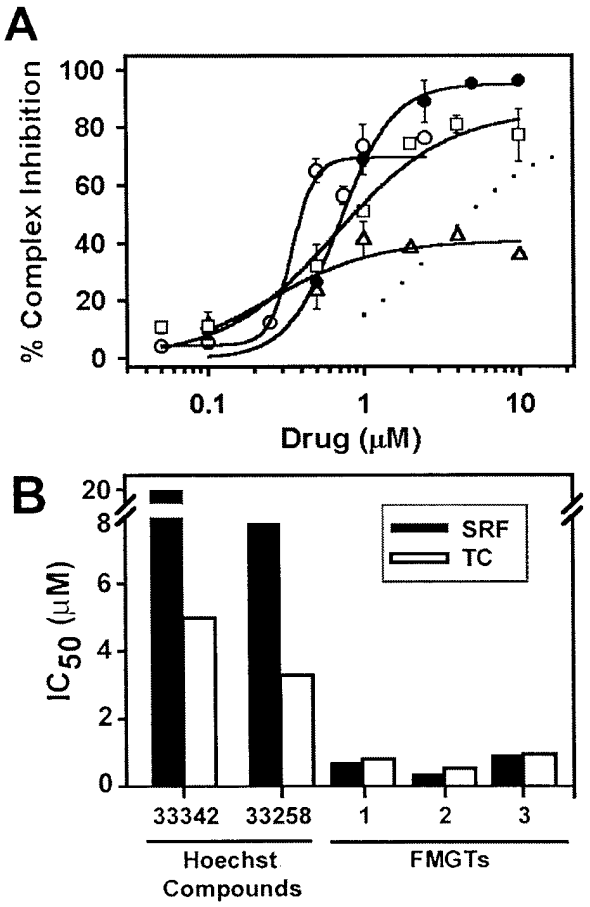
A
% Complex Inhibition
100
80
60
40
20
0
0.1
1
10
Drug (μM)
B
IC50 (μM)
20
8
6
4
2
0
SRF
TC
33342
33258
1
2
3
Hoechst Compounds
FMGTs

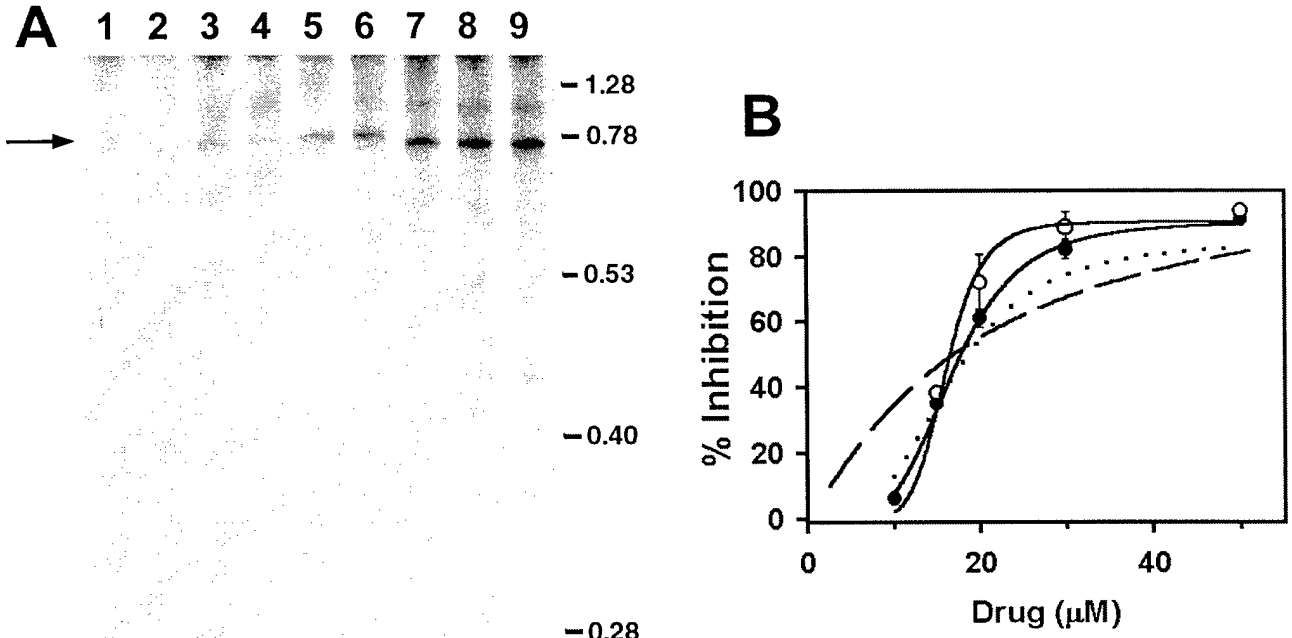
A
1 2 3 4 5 6 7 8 9
1.28
0.78
0.53
0.40
0.28
B
% Inhibition
100
80
60
40
20
0
0
20
40
Drug (μM)